Title No. 60-55

Laboratory Study of a 45-Foot Square Flat Plate Structure

By SIDNEY A. GURALNICK and ROBERT W. LA FRAUGH

Coordinated experimental and analytical studies of reinforced concrete floor systems were conducted at the University of Illinois and the Portland Cement Association laboratories for the purpose of providing a basis for more rational design methods than those now in use. Ultimately, it is expected that more economical floor systems will result from these improved design methods. The experimental program at the University of Illinois involved testing of one-quarter scale models of various floor systems.

To aid interpretation of the one-quarter scale model tests, a flat plate structure constructed at three-quarter scale and 45-ft square was tested at the PCA laboratories. The distribution of moments in the slab found in the tests at service load is compared with values for slab moments obtained by current design methods. Also, the observed behavior at ultimate strength is compared with values for ultimate load predicted by application of the yield-line theory and of a shear strength theory.

Key words: compressive strength; cracking; deflection; failure; flat plate; flat slab; flexural strength; model; moment; reinforced concrete; slab; shear strength; test; two-way slab; ultimate load; ultimate strength.

■ RECENT ADVANCES IN THE development and practical application of ultimate strength theories in structural concrete design have emphasized the need for re-evaluation and improvement of design methods for reinforced concrete floor systems. To accomplish this purpose, Committee 421 on Design of Reinforced Concrete Slabs was organized in 1941 by the American Concrete Institute and became joint with the American Society of Civil Engineers in 1953. The committee's studies led to development of an extensive experimental and analytical research program. Execution of this program began at the University of Illinois in 1956. The experimental work involves tests of two flat slabs, one flat plate, and two types of two-way slab construction.[1] An extensive analytical research program considering both elastic and inelastic behavior is also in progress at the University of Illinois.

The experimental work at the University involves ¼-scale models of typical floor systems, each model consisting of nine square panels arranged three-by-three, and constructed from portland cement mortar reinforced with ⅛ in. square steel bars. The panel size used is 5 x 5 ft as compared to 20 x 20 ft in the full-size prototype structures considered. Studies by ACI-ASCE Committee 421, and test results obtained so far at the University, indicate that significant changes and improvements in design practice may be expected to result from the current research-

ACI member **Sidney A. Guralnick** is associate professor of civil engineering, Illinois Institute of Technology, Chicago. His duties combine teaching and research in structural theory, reinforced concrete, and thin shell construction. Previously, Dr. Guralnick had engaged in research in the deflection and shear strength of reinforced concrete beams while serving as manager of the Structural Research Laboratory at Cornell University. During the course of the research reported in this paper, he served as a development engineer with the Structural Development Section of the Research and Development Laboratories of the Portland Cement Association.

Dr. Guralnick is a member of ACI-ASCE Committee 421 (321), Reinforced Concrete Slabs, and 441 (341), Reinforced Concrete Columns; and a member of ACI Committee 439 (339), High Strength Reinforcement for Concrete.

ACI member **Robert W. LaFraugh** has been an associate development engineer, Structural Development Section, Portland Cement Association since 1960. He received his BS degree in civil engineering at Michigan State University in 1958. Mr. LaFraugh was appointed a part-time instructor in the Civil Engineering Department at Michigan State in 1958 and received his MS in structural engineering from this University in 1960.

es. It was considered essential, therefore, that interpretation of the University's one-quarter scale tests in terms of full-scale structural performance be aided by securing laboratory test data for a larger structure. The PCA Structural Laboratory undertook this supplementary testing because it is well equipped to conduct tests of large structures.

To aid interpretation of model test data, the large test structure should, of course, duplicate one of the five one-quarter scale floor systems involved in the University of Illinois work. The flat plate floor system was selected as best serving the dual purpose of obtaining needed performance characteristics, as well as obtaining data for model interpretation.

PURPOSE

The purpose of this report is to present the results of an experimental study of the performance under load of the three-quarter scale flat plate structure, and to compare these results with those obtained in the one-quarter scale model test conducted at the University of Illinois. In addition to a consideration of model effects, a further purpose is to evaluate certain existing design procedures on the basis of the experimental results obtained.

The results of this study together with those of the extensive research programs being conducted at the University of Illinois and at other institutions in the United States and abroad should materially aid ACI-ASCE Committee 421 on the Design of Reinforced Concrete Slabs toward development of improved design methods.

SCOPE

A three-quarter scale flat plate test specimen, having over-all dimensions 45 x 45 ft and consisting of nine 15 x 15-ft panels arranged three-by-three, was subjected to a series of load tests culminating in a final

test to destruction. The slab was approximately 5¼ in. thick and was supported on 16 columns. The four interior columns supported the slab without the use of drop panels, column capitals or supporting beams. Shallow spandrel beams, 8¼ in. deep and 12 in. wide, intersected the exterior columns along the west and north edges of the test structure; deep spandrel beams, 15¾ in. deep and 6 in. wide, intersected the exterior columns along the east and south edges. All reinforcement was intermediate grade deformed steel bars with a yield point of approximately 45,000 psi.

The test program was designed primarily to investigate the over-all general performance of the flat plate structure, and the following major items were investigated:

1. Slab deflections at various load levels from the service load range to the ultimate load.
2. Development of cracking at service load and at ultimate load.
3. Distribution of steel stresses throughout the slab at service load.
4. Distribution of bending moments throughout the slab at service load.
5. Behavior at high overloads and final mode of failure.

The distribution of moments in the slab at service load was compared with the distribution assumed in current design methods. The measured ultimate strength was compared with values for the ultimate load predicted by application of the yield-line theory and various shear strength theories.

NOTATION

The mathematical notation of this paper generally follows that of the 1956 ACI Building Code. A list of notation is given at the end of the paper following the Appendix.

EXPERIMENTAL WORK

The prototype structure, on which the test structure was based, was designed for the University tests by Di Stasio and van Buren, consulting engineers, New York City, as a typical floor of a multistory building according to the empirical method, Section 1004, of the 1956 ACI Building Code (ACI 318-56). The square layout shown in Fig. 1 was selected for the prototype structure with nine 20 ft square panels arranged three-by-three in each direction. With this arrangement every type of panel condition, with the exception of an interior panel more than one panel distant from a discontinuous edge, could be investigated.

The prototype slab was 7 in. thick and was supported at its discontinuous edges by spandrel beams. Two adjacent spandrel beams were narrow and deep, so that they had a relatively high flexural rigidity. The other two spandrel beams were wide and shallow, providing a condition of relatively low flexural rigidity. On the basis of the simple St.

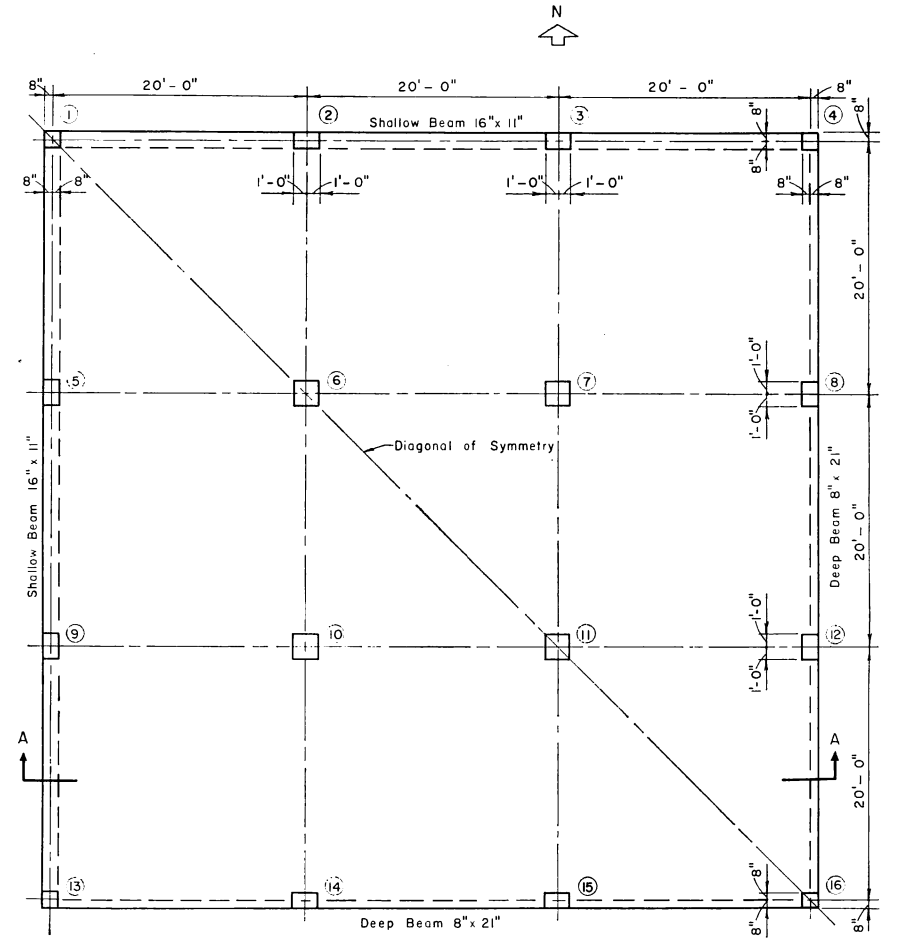

PLAN OF SLAB

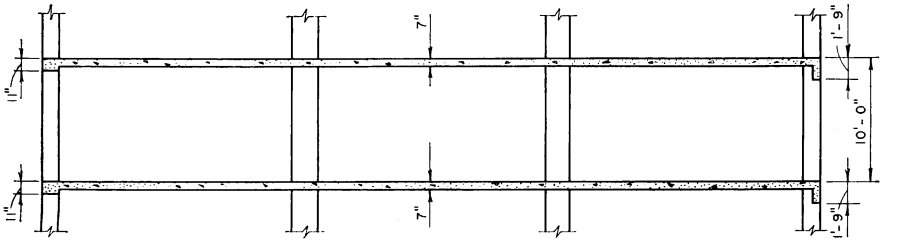

SECTION A-A

Fig. 1—Prototype structure

Venant torsional formula for rectangular sections, the torsional rigidity of the shallow beam was approximately 1½ that of the deep beam. This arrangement of edge beams produced a structure symmetrical about a diagonal running through Columns 1, 6, 11, and 16 as shown in Fig. 1.

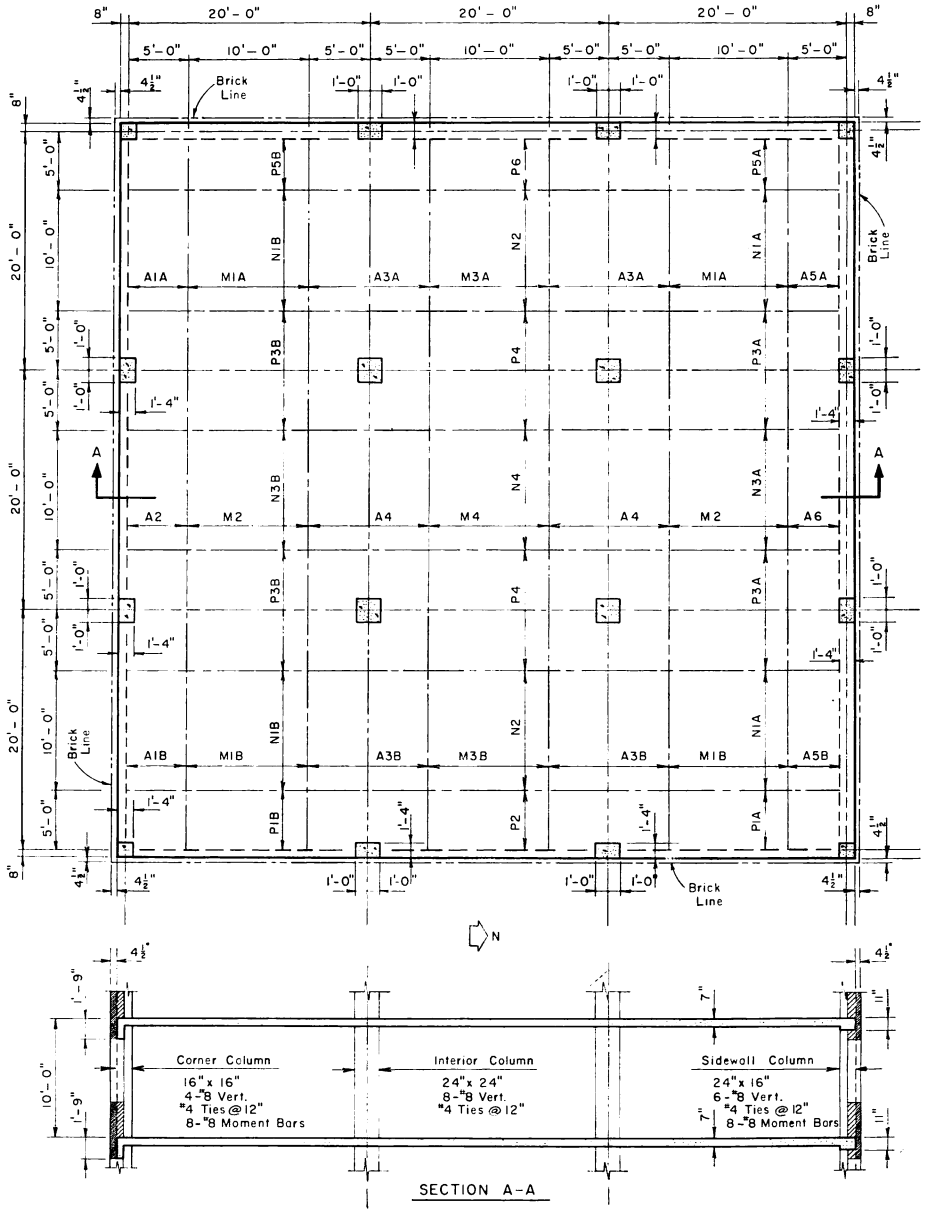

Fig. 2—Prototype steel layout

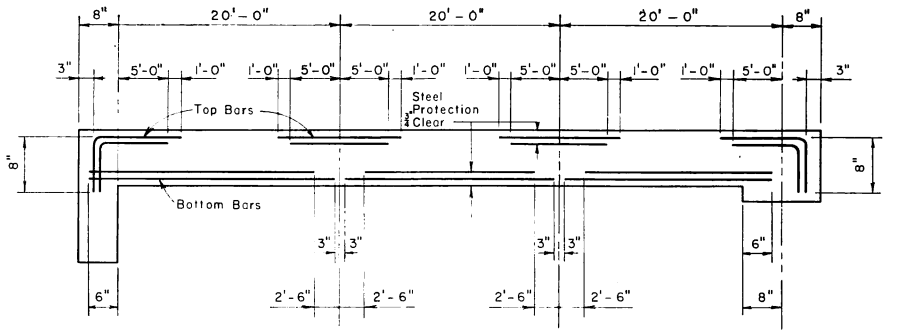

2-½"□ x 7'-0" | Top 2-½"□ x 6'-0" | Alt. @ 14"	4-½"□ x 12'-0" | Top 3-½"□ x 10'-0" | Alt. @ 8½"	4-½"□ x 12'-0" | Top 3-½"□ x 10'-0" | Alt. @ 8½"	3-½"□ x 7'-0" | Top 2-½"□ x 6'-0" | Alt. @ 12"
2-½"□ x 20'-3" | Bottom 2-½"□ x 18'-0" | Alt. @ 14"	2-½"□ x 19'-6" | Bottom 2-½"□ x 15'-0" | Alt. @ 14"	2-½"□ x 19'-7" | Bottom 2-½"□ x 17'-4" | Alt. @ 14"	
BANDS P1B, A1B	BANDS P2, A2	BANDS P1A, A1A	
3-½"□ x 7'-0" | Top 3-½"□ x 6'-0" | Alt. @ 10"	5-½"□ x 12'-0" | Top 5-½"□ x 10'-0" | Alt. @ 6"	5-½"□ x 12'-0" | Top 5-½"□ x 10'-0" | Alt. @ 6"	4-½"□ x 7'-0" | Top 4-½"□ x 6'-0" | Alt. @ 7½"
3-½"□ x 20'-3" | Bottom 3-½"□ x 18'-0" | Alt. @ 10"	3-½"□ x 19'-6" | Bottom 2-½"□ x 15'-0" | Alt. @ 12"	3-½"□ x 19'-7" | Bottom 3-½"□ x 17'-4" | Alt. @ 10"	
BANDS P5B, A5B	BANDS P6, A6	BANDS P5A, A5A	
9-½"□ x 7'-0" | Top 8-½"□ x 6'-0" | Alt. @ 7"	13-½"□ x 12'-0" | Top 13-½"□ x 10'-0" | Alt. *	13-½"□ x 12'-0" | Top 13-½"□ x 10'-0" | Alt. *	11-½"□ x 7'-0" | Top 10-½"□ x 6'-0" | Alt. @ 5¾"
8-½"□ x 20'-3" | Bottom 7-½"□ x 18'-0" | Alt. @ 8"	6-½"□ x 19'-6" | Bottom 5-½"□ x 15'-0" | Alt. @ 11"	8-½"□ x 19'-7" | Bottom 7-½"□ x 17'-4" | Alt. @ 8"	
BANDS P3B, A3B	BANDS P4, A4	BANDS P3A, A3A	

* Spacing of Top Bars Over Interior Columns. (See Drawing Below)

NOTE: All Reinforcing Bars ½" Square, ¾" Steel Clearance.

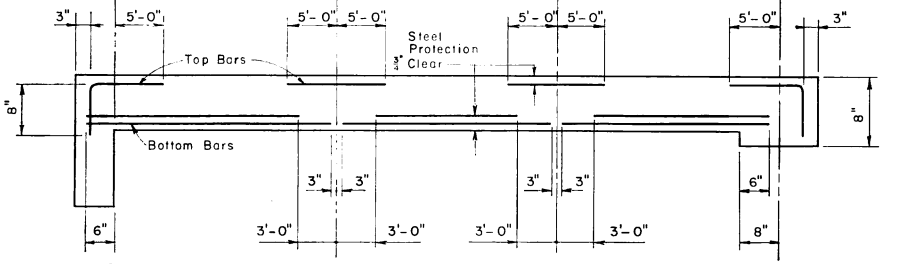

10-½"□ @ 12" Top x 6'-0"	9-½"□ @ 13½" Top x 10'-0"	9-½"□ @ 13½" Top x 10'-0"	9-½"□ @ 13½" Top x 6'-0"
5-½"□ x 20'-3" | Bottom 5-½"□ x 17'-6" | Alt. @ 12"	5-½"□ x 19'-6" | Bottom 4-½"□ x 14'-0" | Alt. @ 13½"	5-½"□ x 19'-7" | Bottom 5-½"□ x 16'-10" | Alt. @ 12"	
BANDS M1B, M3B, N1B, N3B	BANDS M2, M4, N2, N4	BANDS M1A, M3A, N1A, N3A	

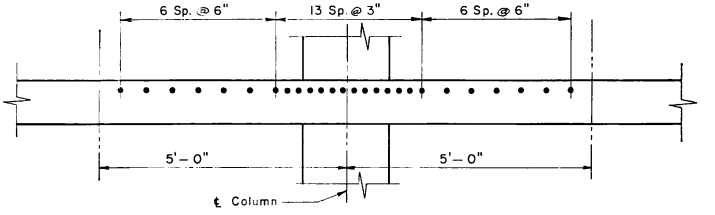

SKETCH SHOWING SPACING OF TOP BARS OVER INTERIOR COLUMNS

Fig. 3—Prototype slab bar schedule

The slab was designed for a live load of 70 lb per sq ft and a dead load of 86 lb per sq ft, making a total design service load of 156 lb per sq ft. The basic design stresses were:

Concrete compressive stress ..... f_c = 1350 psi (f_c' = 3000 psi)

Concrete shear stress ..... v = 90 psi (0.03 f_c')

Steel stress ..... f_s = 20,000 psi (intermediate grade)

Reinforcement for the prototype slab consisted of ½ in. square bars so that the reduction in scale to the one-quarter scale model tested at the University of Illinois could be made directly through the use of ⅛ in. square bars for model slab reinforcement.

Columns for the prototype structure varied in cross section from 16 x 16 in. at the corners to 24 x 24 in. at interior locations. As is typical in flat plate construction, neither column capitals nor drop panels were provided.

Spandrel beams of the prototype structure were designed for a portion of the panel load, in accordance with the provisions of Section 1904 of the 1956 ACI Building Code, as well as for a uniformly distributed load of 600 lb per lineal foot. The latter included the self weight of the beam plus the weight of an exterior curtain wall. All beams were designed by the working stress design method using the moment and shear values given by Section 701(c) of the 1956 ACI Code. Reinforcement details for the prototype slab and beams are given in Fig. 2 and 3.

Test structure

The over-all size of the prototype, 60 x 60 ft, slightly exceeds the maximum size that can be accommodated in the PCA Structural Laboratory.[2] Hence, a three-quarter scale test structure was chosen, which is large enough to permit the use of normal concretes, deformed reinforcing bars and customary construction procedures.

The prototype flat plate was designed as a typical floor of a multistory building, so that columns extended both above and below the slab. In designing the test structure, it was necessary to remove the columns above the slab. To compensate for the corresponding reduction of the ratio of column stiffness to slab stiffness, the height of the columns below the slab was halved. The column end conditions in the prototype structure were approximated in the test structure by fixing the lower ends of the reduced-height columns.

The plan and a cross section of the test structure are shown in Fig. 4. Geometric similarity between test structure and prototype was maintained by making all linear dimensions of the test structure three-quarters as large as corresponding dimensions of the prototype. Because of this form of geometric similarity, the test structure is a linear scale model of the prototype. For this type of model, a given intensity

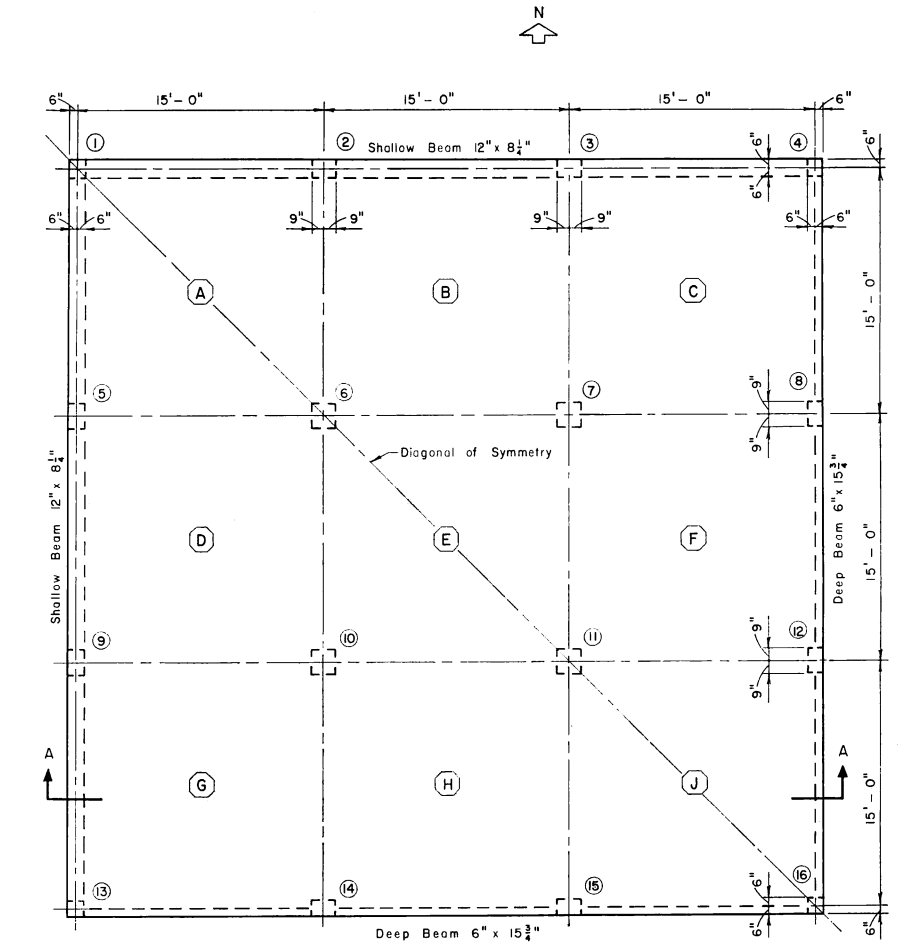

Fig. 4—Layout of test structure

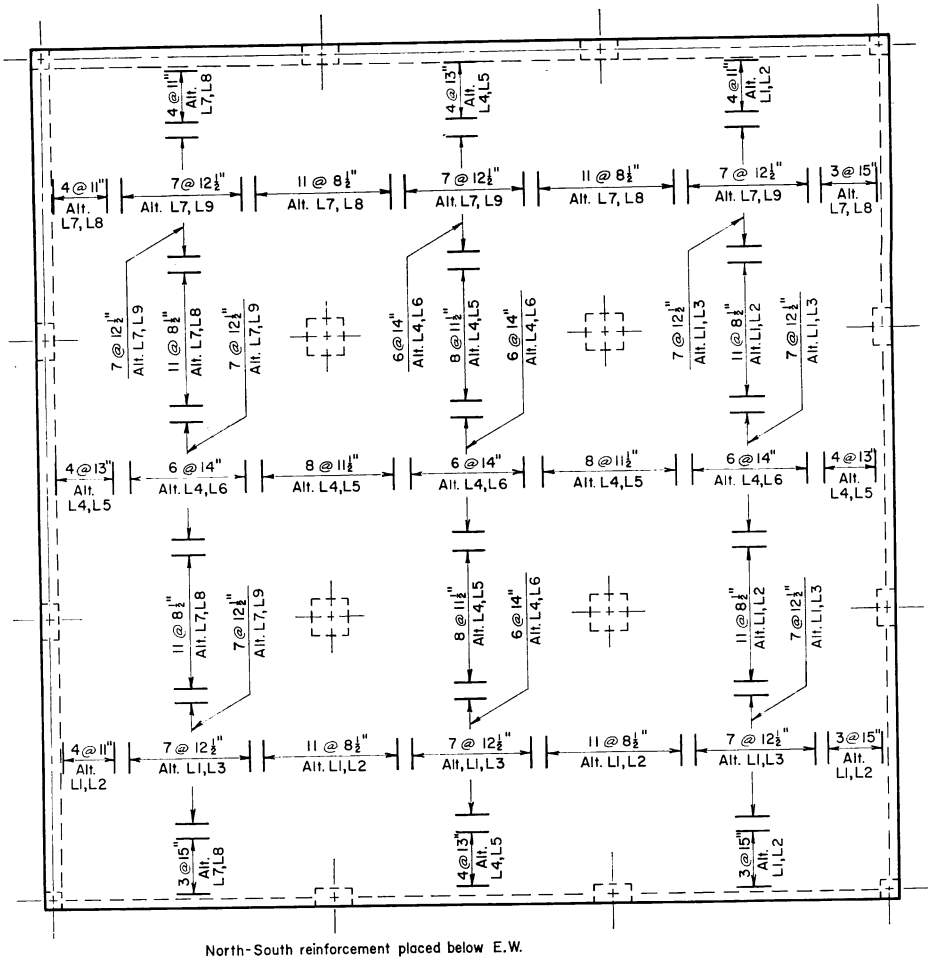

North-South reinforcement placed below E.W.

BAR DESIGNATION	
Mk	Length
L1	15' 2¼"
L2	13' 6"
L3	13' 1½"
L4	14' 7½"
L5	11' 3"
L6	10' 6"
L7	14' 8¼"
L8	13' 0"
L9	12' 7½"

Fig. 5—Test slab bottom steel

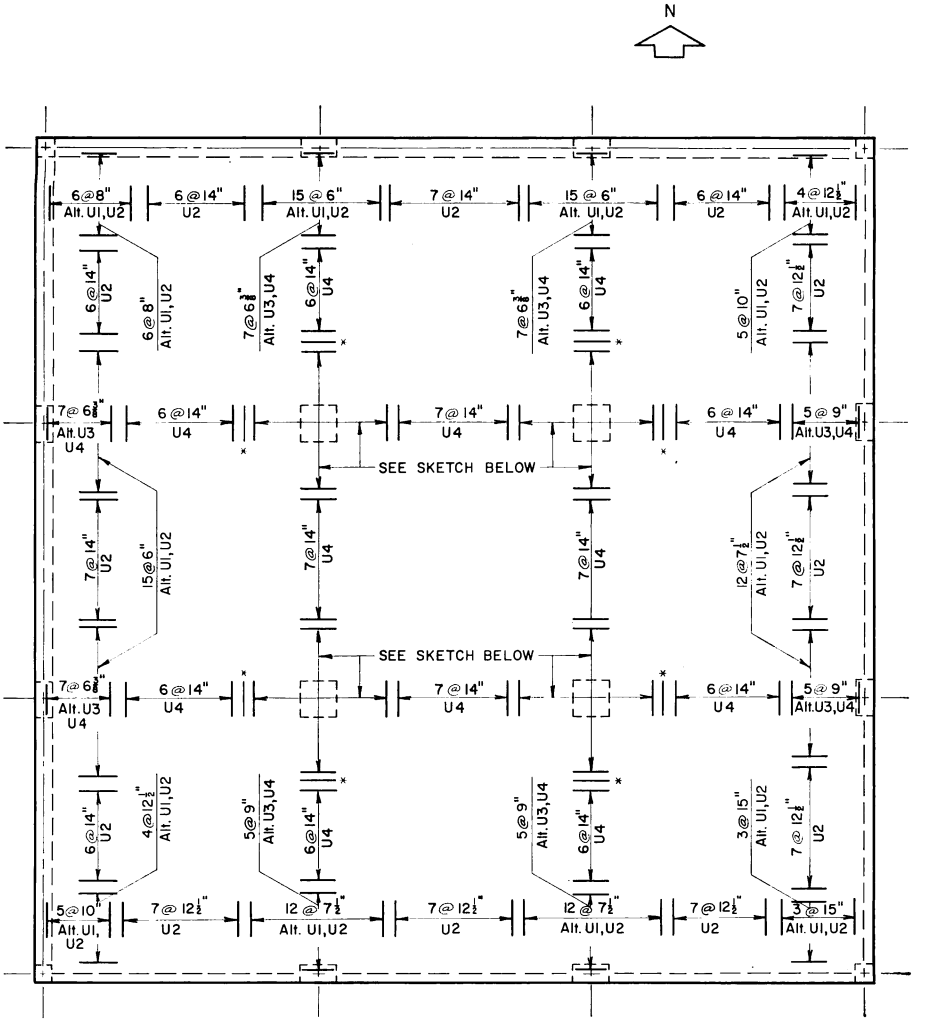

North-South reinforcement placed above E.W.

* Single bar

BAR DESIGNATION			
Mk	Bend	x	y
U1	x, y	4'-9¾"	6"
U2		4'-0¾"	6"
U3	STRAIGHT	9'-0"	
U4	STRAIGHT	7'-6"	

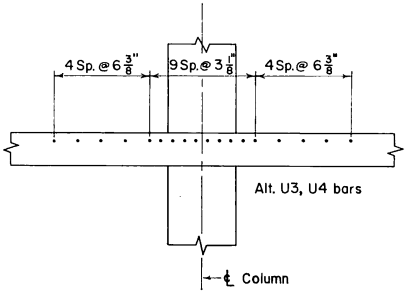

Fig. 6—Test slab top steel

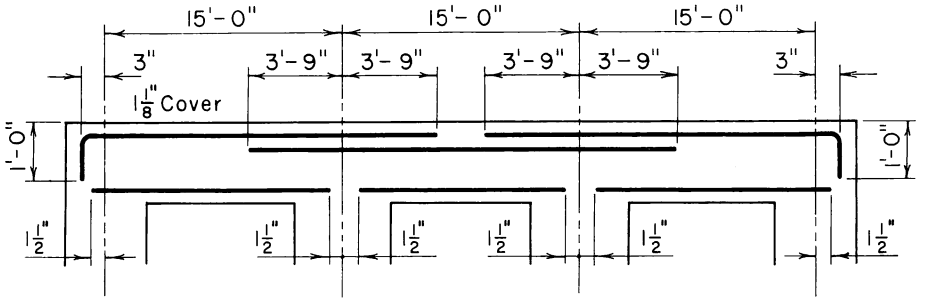

Deep Beam (6"x15 1/4")

L1	L2	L1
2 #6x20'-0" Top	1 #4x22'-6" Top	2 #6x20'-0" Top
2 #6x15'-0" Bottom	1 #5x22'-6" Top	2 #6x15'-0" Bottom
	2 #6x14'-9" Bottom	

Shallow Beam (12"x8 1/4")

L3	L4	L3
3 #6x20'-0" Top	1 #3x22'-6" Top	3 #6x20'-0" Top
4 #6x15'-0" Bottom	2 #5x22'-6" Top	4 #6x15'-0" Bottom
	3 #6x14'-9" Bottom	

STIRRUPS

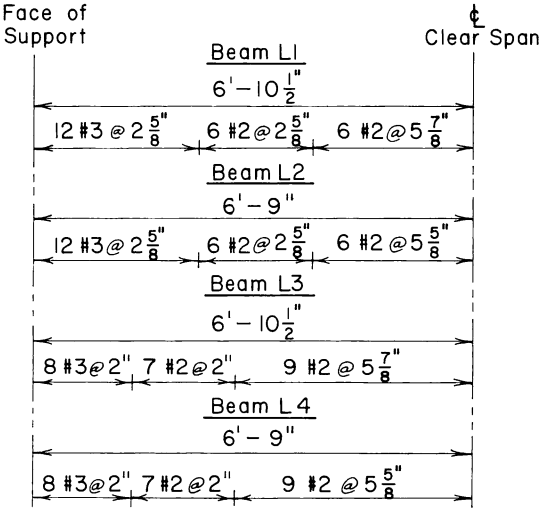

Fig. 7—Test slab spandrel beam steel

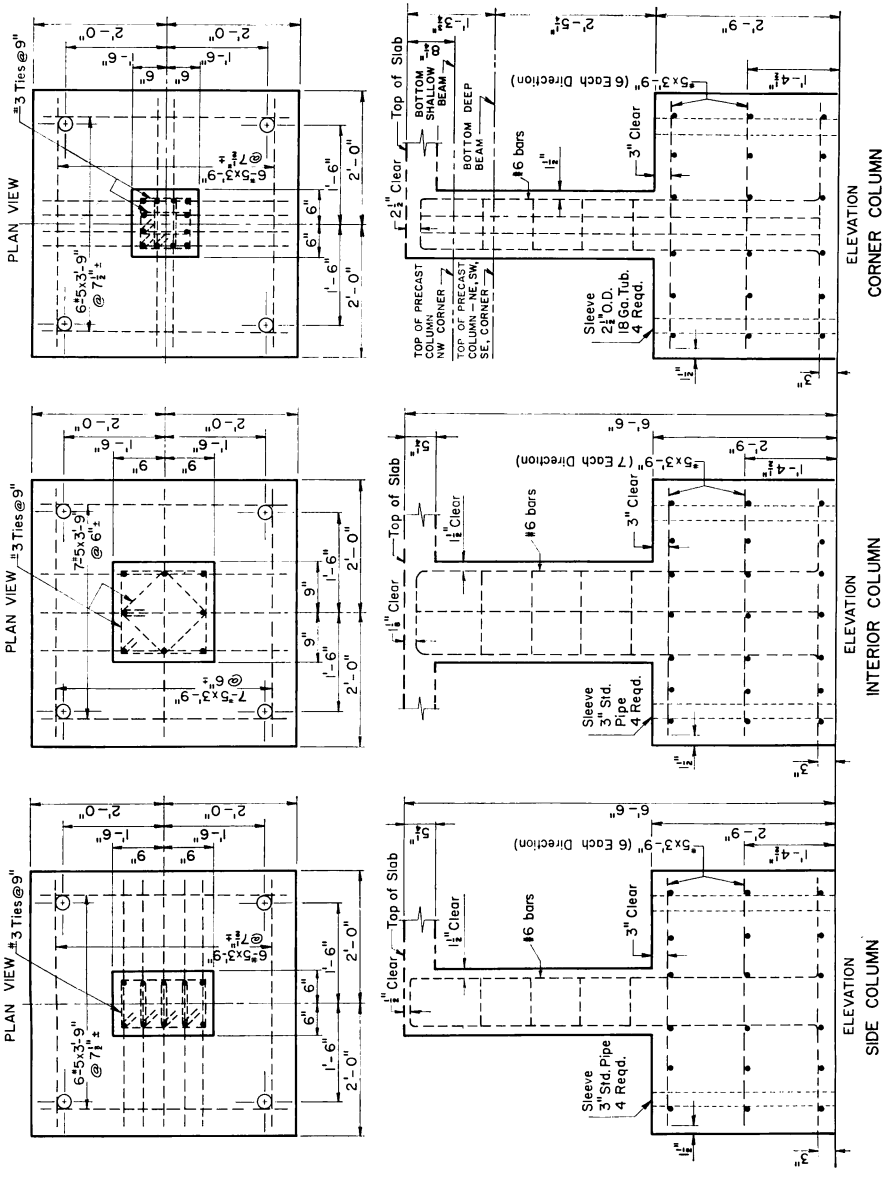

Fig. 8—Test structure column and column base steel

of uniformly distributed load per unit area will produce the same stresses in both the model and the prototype structure.

Perfect geometric similarity between test structure and prototype would require ⅜ in. square bars for the slab reinforcement. However, it was considered desirable to use a standard type of deformed reinforcement, and #4 round bars were chosen for the slab reinforcing. This necessitated a minor rearrangement of slab bar spacings in the test structure to preserve the proper scale in reinforcement percentage per unit width. Similarly, the proper scale cover of 9/16 in. was reduced to 7/16 in. to obtain effective depths to proper scale. Slab reinforcement placement details for the test structure are given in Fig. 5 and 6. The concentration of top slab bars over interior columns is also shown in Fig. 6.

Details of reinforcement for the test structure spandrel beams are given in Fig. 7. Round bars of #4, #5, and #6 sizes were required for longitudinal reinforcement of the spandrel beams. A significant weak-

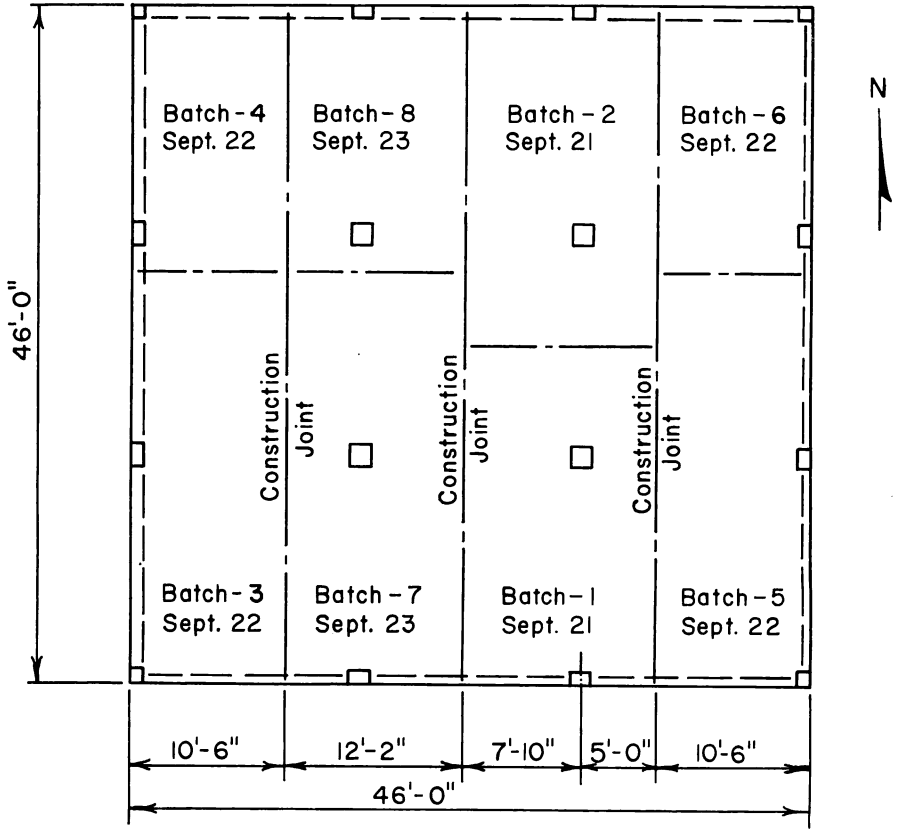

Fig. 9—Location of concrete batches in slab

ness in torsional strength of the spandrel beams had been disclosed by the tests at the University of Illinois.[4] To preclude the possibility of a premature torsional failure of the spandrel beams it was decided to increase the web reinforcement provided in these beams. This was accomplished by arbitrarily increasing the size of the vertical stirrups from #2 to #3, by halving the spacing, and by changing the shape of the stirrups from the open U-type to the completely closed type.

Columns were reinforced with #6 vertical bars and #3 ties spaced 9 in. on centers as shown in Fig. 8. To transfer moments from column

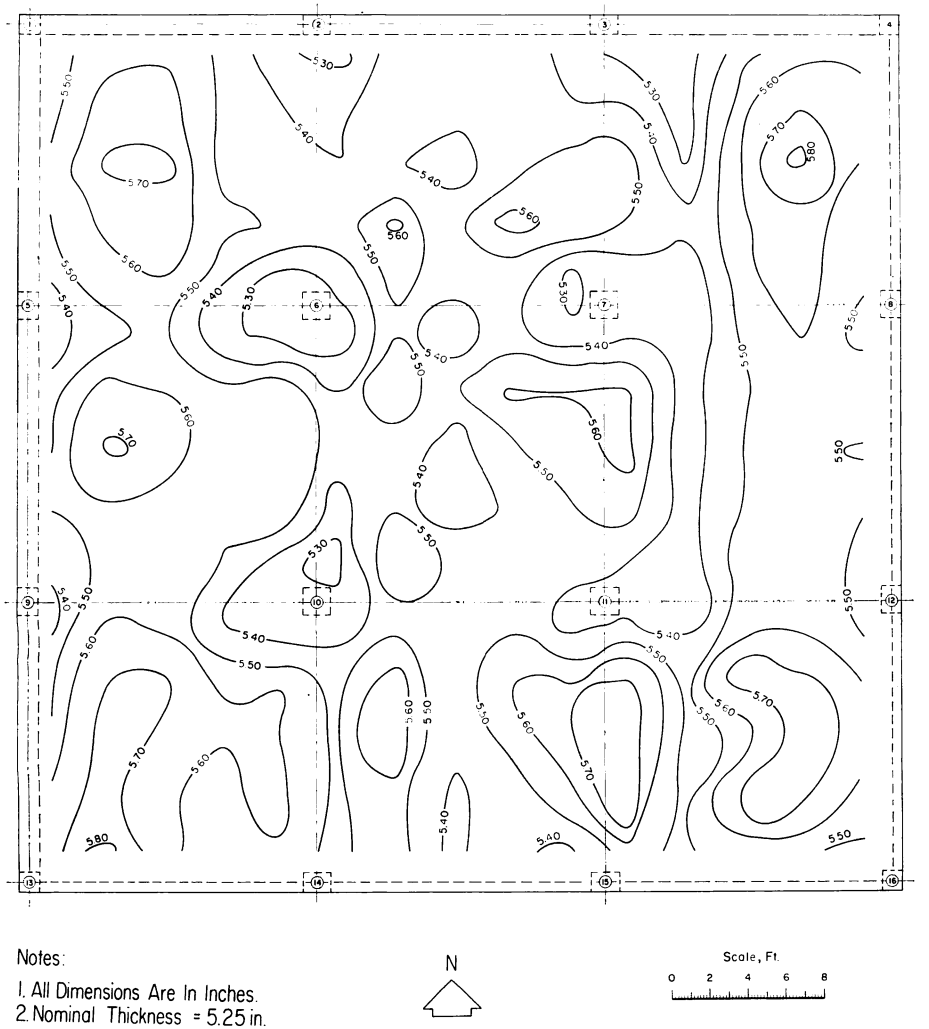

Fig. 10—Slab thickness contour

to slab, the vertical column bars were bent into an inverted U-shape to provide anchorage and continuity at the slab junction.

The fixed end condition for the lower ends of the columns was achieved by making the columns continuous with heavy concrete blocks, which were in turn fixed to the laboratory test floor by tensioned bolts. Details of this construction can be seen in Fig. 8 and 12.

TABLE 1—GRADING OF AGGREGATES

Sieve size	Cumulative percent retained	
	Sand	Gravel
1 in.	0	0
¾ in.	0	0
½ in.	0	63
⅜ in.	0	87
No. 4	0	99
No. 8	11	100
No. 16	32	100
No. 30	53	100
No. 50	81	100
No. 100	96	100

Fineness modulus of sand = 2.73
Unit weight of dry rodded gravel = 103.6 lb per cu ft

TABLE 2—MIX PROPERTIES

Property	Amount
Yield	1 cu yd
Sand	1640 lb (surface dry)
Gravel	1600 lb (surface dry)
Type I cement	423 lb (4½ sacks)
Water	317 lb (38 gal.)
W/C	8.44 gal. per sack
Slump	3 to 4 in.

Concrete

Cement used was Type I portland cement which was purchased and stored in one lot of sufficient quantity to supply the needs of the whole project.

Natural sand and gravel aggregate obtained from local sources and having a maximum gravel size of ⅝ in. was used in all concrete for the project. The grading of the aggregates, the fineness modulus of the sand, and the unit weight of the bulk gravel are given in Table 1.

The mix proportions, as given in Table 2, were selected to yield a concrete which, in strength and workability, closely resembled concretes used for the same purpose in current construction practice.

Reinforcement

Because of cold working during the ordinary rolling process, the smaller sizes of reinforcing bars generally have higher yield points than the specified yield point for the grade of steel involved. Since #4 bars were used for the slab reinforcement and since it was necessary to obtain reinforcement having a yield point close to 40,000 psi to permit correlation of results with those of the one-quarter scale model test, the slab reinforcement was specially rolled from one heat of steel. This specially-rolled reinforcement had deformations conforming to ASTM Standard A 305. A typical stress-strain curve for these #4 bars is shown in Fig. 17.

Longitudinal reinforcement for spandrel beams and columns consisted of commercially available #6 intermediate grade steel bars having a yield point of 45,000 psi.

Construction

The columns and their bases were fabricated in position on the test floor and tied down as shown in Fig. 12. When all 16 columns had been cast and fixed to the floor, formwork for the slab was erected. This formwork consisted of 4 x 8 ft plywood panels, ¾ in. thick, supported on 2 x 4-in. stringers which in turn were supported by telescoping steel trussed beams. Particular care was exercised in maintaining close tolerances to design dimensions and in keeping horizontal surfaces of beam and slab formwork level.

Ready-mixed concrete in 4 cu yd batches was supplied according to specifications drawn up by the project staff. To produce a uniform slab thickness, time consuming extra finishing operations were required. It was decided, therefore, to cast the slab in four strips, as shown in Fig. 9 which also shows the sequence of casting, and the location of the various batches of concrete in the test structure.

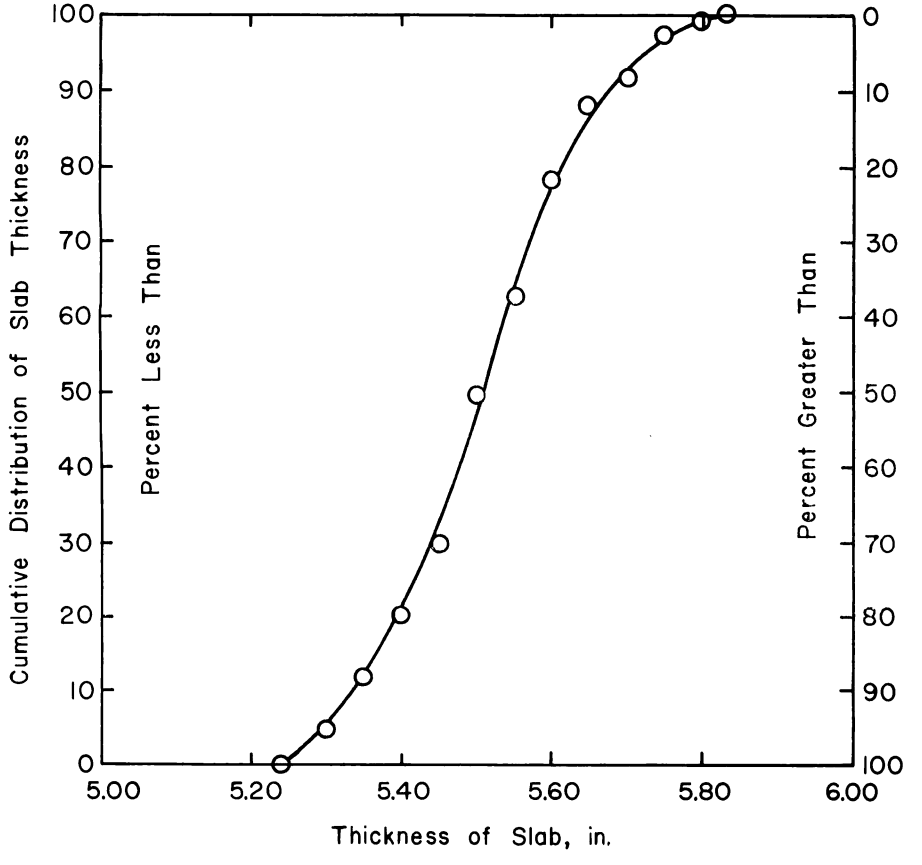

Fig. 11—Cumulative frequency distribution of slab thickness

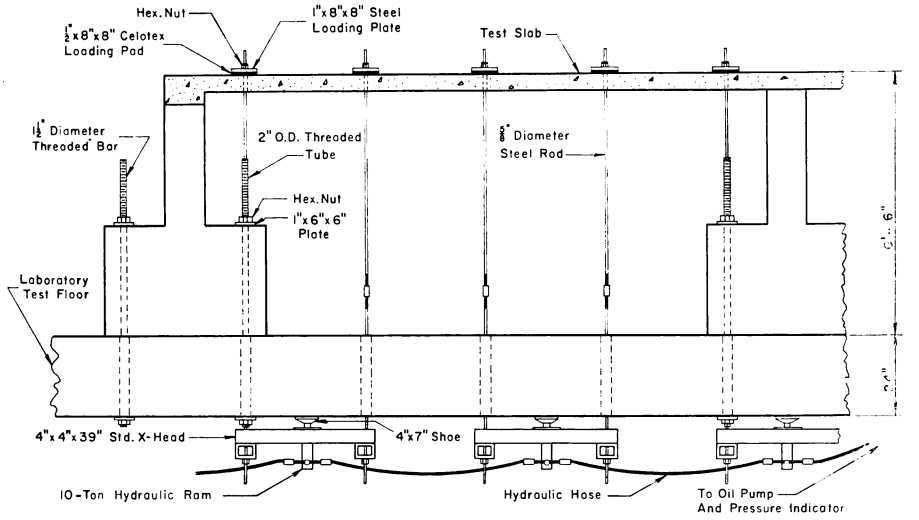

Fig. 12—Elevation of loading system

The concrete in columns and beams was vibrated internally and the slab concrete was compacted with a vibrating screed supported on the construction joint formwork. Finish screeding was accomplished with several passes of a 14 ft long aluminum box-section screed. Several hours after casting was completed, the surface of the slab was worked with a power-driven steel float finishing machine.

Polyethylene plastic cover sheets were applied to all exposed surfaces of the structure and all control specimens approximately 4 hr after casting was completed. These cover sheets effectively prevented drying and permitted the concrete to cure in the moist condition. Seven days after casting, the plastic sheets were removed and the forms were partially dismantled. All vertical shores, however, were kept in place until at least 2 weeks after casting.

Thin-walled steel conduit was installed in the slab formwork prior to casting to provide holes in the finished slab through which loading rods could pass. After the slab was cured, thickness measurements were taken near each of the 225 hole locations, using a dial gage device which could pass through the slab holes, and the thickness contour chart given in Fig. 10 was constructed. The slab thickness was found to vary from 5.25 to 5.80 in. The cumulative frequency distribution of the slab thickness in Fig. 11 shows that the mean value of slab thickness was approximately 5.50 in.

Because the top reinforcement was accurately located and securely held in position by bar supports tied to the formwork, the excess slab thickness probably had little influence on the slab negative moment strength or stiffness. On the other hand, the positive moment strength

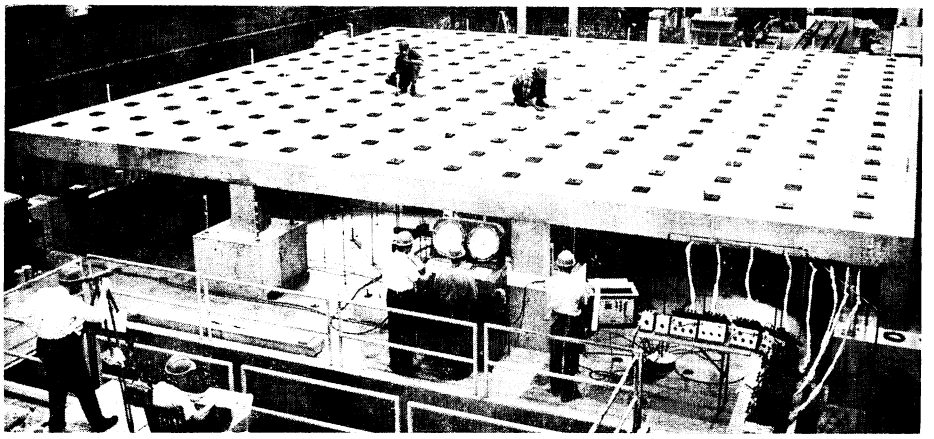

Fig. 13—Flat plate structure under load

and stiffness was increased significantly in certain areas by excess slab thickness and this was taken into account in the appropriate computations of theoretical slab flexural strength.

After all formwork had been removed, the slab was inspected for shrinkage cracks. Several very small local shrinkage cracks in the vicinity of the construction joints and one major shrinkage crack shown by the dashed line through Column 7 in Fig. 26 were found.

Test methods and apparatus

Loading—The uniformly-distributed load condition was simulated by the application of 25 concentrated loads to each panel. The concentrated loads were applied to the structure through 8 x 8 in. steel plates resting on ½ in. thick celotex pads. A tie rod extended through each steel loading plate, the test slab and the laboratory floor, to systems of cross beams and hydraulic rams as shown in Fig. 12. The hydraulic connections were so arranged that any panel or combination of panels could be loaded as desired. The twin dial console for controlling and measuring hydraulic ram pressure is shown in the center foreground of Fig. 13.

A load cell[2] was installed between one ram and the undersurface of the laboratory floor in each panel to provide a continuous check on the ram calibration factors and the hydraulic load measuring system. The load cells instantaneously indicated any system faults that might cause loss of load, such as oil leakage or malfunction of rams. A discussion of the accuracy and additional details of the loading system is given elsewhere.[2]

Strain—To measure the distribution of slab strains which in turn could be converted to stresses and moments, 240 electric resistance strain gages were attached to the slab reinforcing bars, waterproofed,[2] and embedded in the concrete. The strain gage locations, shown in Fig. 14

and 15, were so chosen that the distribution of moments across column lines and panel center-lines could be measured to provide a basis for comparison with design moments computed according to the 1956 ACI Building Code.

The symmetry of the test structure about a diagonal running through its northwest and southeast corners was used to reduce the total number of gages required. The northeast half of the structure was fully instrumented and a few extra gages were applied at various locations in the

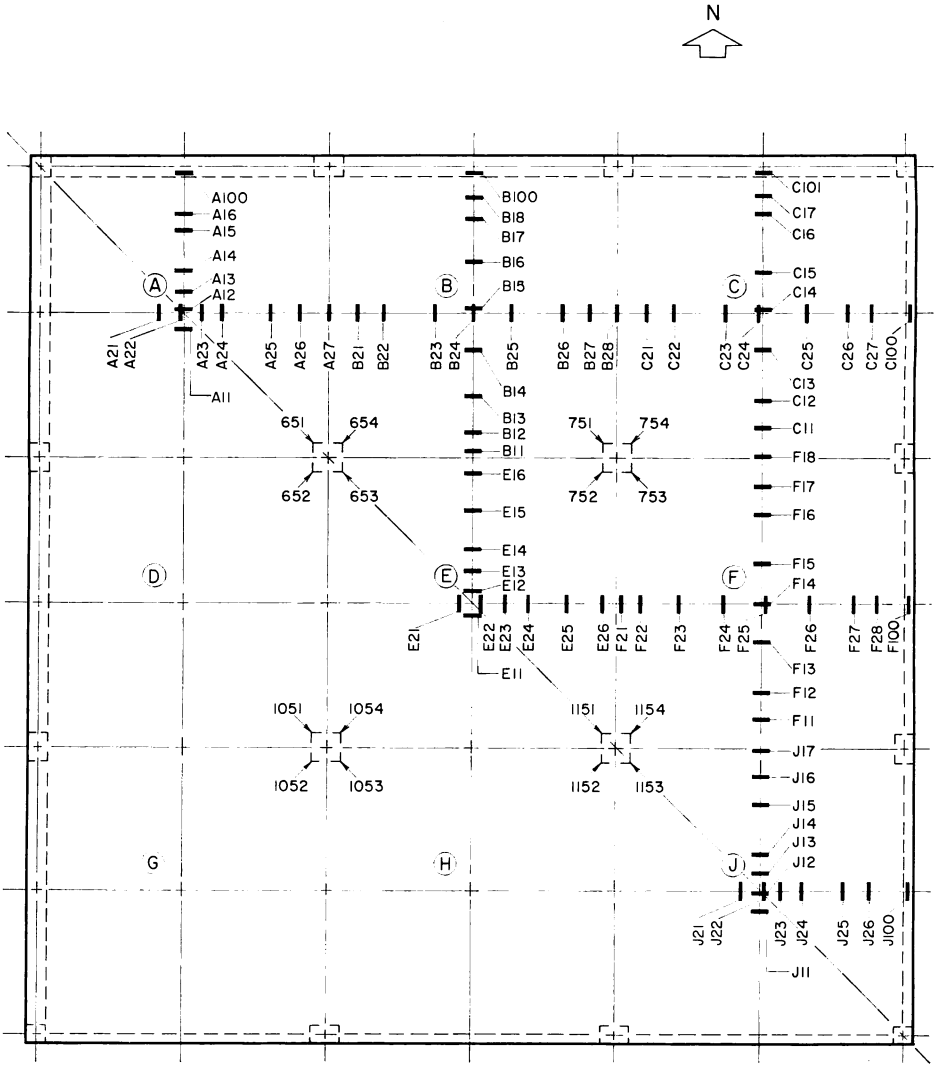

Fig. 14—Location and designation of strain gages on bottom reinforcement

symmetrical southwest half as check gages. The edge beams were provided with strain gages on the bottom steel at midspan and on the top steel at the column faces. All gages used throughout the project were SR-4 strain gages having a 1 in. nominal gage length.

Apparatus for recording strains consisted of a bank of eight 30-channel switching and zero-balancing units and a self-balancing resistance bridge indicator, mechanically linked to a digitizer which provided digital information for a print-out unit. Each strain gage or load cell was connected to a set of terminals on one of the 30-channel switching units which in turn was connected to the strain indicator. The process of switching, balancing, and recording strains was semiautomatic in that switching was done manually, whereas balancing and recording were accomplished automatically by the strain indicator and print-out units. The time required to record all the strain gage data for any one load increment was approximately 15 min. The strain gage switch bank and recording instruments are shown in operation in the right-hand foreground of Fig. 13. Further details of the construction, circuitry, and accuracy of the strain recording system are given elsewhere.[3]

Deflection—The vertical deflections of the slab were measured at 33 locations using a precision surveyor's level, reading against graduated rods fixed to the surface of the slab. This level has an internal optical micrometer with graduations corresponding to 0.001 in. and a range of ½ in. through which the line of sight may be moved vertically. The leveling rods were made of machine-engraved vinylite scales, with ½-in. graduations which were mounted on aluminum stands cemented to the slab surface.

The leveling rods were located at the midpoint of each panel, at the midspan of each spandrel beam, and half-way between columns on each set of column center lines. The graduated-scale face of each leveling rod was so oriented that readings for all 33 level rod locations could be taken at a single instrument station. The instrument station which was used throughout the test is shown in the left foreground of Fig. 13, and the level rods projecting from the slab surface may also be seen in this view.

For the purpose of obtaining information on the probable location of yield lines, it was deemed necessary to obtain a complete deflection contour map of the surface of the test structure when subjected to a high overload. To reduce the time needed to obtain the required data for contour mapping, photogrammetric techniques were used. A specially calibrated aerial photography camera was mounted between the trolley girders of the laboratory overhead crane, and a series of overlapping photographs of the slab surface were taken as crane and camera were made to traverse the test structure. To obtain the relative vertical displacements between the unloaded and loaded states of the test struc-

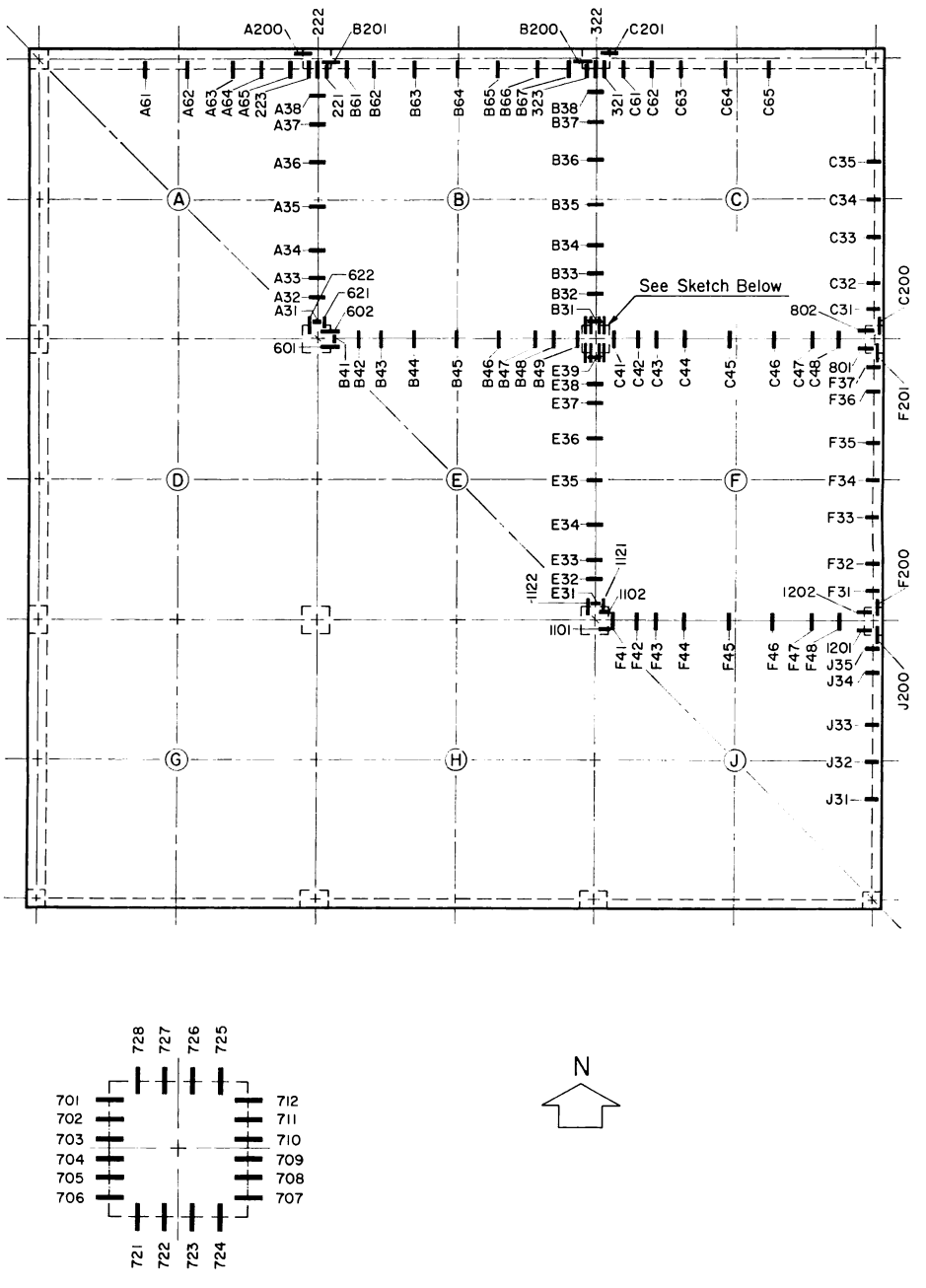

Fig. 15—Location and designation of strain gages on top reinforcement

ture, photographs were taken at zero load and at twice the design live load. The time required to take a complete set of photographs of the test structure was approximately 50 min.

Spot elevations of points on the slab surface defined by a 1 ft square grid were obtained from the photographs using a high-precision stereo plotting instrument. Elevations were obtained on one-half of the symmetrical slab for the two states of superimposed load. These were used to determine relative deflections which in turn were used to plot the deflection contour map shown in Fig. 23.

Testing procedure

The objective of the program of tests numbered 1 through 13 in Table 3 was to assess the performance of the test structure under various load patterns and under load intensities up to the service load level. Tests 14 through 16 were designed to yield information on the performance of the test structure at overloads. Test 17 was the final test to failure with all panels loaded to the same intensity.

The dead weight of the slab of the test structure was 65.7 lb per sq ft and the dead weight of the loading system suspended from the slab was 7.3 lb per sq ft making a total dead weight load of 73.0 lb per sq ft which was in place for the duration of the test program. The additional load superimposed on the test structure by the hydraulic rams is termed the *applied load* and the sum of the 73.0 lb per sq ft dead load and the applied load is termed the *total load*. The dead load of the prototype slab

TABLE 3—TEST PROGRAM

Test No.	Date	Panels* loaded	Maximum total load,† lb per sq ft
1	October 28	All	Design load = 156
2	October 28	All	Design load = 156
3	October 31	All	Design load = 156
4	November 3	BCEFG	Design load = 156
5	November 3	BCEFG	Design load = 156
6	November 4	BCEF	Design load = 156
7	November 4	BCEF	Design load = 156
8	November 7	ABDE	Design load = 156
9	November 8	ABDE	Design load = 156
10	November 8	BDFH	Design load = 156
11	November 9	BDFH	Design load = 156
12	November 9	ACEGJ	Design load = 156
13	November 10	ACEGJ	Design load = 156
14	November 10	All	DL + 1.5 LL = 191
15	November 10	All	DL + 1.5 LL = 191
16	November 11	All	DL + 2.0 LL = 226
17	November 11	All	Test to failure = 369

*See Fig. 4 for location of panels.
†Values of uniform load include weight of the slab and the loading system.

TABLE 4—PROGRAM OF LOADING IN SERVICE LOAD TESTS

Order of application	Type of loading applied	Intensity of load, lb per sq ft
1	Self weight of slab and loading equipment	73
2	Full dead load (prototype)	86
3	Dead load + ½ live load	121
4	Dead load + live load	156
5	Dead load + ½ live load	121
6	Full dead load (prototype)	86
7	Self weight of slab and loading equipment	73

was 86 lb per sq ft and its design live load was 70 lb per sq ft making a total slab service load of 156 lb per sq ft.

The program of loading for each of the service load tests, numbered 1 through 13, is given in Table 4. The first increment of applied load was 13 lb per sq ft while subsequent increments were 35 lb per sq ft (i.e., ½ live load).

The program of loading for Tests 14, 15, and 16 was similar to the above except that extra 35 lb per sq ft increments of load were applied to reach the respective maximum loads given in Table 3.

Test 17, the final test to destruction, was programmed initially in a manner similar to the service load tests; however, after a load of 226 lb per sq ft was reached the applied load increments were reduced to approximately 23 lb per sq ft and loading proceeded until failure occurred.

A full set of strain and deflection readings was taken at each load increment in each test. Also slab and beam crack surveys were made at high load stages for each test.

After the service load tests (Tests 1 through 13) had been completed, all top surface slab cracks were heavily outlined with black paint and a series of photographs covering the whole slab surface was taken. Fig. 24, which shows the whole top surface crack pattern at design load, was prepared from a mosaic of the slab photographs. Fig. 25 and 26, which show, respectively, top and bottom surface crack patterns at failure, were prepared in a similar way by outlining those cracks which appeared during the course of Test 17.

To obtain the relative vertical displacements between the unloaded and loaded test structure for the photogrammetric study, it was necessary to obtain a set of photographs at zero applied load. To minimize the effects of dead load creep deflections, 24 days were allowed to elapse between the time that formwork was completely stripped from the test structure and the zero applied load photographs were taken. The second set of photographs for the photogrammetric study were taken during Test 17 at a total load level of 226 lb per sq ft (dead load plus twice live load).

TEST RESULTS

Mechanical properties of materials

Concrete—Table 5 gives the compressive strength of 6 x 12-in. cylinders at 7, 28, and 50 days after casting of the concrete used in the various portions of the slab. Values of modulus of rupture and modulus of elasticity are also reported.

Fig. 16 is a typical stress-strain curve for the concrete used in the slab of the test structure. The stress-strain curves were obtained from tests of 6 x 12-in. cylinders and the strains were measured using an 8 in. gage length mechanical compressometer. As shown in Fig. 16, the modulus of elasticity was obtained as the secant modulus at 0.45 f_c' using the second loading cycle.

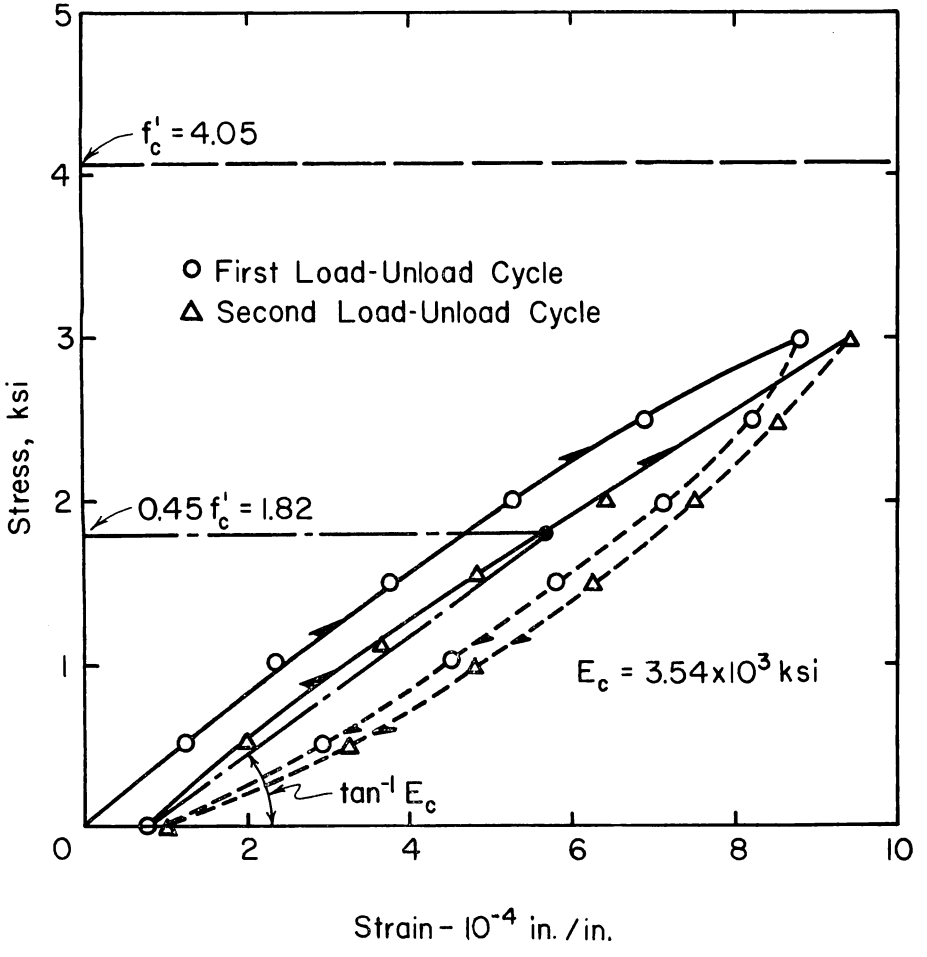

Fig. 16—Typical stress-strain curve for slab concrete

TABLE 5—PROPERTIES OF CONCRETE

Batch No.	Compressive strength						Modulus of elasticity		Modulus of rupture	
	7 days		28 days		50 days		28 days		28 days	
	No. of tests	f_c' psi	No. of tests	f_c' psi	No. of tests	f_c' psi	No. of tests	E_c* 10^6 psi	No. of tests	f_r psi
1	3	2650	3	4390	3	5045	2	3.66	3	491
2	3	2570	3	4110	3	4967	2	3.68	3	499
3	3	2470	3	3990	3	4388	2	3.54	3	554
4	3	2520	3	3532	3	4292	2	3.35	3	454
5	3	3000	3	4452	3	4985	2	3.91	3	571
6	3	2780	3	4147	3	4758	2	3.78	3	592
7	3	2400	3	4030	3	4540	2	3.88	3	495
8	3	2630	3	4190	3	4757	2	3.55	3	489
Averages		2630		4105		4715		3.67		518

*E_c is the secant modulus at 0.45 f_c'

Steel—Average mechanical properties of the steel used for slab reinforcement are given in Fig. 17. Results from tension tests on a number of samples of slab reinforcement were uniform and maximum deviation of the properties measured was generally less than 3 percent of the average.

Tension tests were also performed on the #6 bars used for spandrel beam and column reinforcement and these bars exhibited mechanical properties very similar to those of the slab reinforcement.

Outline of tests

Tests 1 through 13 in Table 3 were designed to assess the performance of the test structure under various load patterns and under a maximum intensity of load equal to the service load. Tests 1, 2, and 3 were performed with all panels loaded. Tests 2 and 3 were, of course, simple repeats of Test 1. These repetitions were performed to contrast the behavior of the slab both before and after initial cracking had occurred.

A load pattern was selected for Tests 4 and 5 to produce the maximum negative moment in each direction over Column 7. Tests 6 and 7 were similar to Tests 4 and 5 except that Panel G, which was farthest removed from Column 7, was not loaded. These latter two tests were performed to ascertain whether the simpler four-panel loading pattern yielded negative moments which were comparable to those obtained in Tests 4 and 5.

Because comparable results were obtained in Tests 4 and 5 and 6 and 7, the simpler four-panel loading pattern was adopted for Tests 8 and 9 which were designed to yield maximum negative moments over Column 6.

Since it was found in the model test conducted at the University of Illinois[4] that maximum negative moments obtained with three-panel

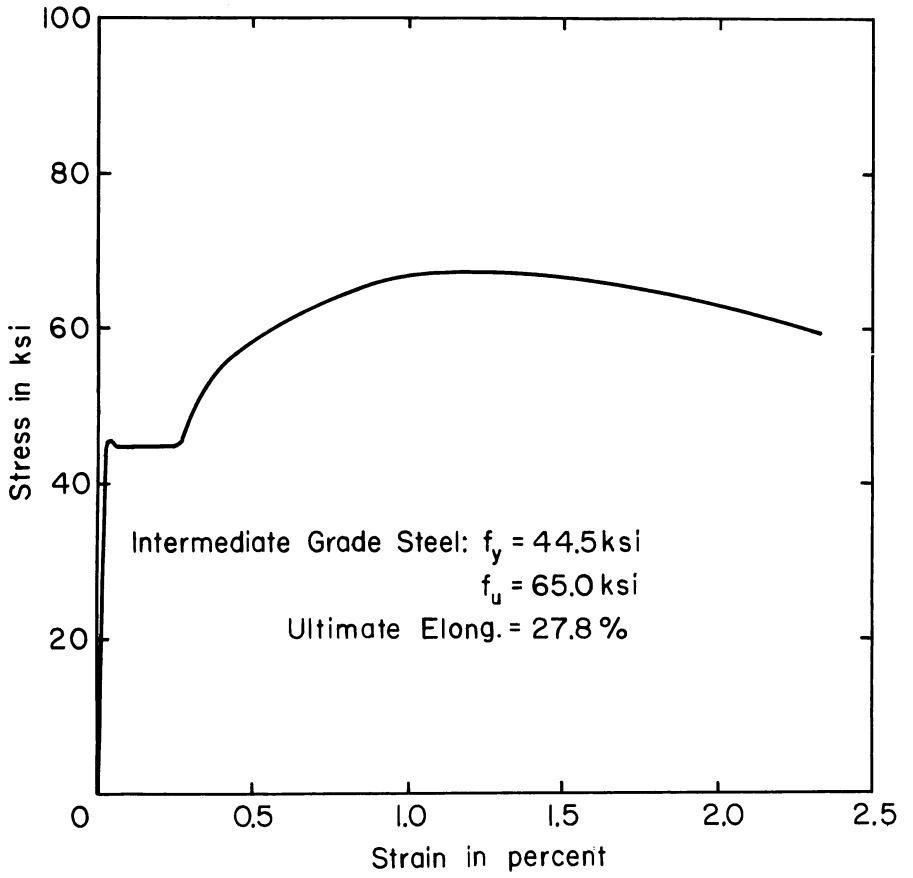

Fig. 17—Typical stress-strain curve for slab reinforcement

strip loadings did not differ significantly from those obtained with all panels loaded, strip loadings were not used in this investigation.

Tests 10 through 13 were "checkerboard" load patterns. The remaining Tests 14 through 17 were with all panels equally loaded to the respective maximum loads given in Table 3.

Deflections

Load-deflection curves for each of four different levels of maximum load are given in Fig. 18 through 21. The deflections plotted are those of the center point of each panel. On first loading, the load-deflection curves shown in both Fig. 18 and 19 exhibit markedly inelastic behavior. However, subsequent unloading and reloading produces almost linear load-deflection curves. The residual deflection on unloading is probably due to an increase in the dead load deflection caused by a reduction in

stiffness of the slab due to cracking, together with a "permanent set" in the slab due to inelastic deformation of the concrete.

Maximum deflection at the 156 lb per sq ft service load level, on initial loading in Test 1, was 0.122 in., and this occurred in Panel B. The maximum deflection on reloading occurred in Panel A, as shown in Fig. 18. Two edges of Panel A were "discontinuous" and supported on shallow spandrel beams offering relatively low flexural rigidity. The deflections of Panel J would be expected to be smaller than those of Panel A because of the higher flexural stiffness of the deep spandrel beams bounding Panel J.

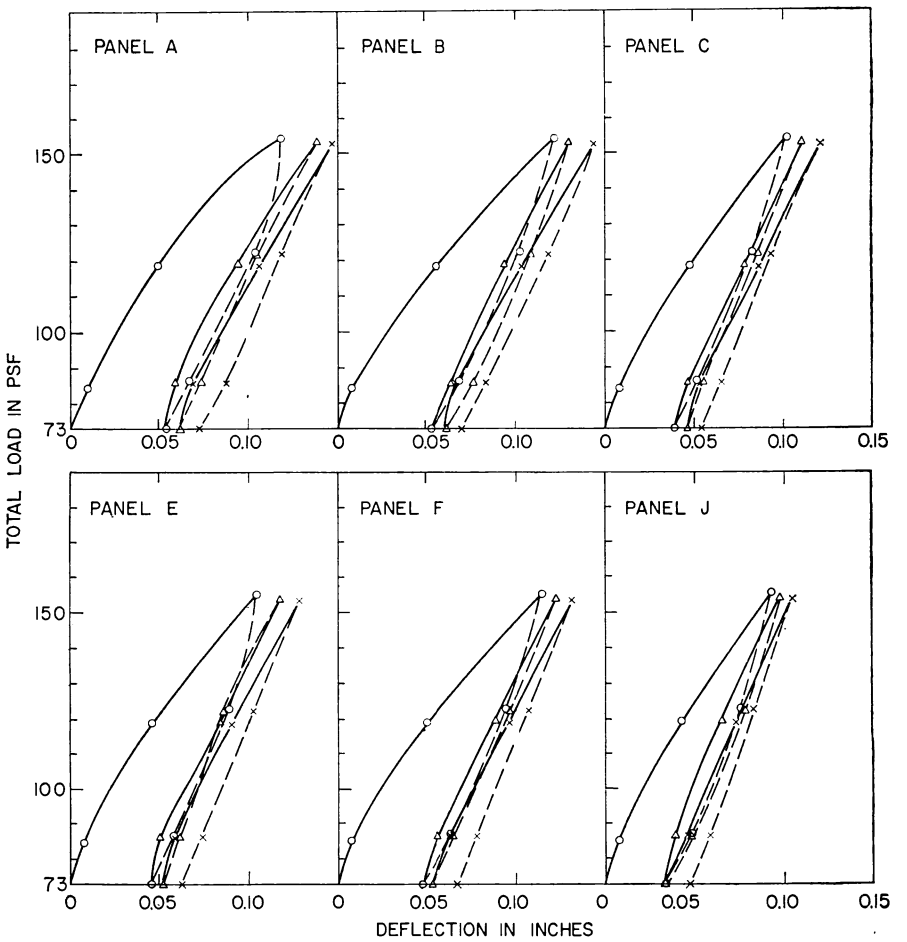

Fig. 18—Deflection of panel center points in Tests 1, 2, and 3 (tests to service load)

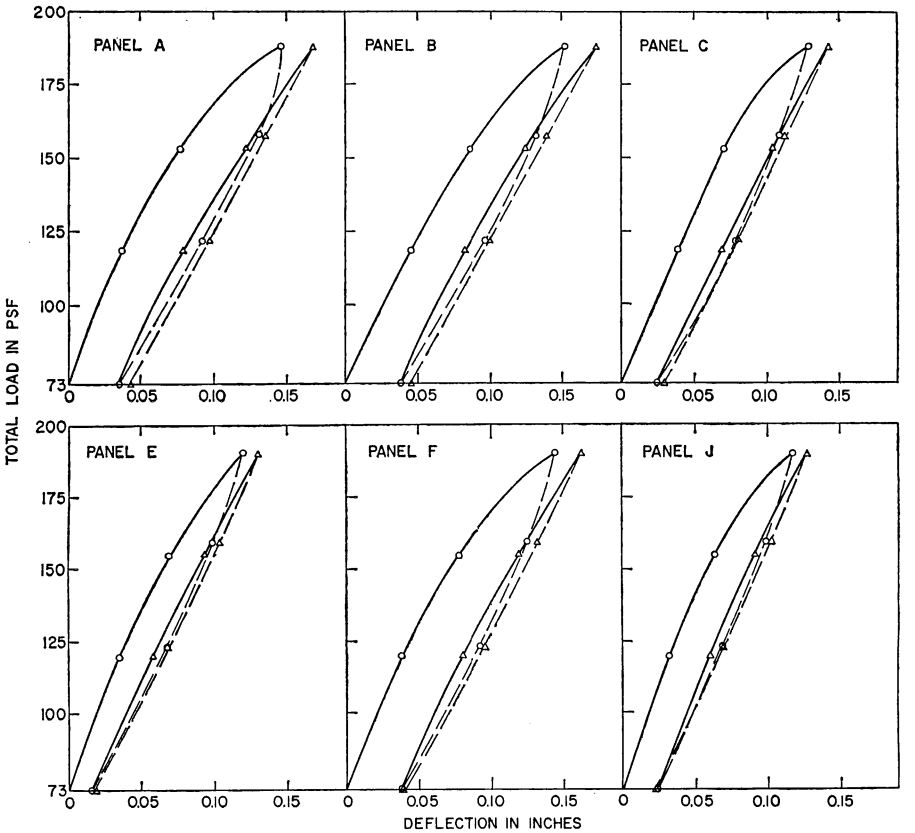

Fig. 19—Deflection of panel center points in Tests 14 and 15 (tests to dead load + 1.5 live load)

The maximum deflection observed during Test 14, on initial loading to 191 lb per sq ft, was 0.151 in. and this occurred in Panel B. The maximum deflections on reloading in Test 15 were practically identical for both Panels A and B, as shown in Fig. 19. The close agreement between the deflections in Panels A and B is probably due to a loss of Panel B edge restraints due to heavy, negative-moment cracking in the slab over the columns as loading progressed. Slab cracking at elevated loads tended to make edge rotations of Panel B comparable to those of Panel A, even though two adjacent edges of Panel A were "discontinuous" and supported on shallow spandrel beams while such a condition existed at only one of the edges of Panel B.

The 226 lb per sq ft maximum total load in Test 16 was equal to the full prototype dead load plus twice the design live load. This is the

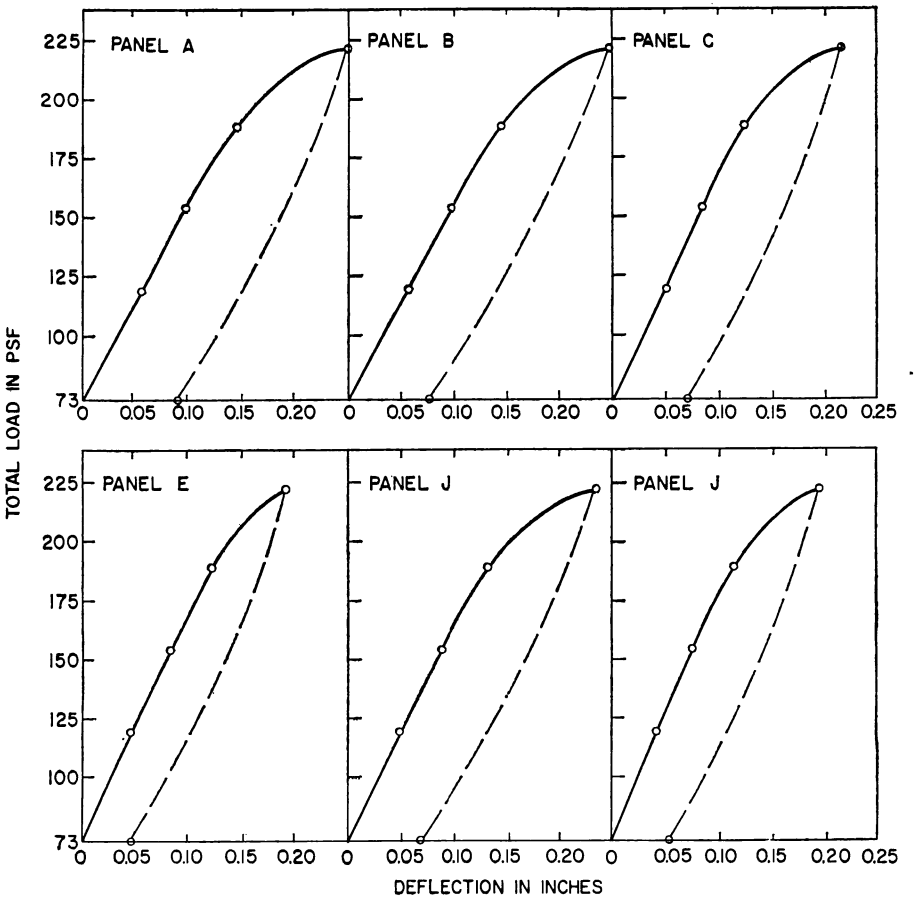

Fig. 20—Deflection of panel center points in Test 16 (test to dead load + 2.0 live load)

maximum load specified in Section 202(c) of the 1956 ACI Building Code for load tests of existing structures. The load-deflection curves for centers of panels for Test 16 are given in Fig. 20. Again, as was the case in Tests 14 and 15, the load-deflection curves for Panels A and B are almost identical. The maximum deflection observed in Panel A was 0.250 in. and in Panel B 0.247 in. The greatest deflection was less than half the acceptance value of $L^2/12{,}000t$ specified in Section 203(b) of the 1956 ACI Building Code. Even though the test load was not allowed to remain in place for a full 24 hr, as specified in Section 203 of the Code, the relatively low value of maximum deflection attained indicates satisfactory load-deflection performance of the test structure.

Fig. 21 gives the load-deflection curves for centers of panels in Test 17, which was the final test to destruction. As cracking progressed under

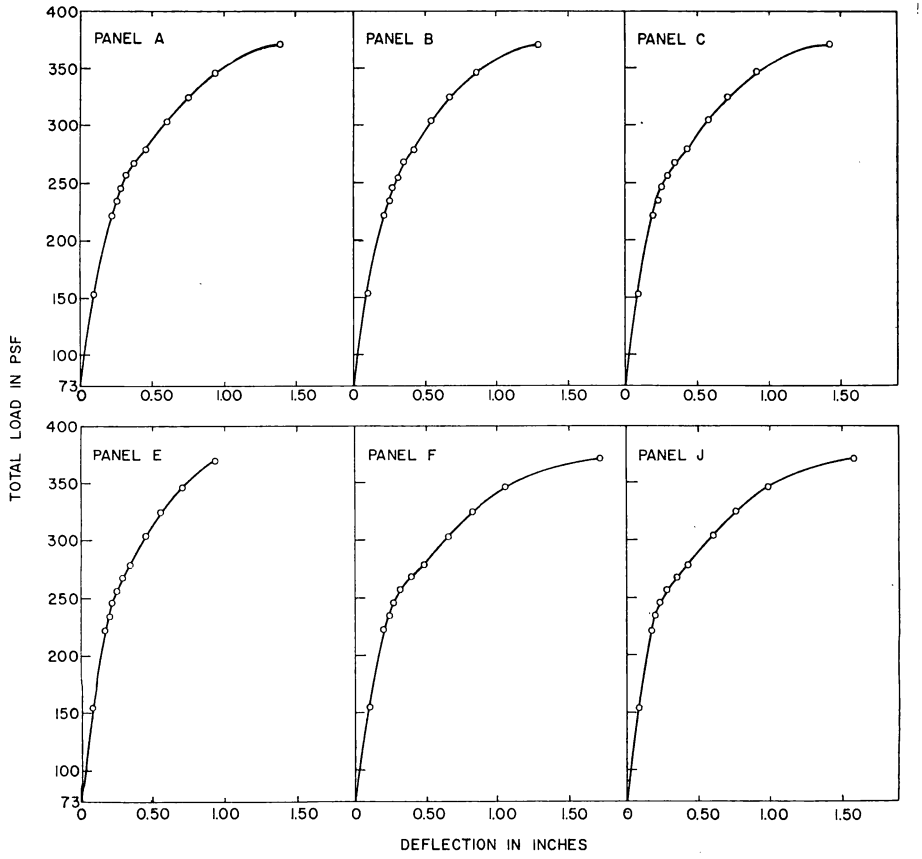

Fig. 21—Deflection of panel center points in Test 17 (test to failure)

increasing load, rotational restraints at the exterior edges of the exterior panels decreased, and the condition of "yield-hinge" or "yield-line" was approached. At total loads in excess of 250 lb per sq ft, the load-deflection curves of the side and corner panels (i.e., Panels A, B, C, F, and J) became more nearly similar. This behavior indicates that, at elevated loads and after considerable cracking has occurred, the various conditions at the exterior edges of the exterior panels tend toward a common type.

A theoretical analysis of a uniformly-loaded elastic plate infinite in extent and supported by rows of equidistant columns whose cross-sectional dimensions are small compared to the distances between columns has been given by Timoshenko and Woinowsky-Krieger.[6] For a plate with square panels made of a material having a Poisson's ratio of 0.2, the equation for the deflection w, at the panel center is:

$$w = 0.00581 \frac{qL^4}{D_e} \quad \text{.....(1)*}$$

where† q is the intensity of load, L is the distance center-to-center of columns and D_e is the effective flexural rigidity of the plate per unit width. Neglecting Poisson's ratio and the contribution of the reinforcement, and assuming that the concrete is uncracked, the effective flexural rigidity D_e, is given by the equation:

$$D_e = \frac{Eh^3}{12} \quad \text{.....(2)}$$

where E is the modulus of elasticity and h is the plate thickness. If the slab concrete is assumed to have cracked and if any contribution of concrete in tension is neglected, then one may use the properties of the transformed cracked section to obtain the effective flexural rigidity.

The load-deflection curve at the center point of Panel E during Test 17 is shown in Fig. 22. Plots of Eq. (1) using three values for the effective flexural rigidity D_e, are also shown in Fig. 22. The line with the steepest slope is obtained if Eq. (2) is used to compute D_e and is termed the "uncracked gross section" line. The other two lines shown in Fig. 22 are graphs of Eq. (1) in which the transformed cracked sections corresponding to middle strip bar spacings (i.e., #4 bars on 14-in. centers) for both N-S and E-W steel are used to compute D_e and they are termed the "cracked transformed section" lines. The difference in slope between the latter two lines is due to the difference in effective depth of the north-south and east-west reinforcement. The experimental load-deflection curve initially follows closely the uncracked gross section line. Above about 200 lb per sq ft, the experimental curve becomes markedly nonlinear and diverges increasingly from the gross section line as the load increases. From a study of the load-deflection curve it becomes apparent that the concrete in tension contributed significantly to the flexural rigidity of the slab through a major part of its loading history.

As an aid to the yield-line analysis of the slab, the deflection contour map shown in Fig. 23 was prepared from the photogrammetric records. This map gives contours of deflection at 0.1-in. intervals due to application of twice the design live load. The contour of greatest deflection is the 0.5-in. line shown at three locations on the northwest portion of the slab in Fig. 23. A long "valley" or "trough" may be observed running

*After completion of this paper, an analysis was made of this type of structure by M. D. Vanderbilt of the University of Illinois. Deflection coefficients for typical interior panels were obtained using finite differences and taking into account the width of the column supports. The coefficient in the equation for the deflection at the center of a square panel with a c/L ratio of 0.1 is approximately 25 percent less than that given in Eq. (1). Use of this more correct coefficient would result in a reduction of the deflections shown by the theoretical load-deflection curves in Fig. 22 by about 25 percent. However, the conclusions drawn from the comparison of theoretical and experimental data given in this paper are still valid.

†A list of notation is given at the end of this paper.

across the centers of all the exterior panels of the structure. Also, it may be observed that the deflected surface descends steeply along diagonal lines from the corner columns and interior columns into these troughs. The shape of the deflected surface shown in Fig. 23 strongly suggests that the mechanism governing the ultimate flexural strength of the slab is most probably that shown in Fig. 42.

Cracking

After Tests 1 through 13 to service load were complete, all the cracks which had been observed during the course of the tests were heavily outlined with black paint and then photographed. Fig. 24, giving the top surface crack pattern which resulted from the service load tests,

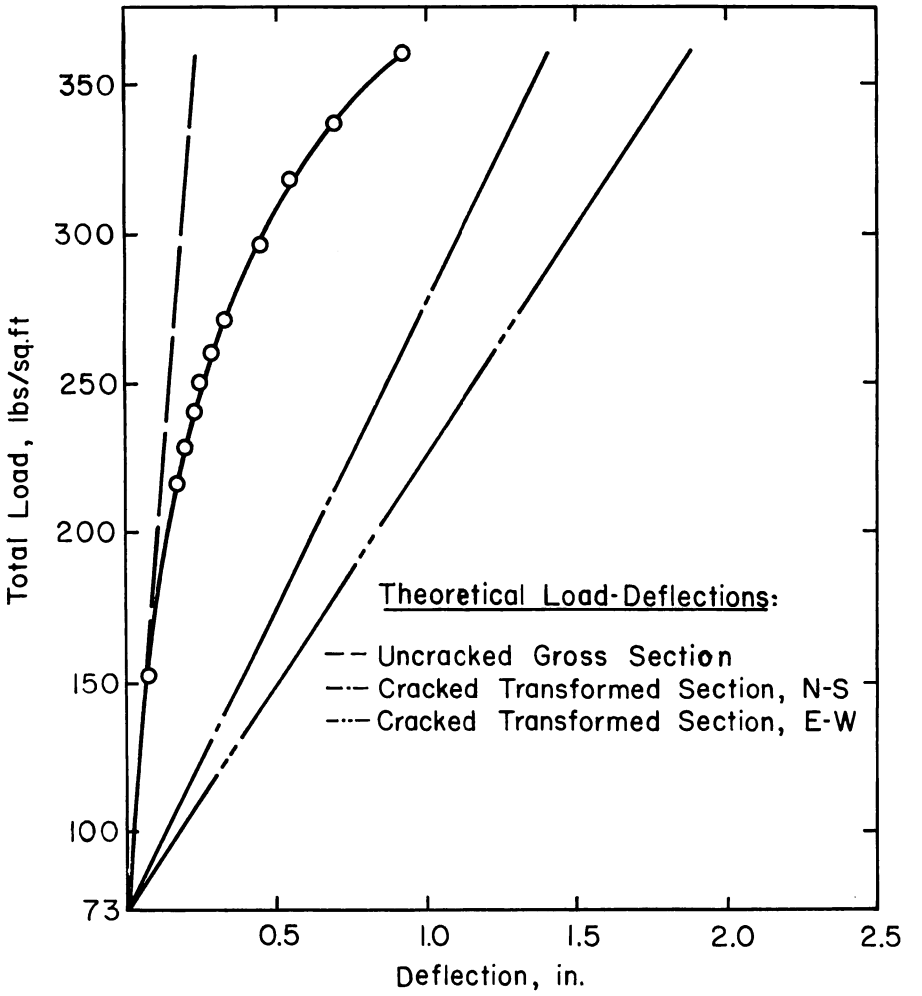

Fig. 22—Load-deflection curve for midpoint of center panel during Test 17

was prepared from a mosaic of 196 individual photographs of the slab surface. The maximum opening of the top surface cracks was approximately 0.005 in. The cracking was mainly confined to areas of the slab directly over the columns with the largest number of cracks occurring in the north-south direction. The spacing and location of the north-south top surface cracks corresponded to the spacing and location of the slab reinforcing bars. Since the north-south bars were placed nearest to the top surface, it appears that these bars acted as crack initiators.

Bottom surface slab cracking during the service load tests was confined to one short crack running in the north-south direction, located in the middle of the center panel plus a few very short localized cracks

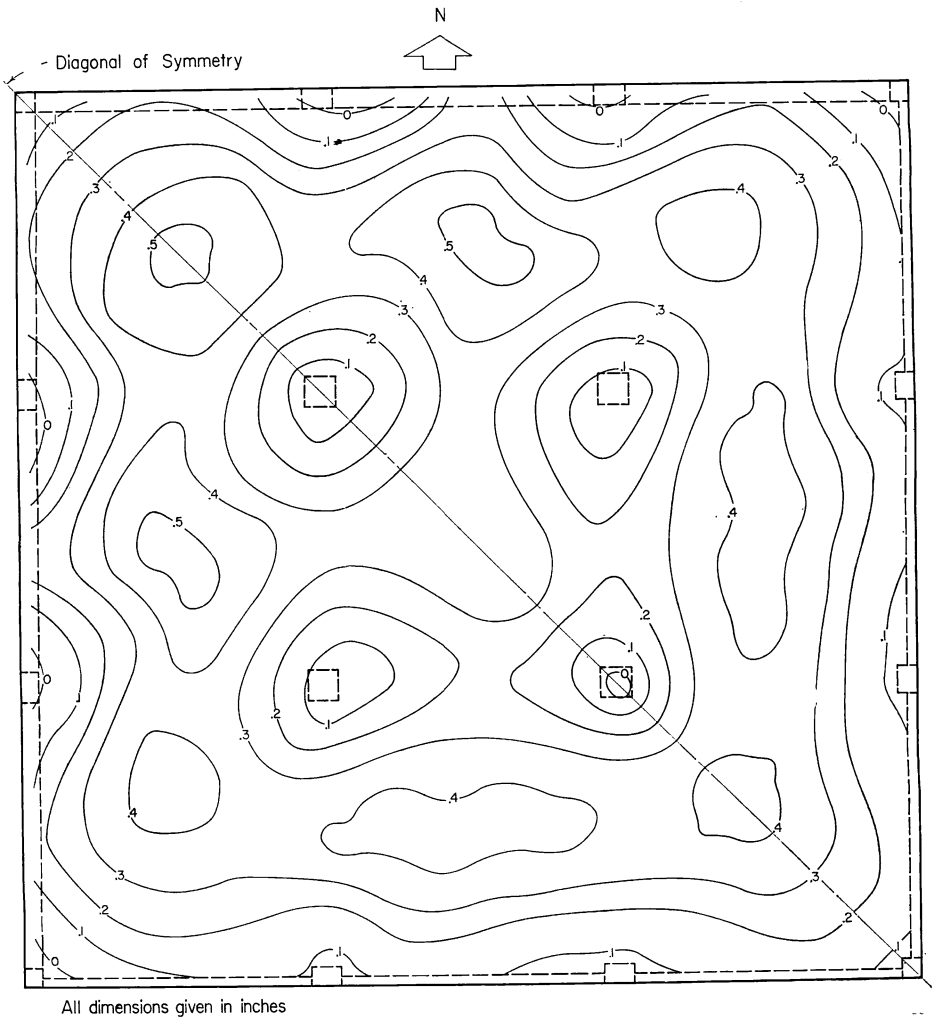

Fig. 23—Slab deflection contours under twice the design live load

at maximum positive moment areas near the construction joints. Because positive moment cracking was extremely slight relative to negative moment cracking, slab cracking behavior for a given total amount of reinforcement could probably be improved by decreasing positive and increasing negative reinforcement.

Fig. 25 and 26 which give, respectively, the top and bottom surface crack patterns at failure were prepared from photo-mosaics by the procedure described previously.

As was the case at service load, slab cracking in both top and bottom surfaces was heaviest in the north-south direction, as may be observed in Fig. 25 and 26. The pattern of bottom surface cracks shown in Fig. 26

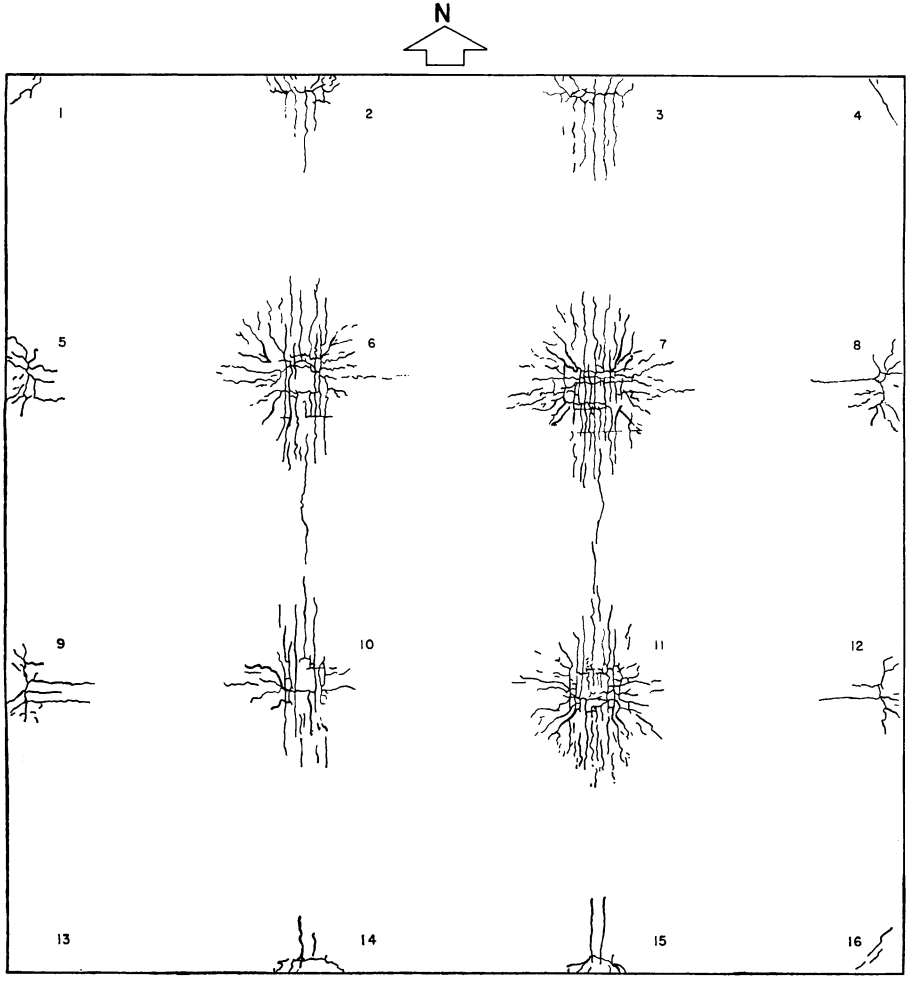

Fig. 24—Top surface crack pattern at design load

appears to be further evidence that the correct mechanism on which to base a yield-line analysis is that given in Fig. 42.

Distribution of steel stresses

Graphs of measured steel stress at service load versus strain gage location for Tests 3 and 16 with all panels loaded are given in each of Fig. 27 through 31. The stresses plotted in these figures were obtained by multiplying the measured strains by the modulus of elasticity of steel, assumed to be 30×10^6 psi. The location of the line across which the stresses were measured is shown in the upper left-hand corner of each figure. Distributions of positive moment steel stresses across panel

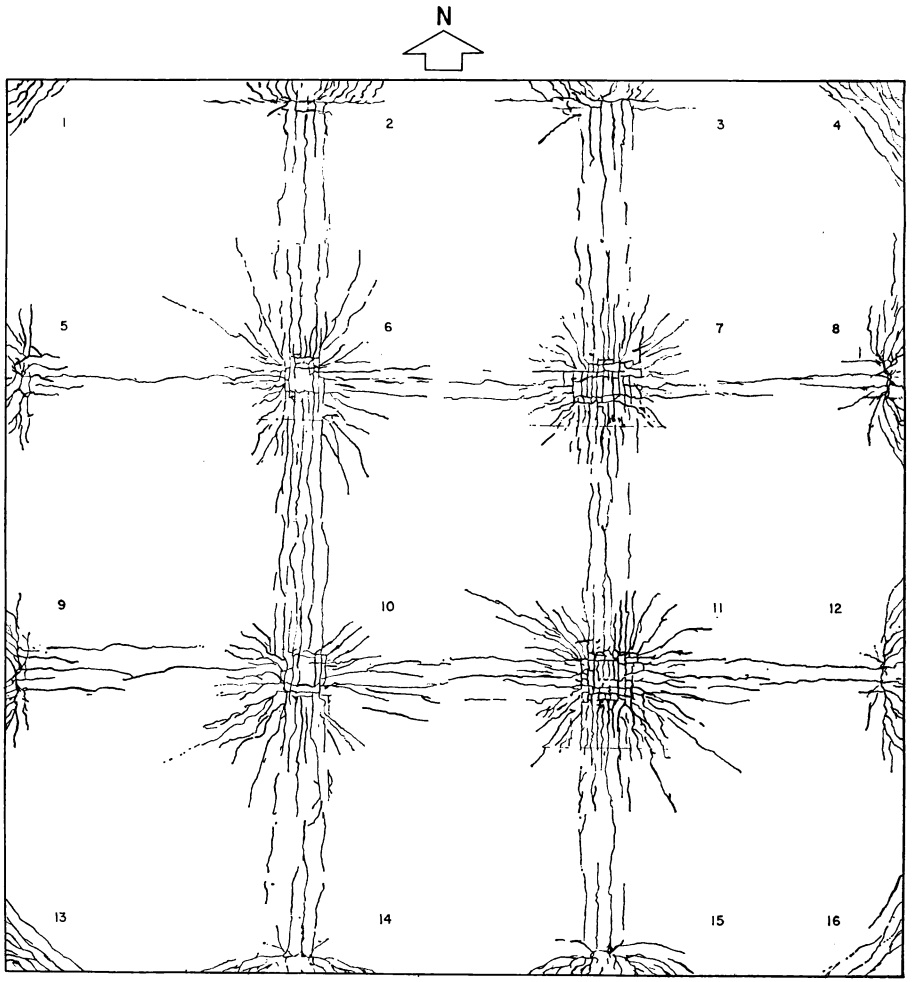

Fig. 25—Top surface crack pattern at ultimate load

center lines are given in Fig. 27, 28, and 29, and distributions of negative moment stresses across column lines are given in Fig. 30 and 31.

Stress distributions obtained during Tests 3 and 16 are shown in each figure to contrast the service load behavior of the test structure before and after a slight overload to 1½ design live loads during Tests 14 and 15. It may be observed in Fig. 27, 28, and 29 that the dashed lines representing the stress distribution for Test 16 indicate that positive moment steel stresses were increased considerably by the previous overloading. On the other hand, the dashed lines in Fig. 30 and 31 generally indicate relatively slight changes in negative moment stresses due to the previous

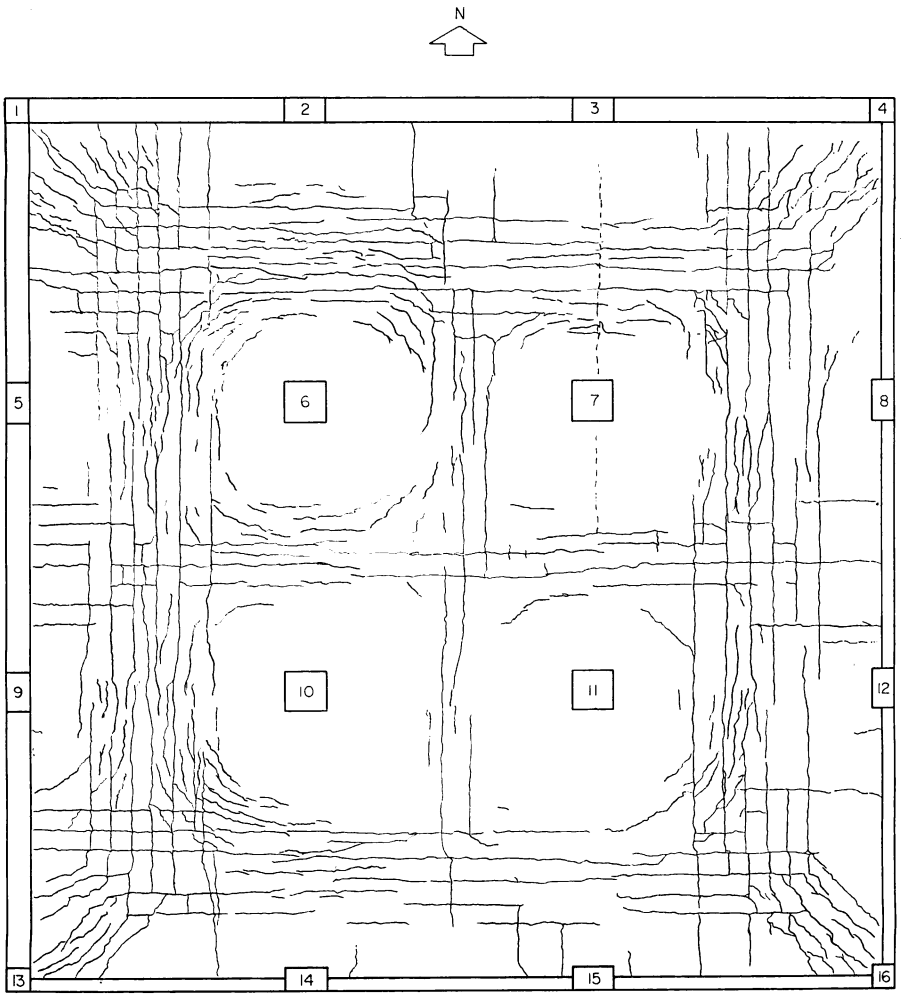

Fig. 26—Bottom surface crack pattern at ultimate load

overloading. This phenomenon of increase in positive moment steel stress without an accompanying increase in negative moment steel stress is probably due to the way in which the crack patterns developed. The negative moment cracks formed first, and at relatively low loads. Significant positive moment cracks did not develop until the total load slightly exceeded the service load. However, once the positive moment cracks started forming, the negative moment cracking did not increase significantly until the applied load exceeded twice the design live load. Thus, at service load in Test 16 the negative moment crack pattern was virtually identical to that at Test 3, while the corresponding positive moment crack pattern in Test 16 was considerably more developed than that in Test 3.

Referring again to Fig. 27 through 31, it may be observed that the magnitudes of the maximum positive moment stresses are approximately half those of the maximum negative moment stresses. Furthermore,

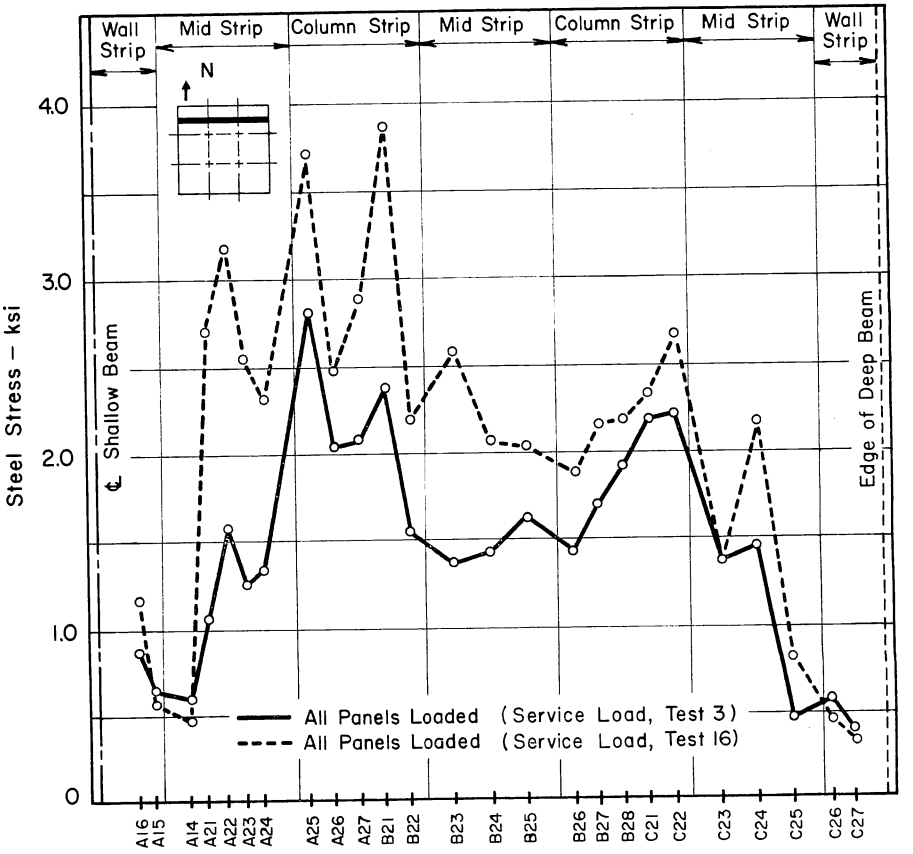

Fig. 27—Distribution of measured stresses in bottom layer of reinforcement across centers of Panels ABC

in no case did the maximum steel stress at service load exceed one-half the design allowable stress of 20,000 psi.* For this reason, to interpret the steel stresses in terms of resisting moment, consideration had to be given to the considerable contribution of the concrete in tension. Hence, the relatively intricate procedure described in the Appendix was required to convert raw strain data into moments per unit width of slab.

Mode of failure

Test 17, the final test performed on the flat plate specimen, was continued until the load-carrying ability of the slab was destroyed. The load versus center-of-panel deflection curves for this test are given in Fig. 21. For loads in excess of approximately 260 lb per sq ft, the curves

*Measured steel stresses do not include those due to the self weight of the test slab.

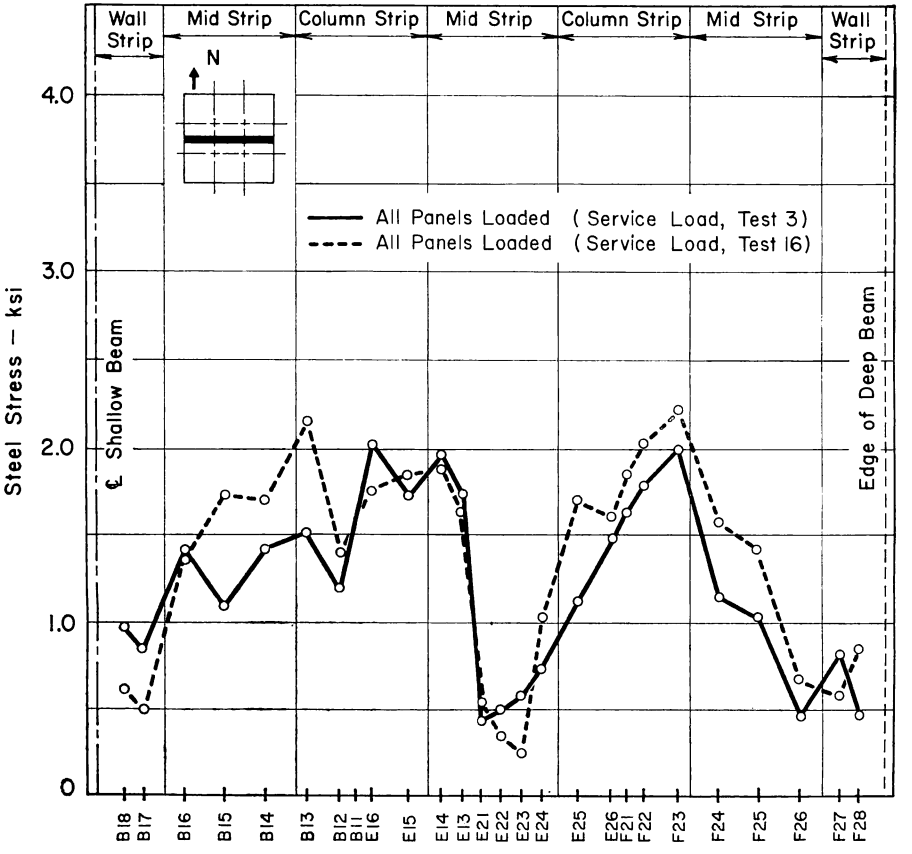

Fig. 28—Distribution of measured stresses in bottom layer of reinforcement across centers of Panels DEF

shown in Fig. 21 become markedly nonlinear, the deflection increasing more and more rapidly with increasing load. At the 260 lb per sq ft load level it was observed that positive moment cracks (center of panel, bottom surface cracks) had increased rapidly in width and number. This cracking had progressed so far at the 260 lb per sq ft load that the outline of the failure-load crack pattern, given in Fig. 26, was already clearly defined. Undoubtedly, this rapid increase in positive moment cracking at 260 lb per sq ft led to the observed onset of nonlinearity in the load-deflection curves. Yielding of the positive moment reinforcement did not take place until the 346 lb per sq ft load level.

Torsional cracking of spandrel beams, present to a slight degree at a load level of approximately 240 lb per sq ft, became quite pronounced at loads in excess of 280 lb per sq ft. The maximum spandrel beam rotation observed was approximately 3 deg at midpoints of the south side deep beams. However, even though torsional twist and torsional

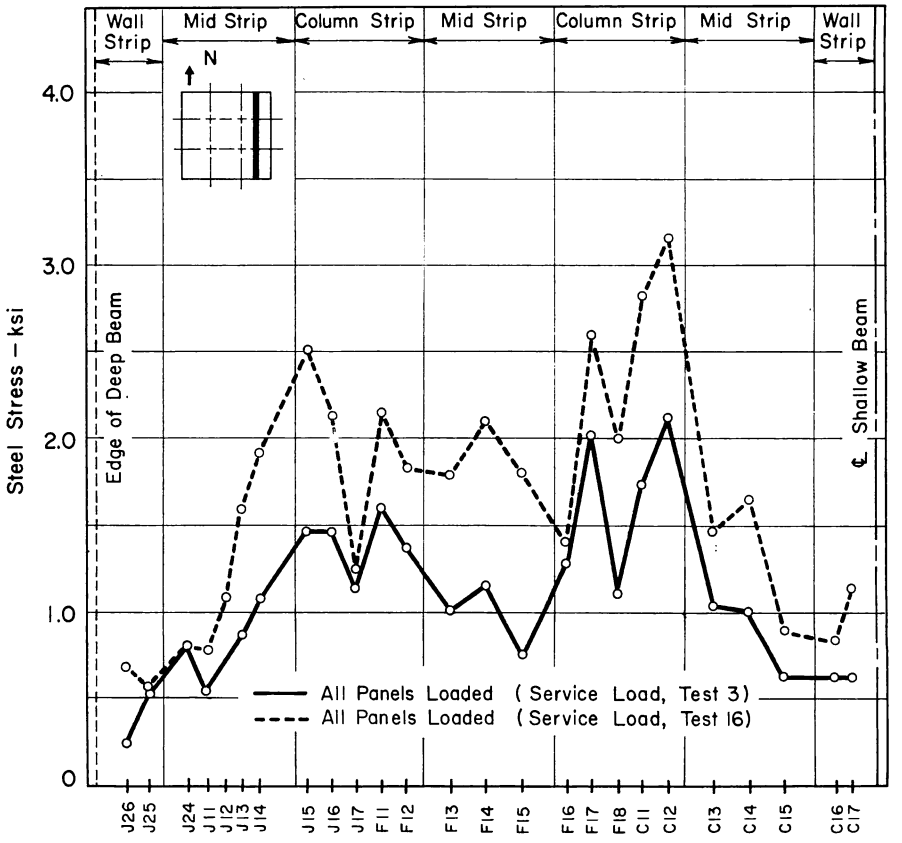

Fig. 29—Distribution of measured stresses in bottom layer of reinforcement across centers of Panels CFJ

cracking of spandrel beams was evident at elevated loads, neither torsional collapse of the spandrel beams nor torsional rupture of the beam-to-column connections occurred. This strength in torsion of the spandrel beams was largely due to the relatively heavy web reinforcement provided.

After application of the next to last load increment, several of the slab top steel strain gages in the vicinity of the columns indicated that yielding of the reinforcement had occurred. Fifteen minutes elapsed between the time the last load increment was applied and the time of failure, thus permitting the recording of most of the strain gage data. After application of the last load increment, approximately 30 percent of the slab top steel strain gages indicated yielding, as did approximately 15 percent of the bottom steel strain gages located along the center line

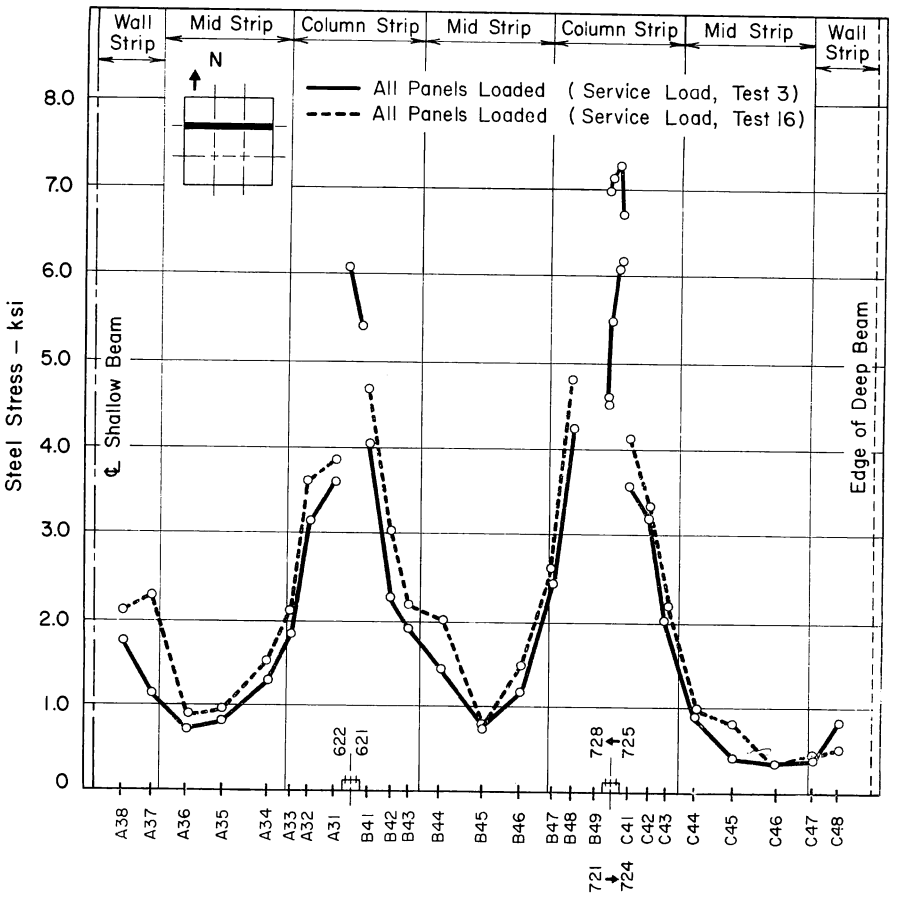

Fig. 30—Distribution of measured stress in top layer of reinforcement across Column Line 5-8

of Panels C, F, and J. The average of the strains indicated by the remaining gages was approximately 75 percent of the yield strain of the reinforcement.

Failure was evidenced by a sudden punching through the slab of the interior column (Column 7) 15 min after a 23 lb per sq ft increment of load was applied to produce a total of 369 lb per sq ft. Because a hydraulic loading system was used, the applied load was lost immediately after the column punched through the slab. After the initial punching failure had occurred, Panels G, H, and J were loaded to their ultimate load carrying capacity. At each of the two adjacent interior column locations (Columns 10 and 11 in Fig. 4), the slab failed by punching shear. Furthermore, in no case did the load causing failure exceed the initial collapse load by more than 1 or 2 percent.

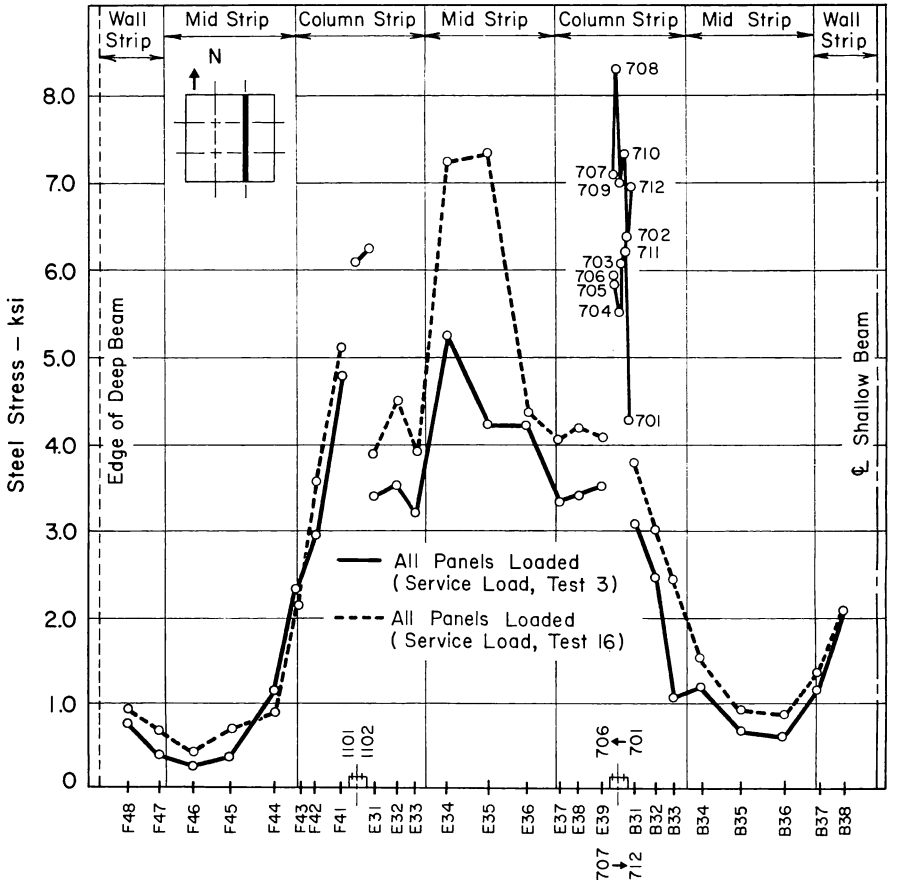

Fig. 31—Distribution of measured stress in top layer of reinforcement across Column Line 3-15

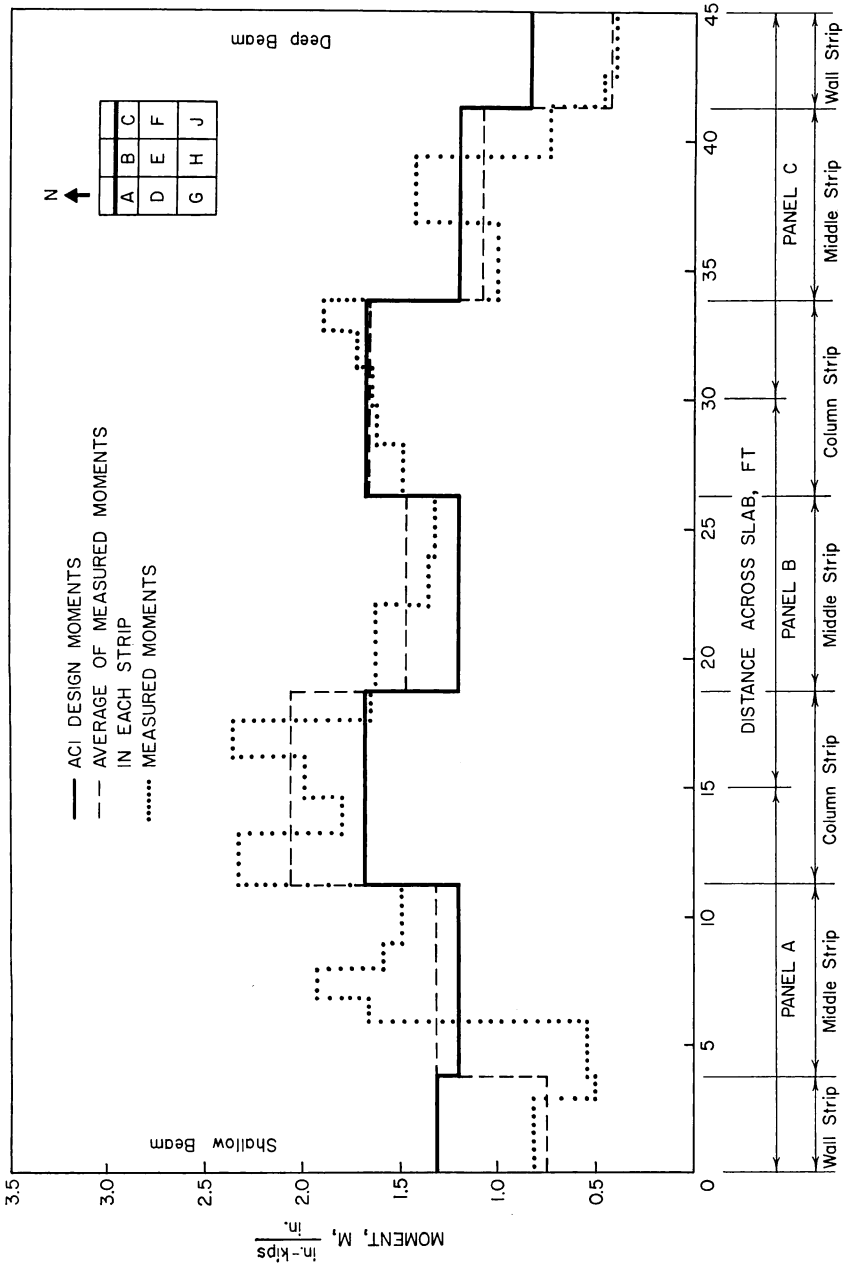

Fig. 32—Comparison of measured positive moments across Panels ABC with design moments

ANALYSES OF EXPERIMENTAL RESULTS

The test findings were analyzed with several objectives in mind. Comparisons were made of measured moments at service load with design moments computed by the empirical method of the 1956 ACI Building Code. The behavior of the three-quarter scale structure was compared with that of the one-quarter scale model tested at the University of Illinois. Finally, the observed ultimate strength of the structure was studied in terms of yield-line analysis for flexure and in terms of ultimate shear strength.

Comparison with design moments of ACI Code

The steel strains measured at service load level in Test 16 were converted to slab moments per unit width for each strain gage location in the slab, using the procedure described in the Appendix. Test 16 with all panels loaded to twice the design live load was selected for the moment comparison to investigate the behavior of the test structure after it had been subjected to a previous test history simulating extremes of possible service conditions, such as pattern loading to produce maximum positive or negative moments, and slight overloading to develop extensive cracking.

Moments in strips—The moments per unit width obtained from the strain measurements are plotted in Fig. 32 through 38. The average measured moment per unit width over each strip, together with corresponding design moments for the empirical method of the 1956 ACI Building Code, Section 1004, are also given in these figures. The distributions of positive moment across panel center lines are given in Fig. 32, 33, and 34, and distributions of negative moment across interior column lines are given in Fig. 35 and 36. The distributions of negative moment across exterior column lines at the junction between slab and spandrel beams are given in Fig. 37 and 38.

As shown in Fig. 32, 33, and 34, reasonable agreement was found between average measured moments and ACI design moments at each panel center line where positive moments were measured. As might be expected, the best agreement between test results and design values occurred across the center lines of Panels DEF. In Fig. 33 it may be seen that in every strip but the west wall strip, the maximum difference between average measured moment and ACI design moment was about 12 percent. Comparing the distribution of measured moments shown in Fig. 32 and 34 it is seen that the agreement between measured moments and design values was closest along the center line of Panels CFJ.

The distributions of negative moment across two of the interior column lines are given in Fig. 35 and 36. For both column lines considered, it can be seen that a high concentration of negative moment was found

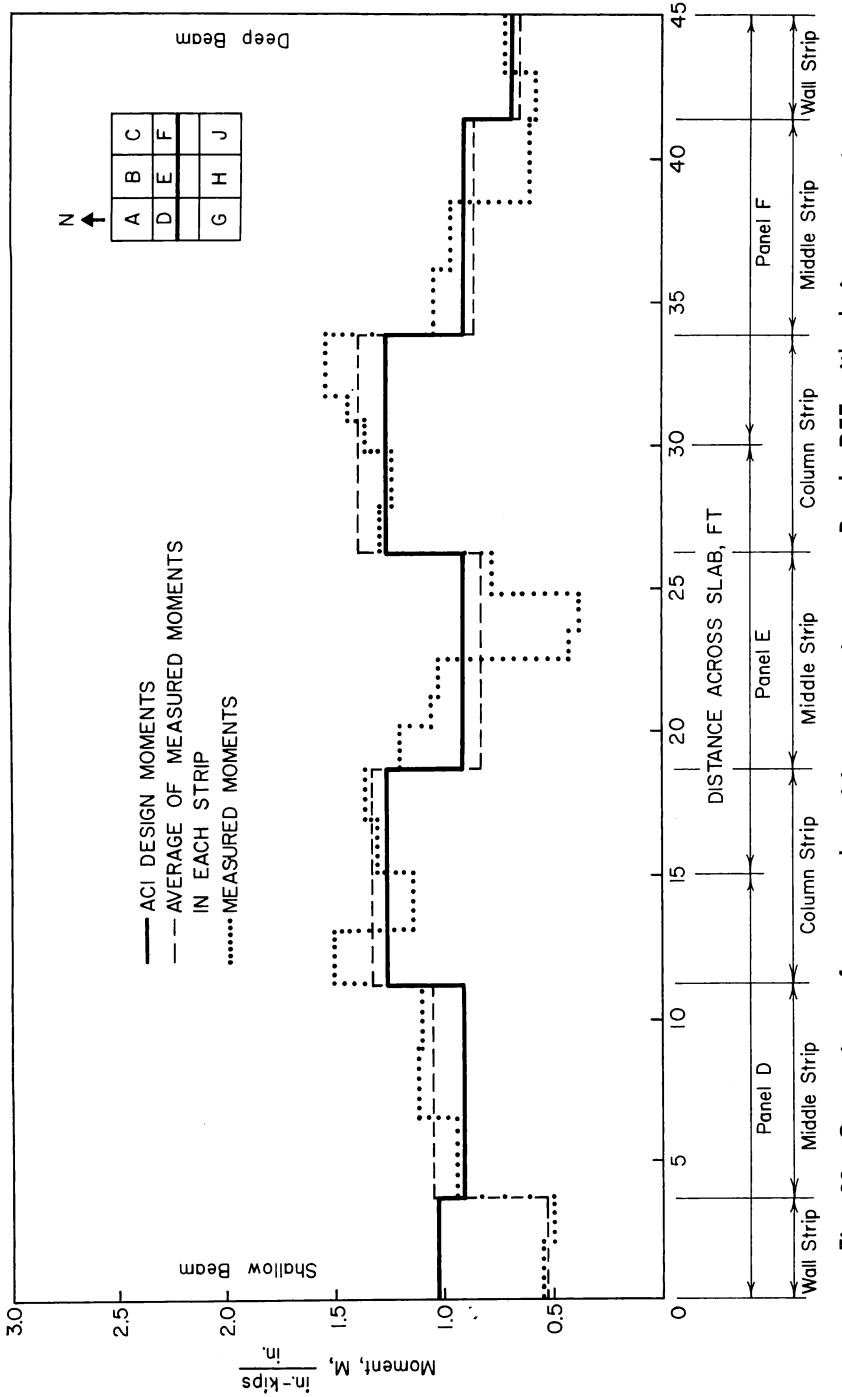

Fig. 33—Comparison of measured positive moments across Panels DEF with design moments

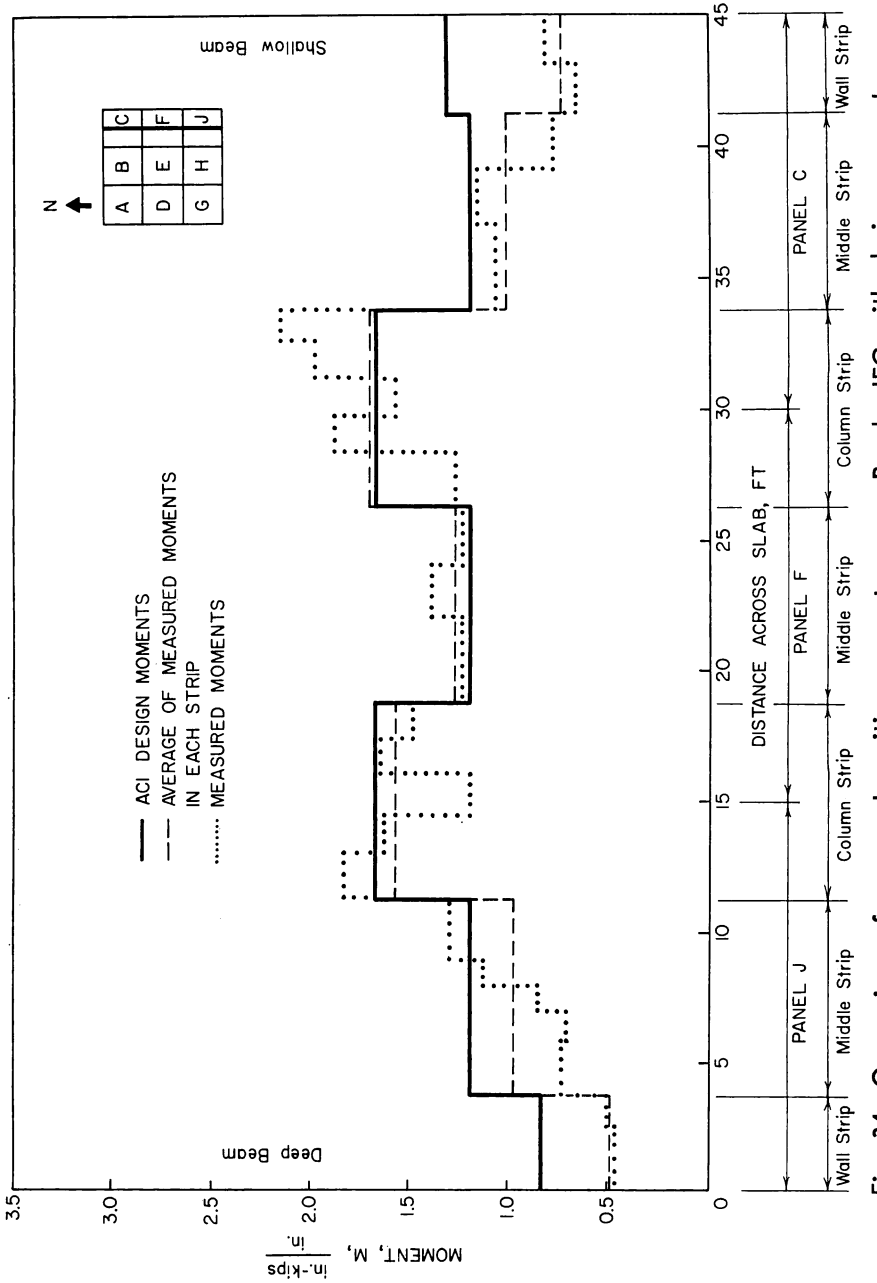

Fig. 34—Comparison of measured positive moments across Panels JFC with design moments

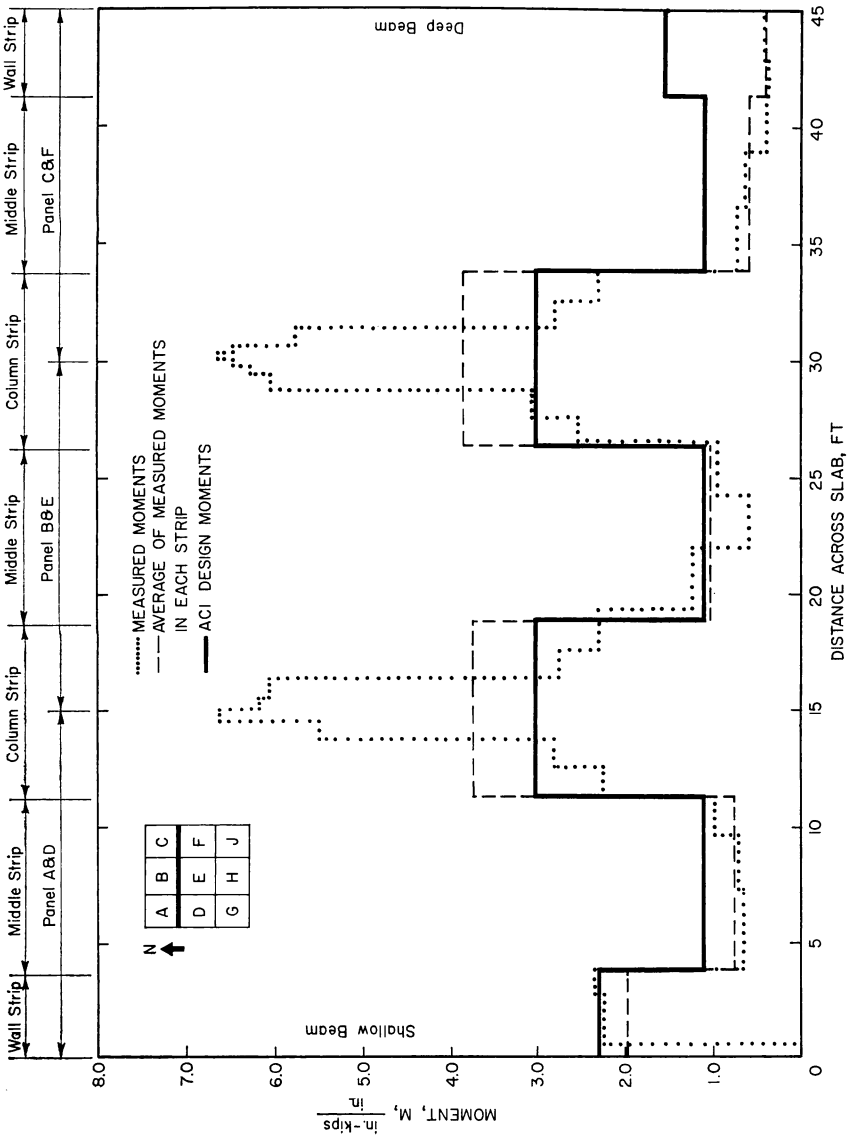

Fig. 35—Comparison of measured negative moments across Columns 5, 6, 7, and 8 with design moments

in the slab at interior column locations. Moments measured in the slab at a number of locations in the vicinity of the interior columns were as much as twice the ACI design moments. Average negative moments over the column strip at the interior column locations were from 25 to 30 percent in excess of the ACI design moments. On the other hand, negative moments in exterior middle strips and wall strips as shown in Fig. 35 and 36 are considerably smaller than the ACI design moments. Agreement between measured negative moment and ACI design moment in the interior middle strips in Fig. 35 and 36 was satisfactory. The negative moments in the wall strips appear to be influenced to a considerable degree by the stiffness of the adjacent spandrel beams. In Fig. 35 and 36 it can be seen that, whereas the measured moment in wall strips adjacent to deep spandrel beams was about 30 percent of the ACI design moment, the measured moment in wall strips adjacent to the shallow spandrel beams was about 80 percent of the ACI design moment.

The distributions of negative moment across two of the exterior column lines at the junctions of the slab and the edge beams, plotted in Fig. 37 and 38, also show concentrations of negative moment in the slab at the inner column locations. These concentrations of negative moment again approach twice the ACI design moment, but over a smaller width than was found at the interior column center line locations. As a result, the average of measured negative moments over the interior column strips was actually less than the ACI design moment in three cases, and only about 4 percent above the ACI design moment in the fourth case investigated. The measured negative moments in the wall strips are seen to approach zero at the junction between the panels and the edge beams. This is probably due to the greater stiffness of the edge beams allowing them to carry much more moment than the slab which is less stiff in this region.

Sections across entire structure—The design moments for various parts of the slab of the test structure, computed according to the empirical method of Section 1004 of the 1956 ACI Building Code, are given in Table 6.

The area under the measured moment curve in Fig. 32 through 38 is the total measured moment M_t, acting on a given section of the slab extending across the entire test structure. Values of M_t together with values of the total design moment M_d are given in Table 7. The total design moment M_d, at a given section of the slab is obtained by evaluating the corresponding area under the "ACI Design Moment" curve shown in each of Fig. 32 through 38.

The extreme right-hand column in Table 7 gives the ratios of total measured moment to total design moment. Agreement between measured total moment and design total moment is satisfactory for the first five entries in Table 7. The last two entries, representing moments along

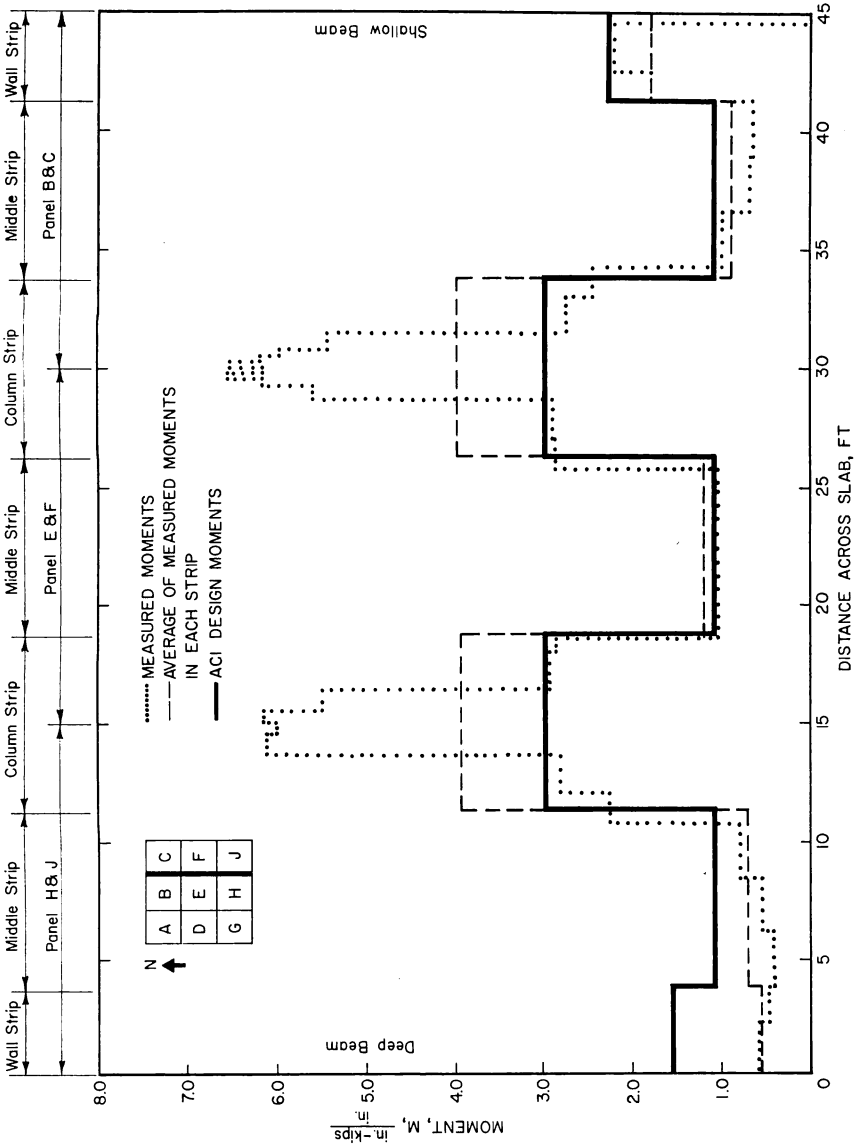

Fig. 36—Comparison of measured negative moments across Columns 3, 7, 11, and 15 with design moments

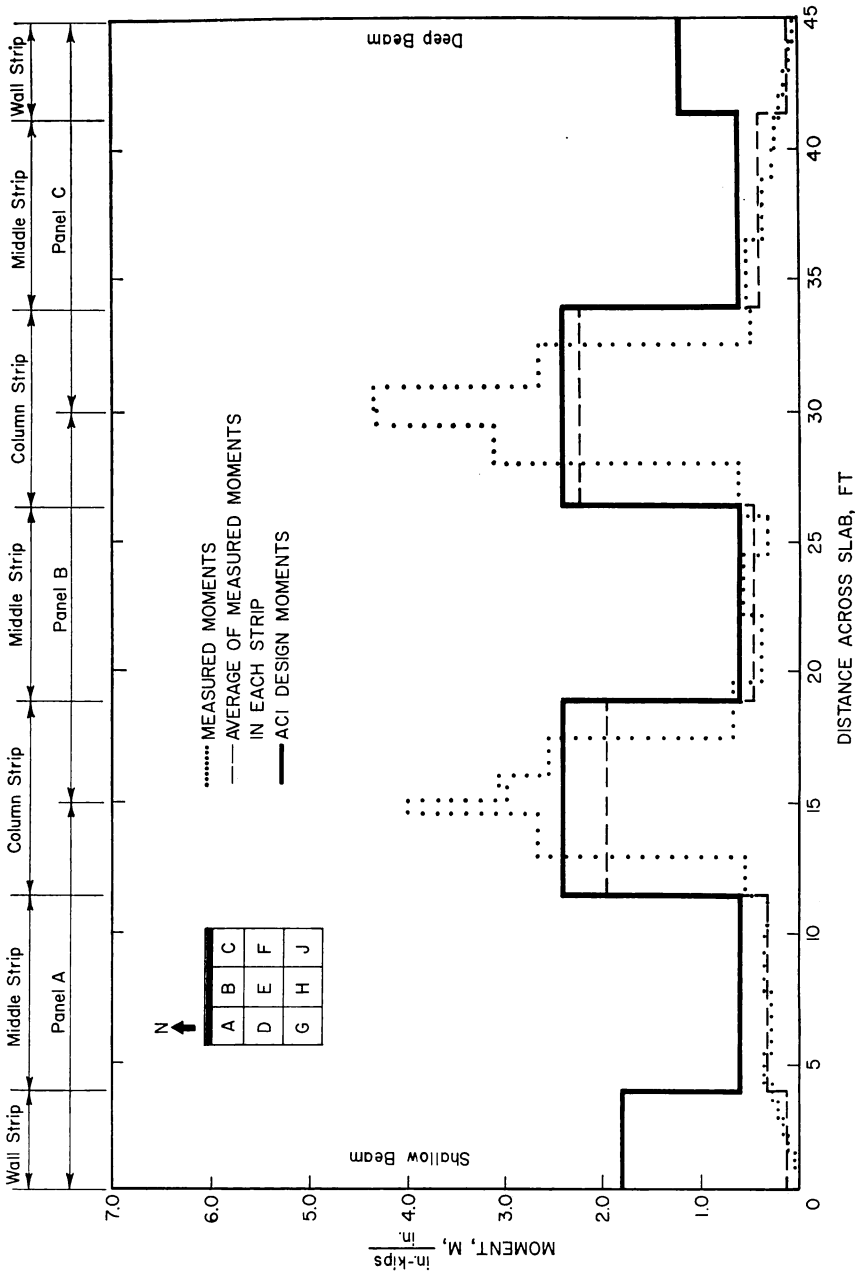

Fig. 37—Comparsion of measured negative moments across Columns 1, 2, 3, and 4 with design moments

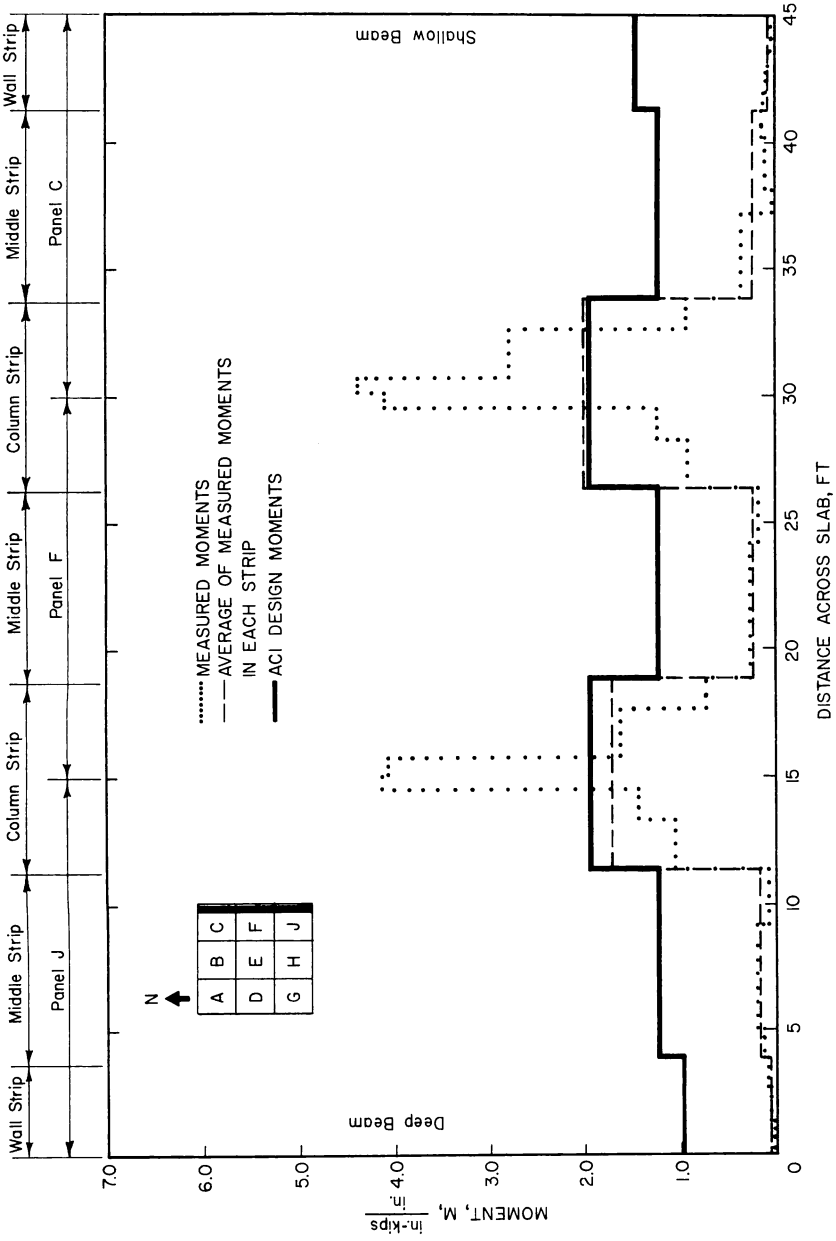

Fig. 38—Comparison of measured negative moments across Columns 4, 8, 12, and 16 with design moments

TABLE 6—DESIGN MOMENTS

Strip type	Location	Exterior panel (M_o = 540 in.-kips) Percent of M_o	Exterior panel (M_o = 540 in.-kips) M, in.-kips	Interior panel (M_o = 516 in.-kips) Percent of M_o	Interior panel (M_o = 516 in.-kips) M, in.-kips
Column	Exterior negative A*	40	216.0	—	—
	Exterior negative B	32	172.8	—	—
	Interior negative	50	270.0	46	237.6
	Positive	28	151.2	22	114.0
Middle	Exterior negative A	10	54.0	—	—
	Exterior negative B	20	108.0	—	—
	Interior negative	18	97.2	16	82.8
	Positive	20	108.0	16	82.8
Wall	Exterior negative 2A	15	81.0	—	—
	Exterior negative 2B	12	64.8	—	—
	Exterior negative 3A	10	54.0	—	—
	Exterior negative 3B	8	43.2	—	—
	Interior negative 2	19	102.6	18	92.4
	Interior negative 3	13	70.2	12	62.4
	Positive 2	11	59.4	9	46.8
	Positive 3	7	37.8	6	31.2

*Support condition, see Table 6A.

the junctions between slab and spandrel beams, indicate that design total moments are greatly in excess of measured total moments. This, of course, could also be observed from the diagrams given in Fig. 37 and 38. On the basis of the above observations, it seems that some reduction in the amount of negative reinforcement in middle strips and wall strips at junctions of the slab and spandrel beams in corner panels would have been possible without impairing the load-carrying capacity of the test structure.

Interior slab panel—An expression for the total static moment in a half panel of a flat plate with circular column capitals has been given by Nichols.[7] The basic assumptions made by Nichols in developing his expression for the total static moment were:

1. The panel is one of an array of identical panels extending indefinitely in both directions.

2. All panels of the array are uniformly loaded to the same intensity of load.

3. The shear (or reaction) is uniformly distributed around the circumference of the column capital.

TABLE 6A—SUPPORT CONDITIONS

Type	Side or end edge condition: Shallow beam 8¼ x 12 in.	Side or end edge condition: Deep beam 15¾ x 6 in.
Side support parallel to strip	2	3
End support at right angles to strip	A	B

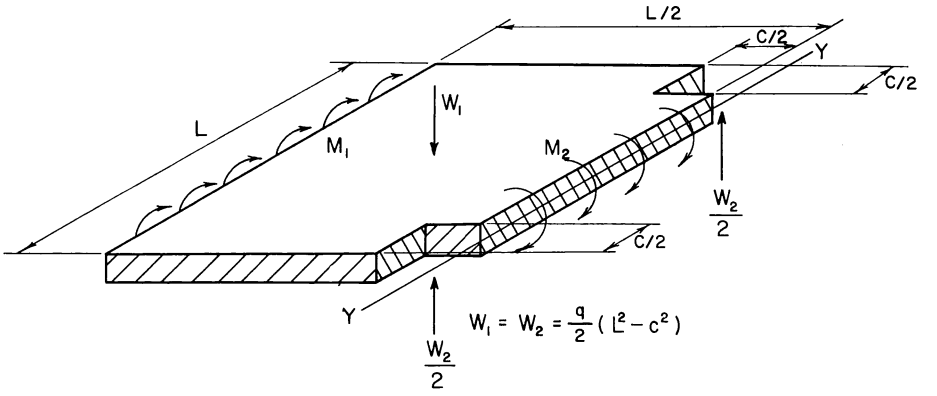

Fig. 39—Free-body diagram of half slab panel

Siess[8] extended Nichols' original work to the case of rectangular panels with rectangular column capitals.

Considering the free-body diagram of a typical half-panel with square columns or column capitals as shown in Fig. 39, no shears exist on any of the long edges of the free body if Conditions 1 and 2 above are fulfilled. Therefore, torsional moments may be neglected in considering the equilibrium of the free body. Two cases may be considered in developing an expression for the total static moment, M_0.*

In the first, which will be denoted Case I, it is assumed that the reaction is uniformly distributed around the periphery of the column or column capital as in Nichols' Assumption 3 above. By writing an equation for the equilibrium of moments about the Y-Y axis shown in Fig. 39, the expression for M_0 becomes

$$M_0 = M_1 + M_2 = \frac{qL^3}{8}\left(1 - \frac{3c}{2L} + \frac{c^3}{2L^3}\right) \quad (3)$$

in which q is the intensity of load, c is the side dimension of the column, and L is the center-to-center span between columns.

A second case, denoted Case II, may be considered in which it is assumed that the whole reaction is concentrated at the corners of the columns. Writing the equation for the equilibrium of moments about the Y-Y axis in Fig. 39 results in an expression for M_0 as follows:

$$M_0 = M_1 + M_2 = \frac{qL^3}{8}\left(1 - \frac{2c}{L} + \frac{c^3}{L^3}\right) \quad (4)$$

*M_0 = sum of the total positive moment at midspan across the full width of the panel and the total negative moment on a parallel column line and around the periphery of the column capitals.
= $M_1 + M_2$ in Fig. 41.

The distribution of shear in the slab around the periphery of a column or column capital in an actual flat plate structure probably lies somewhere between the distributions assumed in the two cases considered above. However, the difference between Case I and Case II values for M_0 rarely exceeds 5 or 6 percent. The Case I expression for the total statical moment always yields the higher value for M_0 and hence leads to a more conservative design. Therefore, the Case I expression for M_0 should perhaps be preferred as a basis for practical design.

Measured moments at service load in Test 16 for the two half-panels of Panel E located adjacent to Column Lines 6-7 and 7-11 are compared in Table 8 with values of M_0 computed according to Eq. (3) and (4).

TABLE 7—COMPARISON OF MOMENTS FOR SECTIONS ACROSS ENTIRE STRUCTURE

Location	Design moment M_d, in.-kips	Test moment M_t, in.-kips	$\frac{M_t}{M_d}$
Center line of exterior row of Panels A-B-C	+ 723.6	+ 734.6	1.015
Center line of interior row of Panels D-E-F	+ 554.4	+ 546.0	0.985
Center line of exterior row of Panels C-F-J	+ 723.6	+ 651.2	0.900
Interior Column Line 5-6-7-8	−1004.4	− 975.4	0.971
Interior Column Line 3-7-11-15	−1004.4	−1015.4	1.011
Exterior Column Line 1-2-3-4	− 729.0	− 477.7	0.655
Exterior Column Line 4-8-12-16	− 777.6	− 385.9	0.496

TABLE 8—COMPARISON WITH NICHOLS' EXPRESSION FOR STATIC MOMENT

Location and type moment	Moment			$\frac{M_1 + M_2^*}{M_0}$	
	M_1, in.-kips	M_2, in.-kips	$M_1 + M_2$, in.-kips	Case I	Case II
Panel E (north half)					
ACI design moment	196.8	367.2	564.0	0.834	0.886
Test moment	195.5	419.7	615.2	0.910	0.967
Panel E (east half)					
ACI design moment	196.8	367.2	564.0	0.834	0.886
Test moment	195.5	440.6	636.1	0.941	0.999

*Case I: $M_0 = 675.9$ in.-kips; Case II: $M_0 = 636.5$ in.-kips.

TABLE 9—COMPARISON OF MOMENTS IN INDIVIDUAL PANELS

	Panel designation								
	A	B	C	D	E	F	G	H	J
Measured M/WL	0.074	0.101	0.060	0.082	0.102	0.067	0.069	0.088	0.058
ACI design M/WL	0.084	0.094	0.077	0.079	0.085	0.069	0.086	0.093	0.079

Design moments for the two half-panels are also compared with computed values of M_0 in Table 8.

It can be seen from Table 8 that the measured values of $(M_1 + M_2)$ are in close agreement with the Case II value of M_0. It can also be seen that the design values of $(M_1 + M_2)$, calculated using Eq. (10) of Section 1004(f) of ACI 318-56, are less than the total static moment M_0, obtained from either Eq. (3) or (4) above.

These results clearly indicate that application of the equations of statics to a suitable free body cut from a typical interior panel leads to a rational expression for M_0 in close accord with the measured sum $(M_1 + M_2)$.

Individual slab panels—Bending moment coefficients M/WL, that were measured in the test structure are compared with design moment coefficients in Table 9. The design values given in the table were obtained by dividing the total moment M, in the north-south direction in each panel by the product of total load per panel and span length WL. The measured total moment in each panel, due to dead plus live load, was obtained by taking the sum of measured positive moments per unit width across the panel center line, and adding to it the average of the sum of the measured negative moments per unit width across the panel edges. Test 16 was selected for this comparison because it was believed that the design load crack pattern was fully developed due to the "exercising" of the test structure by the previous program of tests.

For six of the nine panels, Table 9 shows that the design moment coefficient exceeds the actual moment coefficient. However, for Panels B, D, and E, the measured moment coefficient exceeds the design moment coefficient by 7.5, 3.8, and 20.0 percent, respectively. The underestimation of the measured moment by the design moment in the case of Panels B and D is not too great, but such is not the case for Panel E, which closely represents a typical interior panel of a multibay structure. The design moment coefficient for Panel E is considerably less than the measured moment coefficient, which agrees closely with the coefficient corresponding to the static moment. However, it should be noted that despite this apparent underdesign, the ultimate strength of the test structure was adequate.

Comparison with one-quarter scale model test

One purpose of this investigation is to compare the behavior under load of the test structure with that of the one-quarter scale model tested at the University of Illinois.[4] The one-quarter scale model was constructed from portland cement mortar, reinforced with ⅛ in. square steel bars. Since deflections, bending moments, crack patterns, mode of failure, and load at failure are important phases of the research program at the University of Illinois, it is of considerable importance to investigate the possible influence of scale effects.

Deflection—Equal loads per unit area produce equal stresses in prototype and a linearly-scaled model. However, this is not the case with regard to deflections. Assuming that slab deflections are governed by an equation of the form of Eq. (1), and that the concrete is uncracked, then Eq. (1) may be written in general form as

$$w = C_1 \frac{qL^4}{Eh^3} \quad \text{.....(5)}$$

in which C_1 is a constant dependent on the boundary conditions and geometry of the panel. If subscripts m and p refer to model and test structure respectively, and if s denotes the scale, then the equation for deflection w_p, of the test structure slab is

$$w_p = C_1 \frac{q\,(s_pL)^4}{E_p(s_ph)^3} \quad \text{.....(6)}$$

and the equation for deflection w_m, of the model slab is

$$w_m = C_1 \frac{q\,(s_mL)^4}{E_m\,(s_mh)^3} \quad \text{.....(7)}$$

Dividing Eq. (6) by Eq. (7) results in the expression

$$w_p = \left(\frac{s_p}{s_m}\right)\left(\frac{E_m}{E_p}\right) w_m \quad \text{.....(8)}$$

Since the scale of the test structure was three-quarter and that of the model was one-quarter, Eq. (8) may be written as

$$w_p = 3\,\frac{E_m}{E_p}\,w_m \quad \text{.....(9)}$$

The measured value of E_p at the beginning of testing was 3,670,000 psi and at the end of testing E_p was calculated to be 3,970,000 psi from $E_c = 1.8 \times 10^6$ psi $+ 460\,f_c'$, where $f_c' = 4715$ psi. The measured values of E_m were 2,400,000 and 2,800,000 psi at the beginning and end of testing, respectively.

The model similitude relation, Eq. (9), must be applied to the University of Illinois data so that a direct comparison of deflections for the one-quarter scale model and the test structure may be made.

Deflections due to applied load of various points on the test structure, and of corresponding points on the model, are compared in Fig. 40 and 41. The deflections at the centers of two corner panels, the center panel, and an interior side panel, are shown in Fig. 40 for both structures during the third loading to service load. Deflections due to applied load, when loading the slabs to dead load plus twice the live load, are plotted

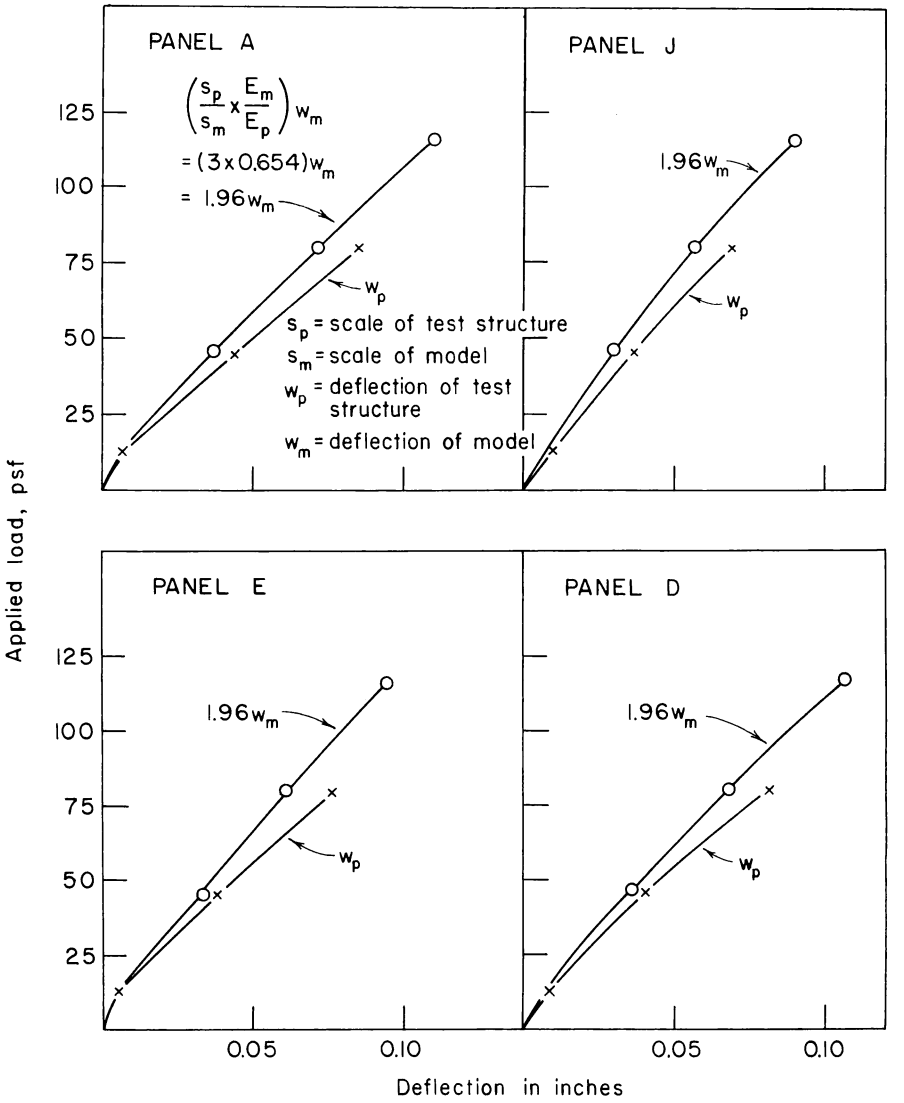

Fig. 40—Comparison of deflections at panel center points between three-quarter scale test structure and one-quarter scale model (Test 3—three-quarter scale test structure; Test 108—one-quarter scale model)

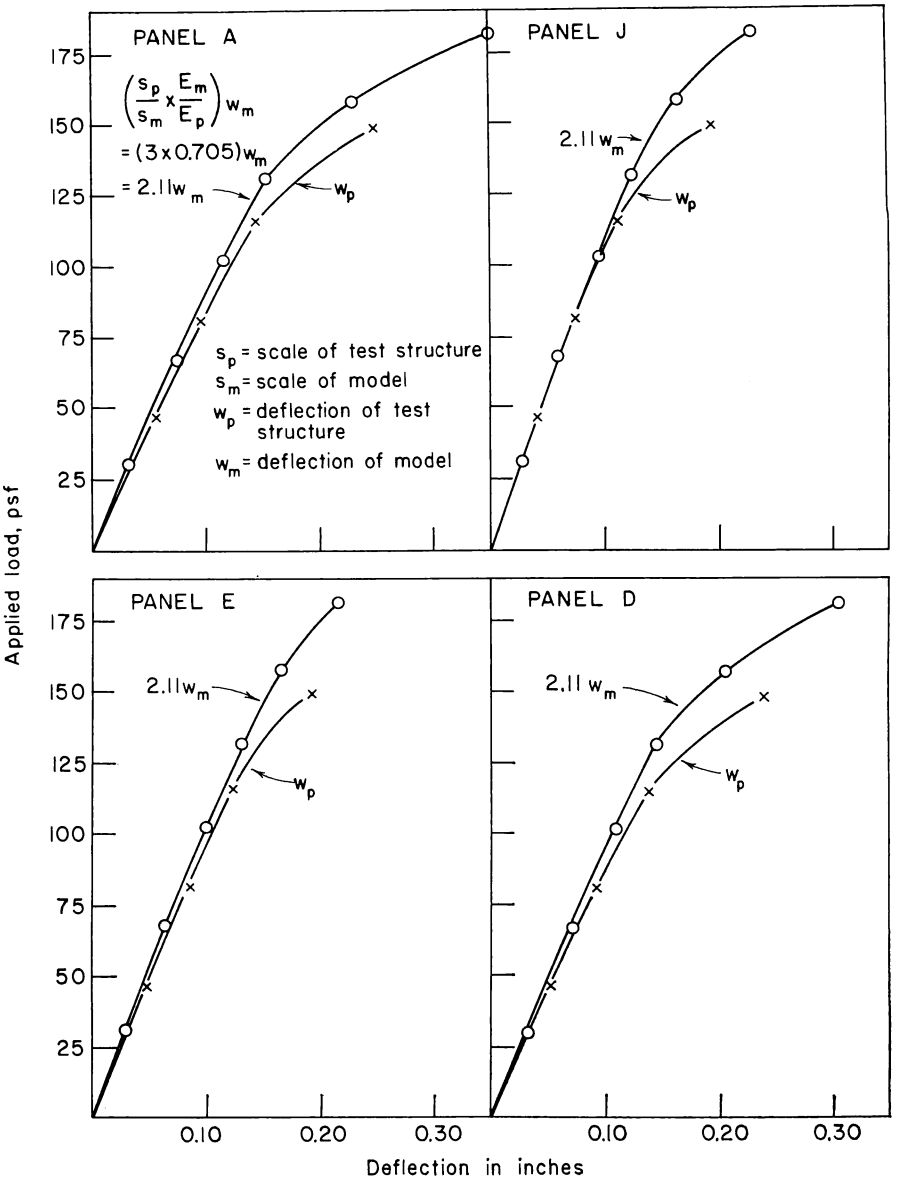

Fig. 41—Comparison of deflections at panel center points between three-quarter scale test structure and one-quarter scale model (Test 16—three-quarter scale test structure; Test 131—one-quarter scale model)

TABLE 10—COMPARISON OF MOMENTS IN INDIVIDUAL PANELS

Measured M/WL	Panel designation								
	A	B	C	D	E	F	G	H	J
Test structure	0.074	0.101	0.060	0.082	0.102	0.067	0.069	0.088	0.058
Model	0.084	0.095	0.069	0.094	0.103	0.065	0.083	0.092	0.066

in Fig. 41 for the same locations as in Fig. 40. In both the above sets of load tests maximum deflections occurred at the center of Panel A both for the test structure and the model.

Fig. 40 and 41 illustrate that satisfactory concordance between the deflections at elevated loads of a reinforced mortar model and the corresponding deflections of a large scale test structure is possible, even though a reinforced concrete slab may hardly be considered to exhibit purely elastic behavior under applied loads as high as twice the design live load.

Bending moments—Table 10 lists the bending moment coefficients that were measured in the test structure and the model due to dead load plus one live load. These moments occurred during Test 16 of the test structure and Test 106 of the model. They represent the resistance of the panels to bending in the north-south direction by summing the positive moments across the panel center line and the average negative moments across the panel edges. The moment resistance of the spandrel beams is not included in these coefficients.

Best agreement of M/WL coefficients between test structure and model occurred in Panel E and the greatest difference occurred in Panel G. This is understandable because the crack patterns in Panel E of test structure and model were symmetrical, thus causing the positive-moment strain gages in each case to yield comparable results since they were located at the panel center lines. On the other hand, crack patterns in Panel G of test structure and model were, understandably, unsymmetrical and slight differences in crack locations between test structure and model could easily cause significant differences in positive-moment strain gage readings since again these gages were located at panel center lines.

Cracking—Although the pattern of cracking at service load and at ultimate load in the quarter-scale model and in the test structure were quite similar in form, the test structure exhibited a far greater number of negative moment slab cracks than did the model. This may have been due, in part, to the fact that the 7/16 in. concrete cover in the test structure was made smaller than the 9/16 in. true scale cover required because of the need to preserve the scale effective depth while using #4 round bars instead of the true scale ⅜ in. square bars. The major interest in the crack study of this investigation was in the pattern of

cracking, particularly as it foreshadowed the formation of yield lines in the slab. Consequently, the discrepancy between number of cracks appearing in the model and in the test structure was not considered to be of particular significance.

Ultimate strength—Failure in the test structure occurred when Column 7 punched through the slab at a total load intensity of 369 lb per sq ft. Just prior to failure, yielding was evident in approximately 30 percent of the negative moment reinforcement and 15 percent of the positive moment reinforcement. The one-quarter scale model exhibited identical behavior at failure and the load which caused Column 7 of the model to punch through the slab was 360 lb per sq ft.

Summary—The striking similarity of structural performance, both qualitative and quantitative, between model and test structure appears to offer impressive support for the increased use of structural model testing as a tool in reinforced concrete research and design.

Yield-line analysis for ultimate flexural strength

The ultimate flexural capacity of the test structure was predicted by a consideration of the statics of the failure mechanisms shown in Fig. 42 and 43 and designated Mechanisms I and II, respectively. The yield moments on any potential yield line of the structure were computed by Eq. (A1) of the Appendix to the 1956 ACI Building Code (ACI 318-56):

$$M_y = bd^2 f_c' \, q \, (1 - 0.59 \, q) \qquad (10)$$

in which M_y is the yield moment, $q = p \, f_y/f_c'$, $f_y = 44{,}500$ psi, and $f_c' = 4715$ psi corresponding to the average 50-day cylinder strength of the slab concrete.

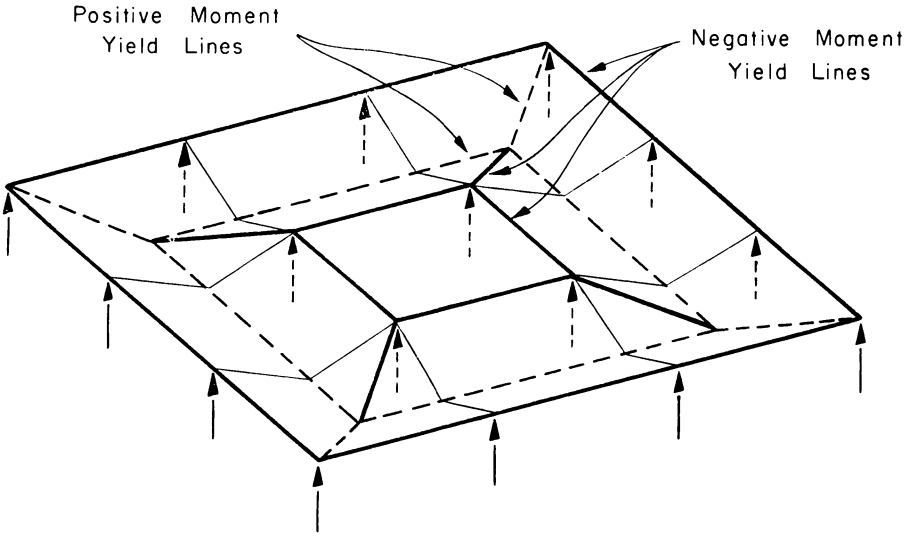

Fig. 42—Slab failure mechanism (Mechanism I)

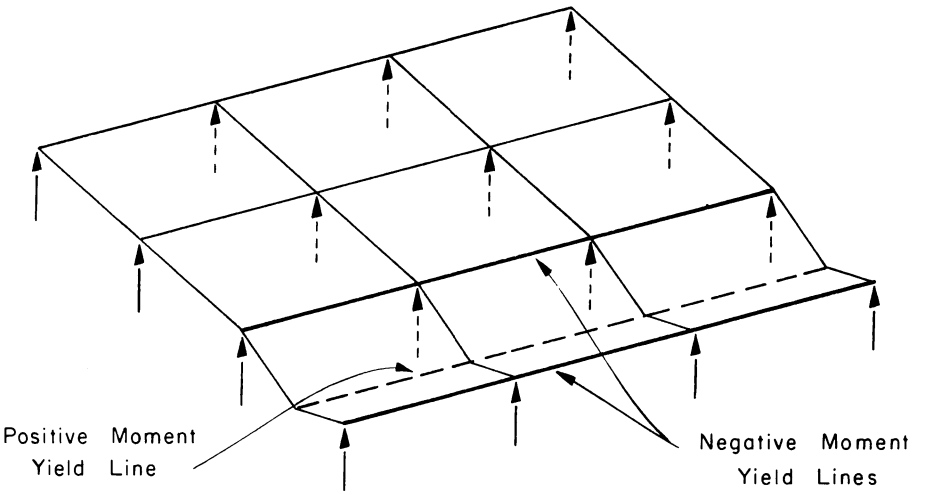

Fig. 43—Structural failure mechanism (Mechanism II)

In Mechanism I of Fig. 42, the collapse mechanism is confined exclusively to the slab and in no way involves the spandrel beams. In addition, only the exterior slab panels participate in the collapse mechanism. Negative moment yield lines, shown by solid lines in Fig. 42, are assumed to occur in the slab at the interior faces of the spandrel beams, along the center lines joining the interior columns, and along the interior half of each diagonal line joining the center of an interior column and its closest exterior corner column. Positive moment yield lines, shown by dashed lines in Fig. 42, are assumed to occur along lines parallel to the outer edges of the structure near midspan and along the exterior half of each diagonal line joining the center of an interior column and its closest exterior corner column.

Mechanism II, which is a simple "valley-type" collapse mechanism, involves a whole row of slab panels extending across the entire width of the structure plus the adjoining short edge spandrel beams. Negative moment yield lines, shown by solid lines in Fig. 43, are assumed to occur in the slab at the interior faces of the spandrel beams and along lines passing through the centroid* of reactions at the interior columns. The positive moment yield line, shown by a dashed line in Fig. 43, is assumed to occur along a line near midspan which is parallel to the two negative moment yield lines. For the test structure there are six possible "valley-type" collapse modes.

*The centroid of one half of the column reaction was located by assuming that the vertical shear transferred from the slab to the column is uniformly distributed around the periphery of the column.

TABLE 11—ULTIMATE LOAD BY YIELD-LINE THEORY

Panel designation	Predicted ultimate load, lb per sq ft	
	Mechanism I	Mechanism II
ABC	428	483
CFJ	350	417
ADG	394	455
GHJ	380	442
BEH	—	446
DEF	—	478

Results of the analysis of each of the four exterior sets of panels of Mechanism I and each of the six possible "valley-type" collapse modes are given in Table 11. The lowest value of the predicted collapse load given in Table 11 is 350 lb per sq ft and it occurs in Panels CFJ of Mechanism I. The lowest predicted collapse load for the Mechanism II mode is 417 lb per sq ft and it also occurs in Panels CFJ. Panels CFJ consistently exhibit the lowest values for the predicted collapse load because these panels combine a long span with a low effective depth caused by the location of all east-west reinforcement layers between the outermost north-south reinforcement layers.

The measured failure load of the test structures was 369 lb per sq ft and the predicted yield line collapse load is 350 lb per sq ft; or, in other words, the failure load was 1.054 times the predicted yield line failure load. However, the observed final mode of failure of the test structure was by shear, by punching through the slab of an interior column. If a shear failure had not intervened, it is possible that the actual collapse load could have risen considerably higher than the observed 369 lb per sq ft. The attainment of failure loads considerably in excess of the predicted yield line collapse loads has often been observed and has been attributed to a variety of factors. The most important of these factors are probably strain hardening of reinforcement in regions of moment concentration, and the development of membrane action in the slab because of the restraints offered by the slab in adjacent panels, the columns and the spandrel beams. However, it should be noted that almost all observed instances of hyper-strength have occurred in slabs supported on beams; in this case the shear strength of the slab is usually more than adequate.

The major reason that yield-line analysis, which is based on full redistribution of moments, appears to be a valid method for predicting a lower limit of the flexural capacity of a flat plate structure is that the usual type of slab appears to be capable of undergoing the rotations and distortions of shape necessary to accomplish the assumed moment redistribution. This ability of slabs to accommodate large rotations and distortions is a result of the very low reinforcement ratios usually employed in flat plate construction.

The center panel (Panel E) of the test structure is the most lightly reinforced panel of the whole structure. However, due to the configuration of adjoining panels, the center panel could only collapse in a simple "valley-type" mechanism in patricipation with two adjoining exterior

panels and the end spandrel beams, or in an "x-type" mechanism such as would occur in the case of a square plate built-in at all four edges. In neither of these two cases would the predicted collapse load of this structure be lower than the minimum predicted collapse load according to Mechanism I. However, if a very large flat plate structure having numerous panels in each direction is considered, then the interior panels would probably collapse in a simple Mechanism II, or "valley-type" mechanism, at a lower load than that corresponding to other collapse modes.

As an illustration of this, the computed collapse load of the center panel (Panel E), alone in a Mechanism II mode is 347 lb per sq ft. This value is 2.22 times the design total load, thus indicating a reasonably conservative safety factor. However, the center panel of the test structure does not represent a typical interior panel, because its edges were the first interior column lines of the structure, and hence more negative reinforcement was provided than would be required for a typical interior panel. In addition, the yield point of the slab reinforcement was 44,500 psi. The computed collapse load for a typical interior panel reinforced with intermediate grade steel having a yield point of 40,000 psi would be 292 lb per sq ft which is 1.87 times the design total load. For a structure composed of many bays of typical interior panels, the collapse load of the interior panels of the structure would probably be close to this predicted collapse load of a single typical interior panel in a Mechanism II mode.

Consideration of shear strength

Effect of flexural intensity — Previous experimental studies of the shear strength of slabs have primarily involved tests of square slabs loaded through a single centrally located column and supported along the edges without moment restraint. For such slab specimens, there are four typical stages of behavior in flexure.[13] In Stage I the slab is uncracked, in Stage II flexural cracking of the slab is spreading from the column along the diagonals toward the corners, in Stage III yielding of the tension reinforcement of the slab is spreading from the column toward the corners, and in Stage IV the slab is in a plastic state of rapidly increasing deflection. The ultimate flexural strength of the slab computed by yield-line theory corresponds to a flexural intensity in the transition between Stages III and IV. Due to strain hardening of reinforcement and membrane action, the loads in Stage IV usually exceed that computed by yield-line theory.

Elstner and Hognestad[13] found that the shear strength of a slab subject to a concentrated force at a column is different for the various stages of flexure. Shear strength decreases as increasing intensities of flexure are combined with shear. They defined punching of the column stub through the slab as a shear failure, provided that such punching

took place before development of the flexural strength of the slab as computed by yield-line theory. A slab failure by rapidly increasing deflection in Stage IV of flexure was regarded as a flexural failure, even when final destruction of the slab took place by punching after large slab deformations.

Moe's analysis—In a study[14] of 183 slab and 120 footing tests, Moe extended the Elstner-Hognestad work, and he developed the following empirical equation for ultimate shear strength:

$$V_u = bd \left[15 \left(1 - 0.075 \frac{r}{d}\right) - 5.25 \phi_0 \right] \sqrt{f_c'} \quad \text{.....(11)}$$

where

V_u = ultimate shear force
b = periphery around the loaded area = 4 x 18 = 72 in. for the flat plate test structure
d = effective depth of slab = 4.31 in. as an average for the two layers of negative reinforcement
r = side dimension of column = 18 in.
ϕ_0 = V_u/V_{flex}
V_{flex} = ultimate shear force if flexural failure had occurred
f_c' = concrete cylinder strength = 4715 psi

The variable ϕ_0 in Eq. (11) is the ratio of shear capacity to the flexural capacity computed by yield-line theory. Most of the laboratory specimens considered by Moe were designed to fail in shear under flexural effects in Stages II and III, so that ϕ_0 was less than unity. For a balanced failure condition, the flexural and shear capacities are reached simultaneously, so that ϕ_0 equals unity. This corresponds to the transition between Stages III and IV of flexure. Since ϕ_0 cannot exceed unity in Moe's equation, Eq. (11) is not applicable in Stage IV of flexure.

Immediately before failure of the present flat plate slab by shear punching around Column 7, the average recorded steel strain at the four faces of the column was about 0.01, which is seven times the reinforcement yield strain. This condition of high steel strain probably corresponds to Stage IV of flexure. If it is assumed that the flexural intensity corresponds to the *beginning* of Stage IV, ϕ_0 in Eq. (11) may be taken equal to unity, so that Eq. (11) becomes:

$$V_u = bd \left(9.75 - 1.125 \frac{r}{d}\right) \sqrt{f_c'} \quad \text{.....(12)}$$

The ultimate shear force V_u, computed by Eq. (12) is 107,700 lb. The column reactions were not measured in the PCA test. The model test at the University of Illinois[4] indicated that the shear force is approximately equal to the load on 1.08 times one slab panel, that is, the load on $1.08 \times 15^2 = 243$ sq ft. The force of 107,700 lb then corresponds to a uniform slab load of 443 lb per sq ft. The observed load of 369 lb per sq ft is only 83 percent of the computed value, which indicates that the flexural intensity may have been well into Stage IV, that is, beyond the range of applicability of Moe's equations.

Committee 426 analysis—Based on Moe's work, the ultimate strength design procedures developed by ACI-ASCE Committee 426 (formerly 326)[15] involve the equation:

$$V_u = 4.0\ bd\sqrt{f_c'} \quad \text{(13)}$$

in which b is the periphery of a pseudo-critical section located at a distance $d/2$ from the periphery of the loaded area, and is equal to 4 (18 + 4.31) in. at Column 7.

The ultimate shear force V_u, computed by Eq. (13) is 106,000 lb, corresponding to a slab load of 436 lb per sq ft. The measured slab load is 85 percent of this computed value.

Condition of test slab at failure—Failure of the present flat plate test structure took place by shear punching around Column 7 at a slab load about 85 percent of that corresponding to shear capacities computed by Eq. (12) or (13). This same ultimate slab load was 105 percent of the flexural capacity computed by the yield-line Mechanism I shown in Fig. 42. It should be noted that this mechanism involves formation of deflected troughs north and east of Column 7.

At failure, the average measured strain in the slab reinforcing bars passing over the faces of Column 7 from the north and east were 0.028 and 0.009, or 19 and 6 times the steel yield strain, respectively. At the same load, most of the gages crossing the positive yield lines in the bottom of the troughs north and east of the column registered only about three-quarters of the steel yield strain. It seems that heavy concentrations of slab rotation were taking place across the negative yield lines at the column, while the positive yield lines were in the process of developing. It is thought, therefore, that the condition of flexure near Column 7 was one corresponding to Stage IV as defined by Elstner-Hognestad and Moe.

The concentration of slab rotation at Column 7 is analogous to the concentration of rotation which occurs in a two-span beam after a yield hinge has formed over the interior support, while redistribution is taking place toward formation of yield hinges in the two spans. It is well known that the rotation capacity of such a hinge in a beam is limited; it becomes exhausted when crushing of the concrete takes place in the compression zone of the hinge. The behavior of the test slab suggests that rotation capacity across certain yield lines in multipanel slab systems may be similarly limited. Rotation capacity may become exhausted near columns by a destruction of the compression zone manifesting itself as shear punching, before a full collapse system of yield lines has formed.

Shear strength in Stage IV of flexure—Since failures of slabs in Stage IV have been defined as flexural failures in previous work, little is

known about shear strength in this stage of flexure. However, certain findings in previous slab tests are believed to be pertinent to the case at hand:

First, tests by Kinnunen-Nylander[16] and Elstner-Hognestad[13] have shown that even lightly reinforced slabs loaded through a column will eventually fail by punching shear. Such slabs develop very large deflections and a flexural strength well in excess of that computed by yield-line theory, but the final destruction of the slab usually takes place by punching.

Secondly, Moe[14] and Kinnunen-Nylander[16] developed methods of detecting internal diagonal cracking in slabs around a loaded column. It was found that cracking along the surface of a truncated cone or pyramid took place at 50 to 75 percent of the ultimate shear capacity. Hence, ultimate strength was governed by destruction of the concrete compression zone directly around the column periphery well after diagonal cracking. The Swedish[16] experiments were particularly convincing in this regard. The shear strength of normal reinforced concrete slabs was compared with special slabs in which diagonal cracking was introduced by a cone-shaped piece of cardboard placed in the form before concreting.

Finally, Kinnunen-Nylander[16] arrived at an improved understanding of the shear failure mechanism in Stage IV of flexure. After diagonal cracking around a column, slab portions adjacent to the column tend to rotate as rigid bodies about axes located in the compression zone below the root of the diagonal cracking. When yielding of the flexural reinforcement crossing the diagonal cracking then develops, these cracks will extend into the compression zone. After a certain amount of steel yielding, accompanied by slab rotation and crack penetration, the compression zone will be destroyed by punching at an abnormally low shear stress.

Summary—The observed ultimate strength of the present flat plate test structure was about 85 percent of the shear capacities computed by Eq. (11) and (12). Extensive yielding of flexural reinforcement at the interior columns was in progress at failure, and the system of yield lines shown in Fig. 42 was in the process of developing. It is believed that a heavy concentration of slab rotation existed across yield lines near the interior columns and caused diagonal cracks to penetrate into the compression zone, thus precipitating a secondary punching shear failure.

It follows from the failure mechanism involved that the shear strength of the test slab could probably have been increased by increasing the amount of negative flexural reinforcement over the interior columns, or possibly by increasing the yield point of that reinforcement, thus delaying yielding and limiting the rotation across negative yield lines required to develop the positive yield lines.

CONCLUDING REMARKS

Service load behavior

In view of the agreement found between measured moments at service load and the computed total static moments, it is confirmed that the equations of statics are applicable to flat plate structures, as they obviously must be. It is desirable to continue recognition of satisfactory service behavior of numerous structures built by current procedures. However, when reduced moment coefficients such as those involved in the empirical method of the 1956 and 1963 ACI Building Codes are used, the true nature of these reductions should be appreciated.

Because positive moment cracking at service load was extremely slight relative to negative moment cracking, and because stresses in negative reinforcement were much higher than in positive reinforcement, there appears to be some justification for re-apportioning the total panel reinforcement so that the proportion of reinforcement provided in the column strips over interior columns is increased.

Measurements of moments along the junction of slab and spandrel beam indicated that some reduction in the amount of negative reinforcement in middle strips and wall strips at the discontinuous edges of corner panels may be possible in common flat plate construction having edge beams and edge conditions similar to those used in this test.

Deflection

At the center point of the interior panel of the test structure satisfactory agreement between measured short-time deflection and deflection computed by Eq. (1) and (2) was obtained for superimposed loads considerably in excess of the design live load. It is therefore concluded that these equations, derived for the uncracked section, provide a reasonably reliable means for predicting service load deflection in interior panels of multibay flat plate structures.

Ultimate flexural strength

Because of the ability of slabs to undergo the large rotations and distortions of shape necessary to accomplish the assumed moment redistributions, yield line analysis appears to be a valid method for predicting the flexural load capacity of flat plate structures. The flexural collapse load of a plate structure composed of many bays of typical interior panels extending in each direction may often be controlled by the flexural resistance of the interior panels acting individually as simple "valley-type" mechanisms.

Shear strength

Because extensive yielding of the negative reinforcement near the interior columns was in evidence just prior to punching of the slab, and because the observed ultimate flexural strength exceeded the ca-

pacity computed by yield-line theory, the mode of failure was classified as a secondary shear failure. Had ultimate slab strength not been governed by shear, it is probable that the collapse load would have been considerably higher than that observed, due to the reserve flexural strength afforded by strain hardening of reinforcement and the development of membrane action in the slab.

Comparison with one-quarter scale model

Deflections, crack patterns, distribution of service load moments, mode of failure, and ultimate capacity of the test structure were closely in agreement with corresponding observations for the one-quarter scale model. It is believed that the value of relatively small scale reinforced mortar models in structural research and design has been convincingly demonstrated.

REFERENCES

1. "Research on Multiple-Panel Reinforced Concrete Floor Systems," ACI JOURNAL, *Proceedings* V. 56, No. 2, Aug. 1959, Newsletter, pp. 11-13.

2. Hognestad, E.; Hanson, N. W.; Kriz, L. B.; and Kurvits, O. A., "Facilities and Test Methods of PCA Structural Laboratory," *Journal,* PCA Research and Development Laboratories, V. 1: No. 1, Jan. 1959, pp. 12-20, 40-44; No. 2, May 1959, pp. 30-37; No. 3, Sept. 1959, pp. 33-51. Also PCA *Development Department Bulletin* D33.

3. Hanson, N. W.; Kurvits, O. A.; and Mattock, A. H., "Semi-Automatic Processing of Strain and Load Measurements," *Journal,* PCA Research and Development Laboratories, V. 3, No. 2, May 1961, pp. 27-31.

4. Hatcher, D. S.; Sozen, M. A.; and Siess, C. P., "A Study of Tests on a Flat Plate and a Flat Slab," *Structural Research Series* No. 217, Civil Engineering Studies, University of Illinois, Urbana, July 1961.

5. Guralnick, S. A., "Some Basic Aspects of the Problem of Shear Strength of Reinforced Concrete Beams," PhD Thesis, Graduate School of Cornell University, Ithaca, N. Y., Feb. 1958.

6. Timoshenko, S. P., and Woinowsky-Krieger, S., *Theory of Plates and Shells,* Second Edition, McGraw-Hill Book Co., Inc., New York, 1959, pp. 245-249.

7. Nichols, John R., "Statical Limitations Upon the Steel Requirements in Reinforced Concrete Flat Slab Floors," *Transactions,* ASCE, V. 77, 1914, pp. 1670-1681.

8. Siess, C. P., "Re-Examination of Nichols' Expression for the Static Moment in a Flat Slab Floor," ACI JOURNAL, *Proceedings* V. 55, No. 7, Jan. 1959, pp. 811-814.

9. Hognestad, E., "Yield-Line Theory for the Ultimate Flexural Strength of Reinforced Concrete Slabs," ACI JOURNAL, *Proceedings* V. 49, No. 6, Mar. 1963, pp. 637-656.

10. Westergaard, H. M., and Slater, W. A., "Moments and Stresses in Slabs," ACI JOURNAL, *Proceedings* V. 17, 1921, pp. 415-538.

11. Mila, F. J., "Relationship Between Reinforcement Strain and Bending Moment in Reinforced Concrete," Unpublished Report, Department of Civil Engineering, University of Illinois, Urbana, July 1960.

12. Lash, S. D., "Ultimate Strength and Cracking Resistance of Lightly Reinforced Beams," ACI JOURNAL, *Proceedings* V. 49, No. 5, Feb. 1953, pp. 573-582.

13. Elstner, R. C., and Hognestad, E., "Shearing Strength of Reinforced Concrete Slabs," ACI JOURNAL, *Proceedings* V. 53, No. 1, July 1956, pp. 29-58.

14. Moe, Johannes, "Shearing Strength of Reinforced Concrete Slabs and Footings Under Concentrated Loads," *Development Department Bulletin* D47, Portland Cement Association, Research and Development Laboratories, Skokie, Ill., Apr. 1961, 130 pp.

15. ACI-ASCE Committee 326, "Shear and Diagonal Tension," ACI JOURNAL, *Proceedings* V. 59, No. 1, Jan. 1962, pp. 1-30; No. 2, Feb. 1962, pp. 277-334; No. 3, Mar. 1962, pp. 352-396.

16. Kinnunen, S., and Nylander, H., "Punching of Concrete Slabs Without Shear Reinforcement," *Transactions,* Royal Institute of Technology (Stockholm), No. 158, 1960, 110 pp.

ACKNOWLEDGMENTS

The investigation reported herein was carried out in the Structural Laboratory of the Portland Cement Association under the direction of Eivind Hognestad, and contributions were made by several members of the laboratory staff. Particular credit is due Alan H. Mattock, principal development engineer; James E. Carpenter, associate development engineer; Ferdinand S. Rostásy, former associate development engineer, as well as B. W. Fullhart and O. A. Kurvits, senior technicians.

APPENDIX

DETERMINATION OF MOMENTS FROM REINFORCEMENT STRAINS

Background and purpose

This Appendix describes an experimental and analytical investigation of the relationship between strains measured in the reinforcing bars and the bending moments acting in a reinforced concrete slab. A careful development of this relationship was necessary in order that the distribution of resisting moments throughout the test structure could be determined.

Similar studies have been made elsewhere,[10,11] but the results reported are not directly applicable in this case.

Scope

Sixteen rectangular beams, simulating strips of the flat plate structure were tested. The results of these tests were used as a basis for the development of a relationship between bending moment and reinforcement strain.

The beams were reinforced in tension only, with reinforcement percentages identical to those used in the test slab. The depth of the beams was 5¼ in., equal to the nominal thickness of the slab, while the width was varied as whole multiples of the bar spacings and ranged from 11½ to 17 in. The effective depth of the reinforcement was either 4 1/16 or 4 9/16 in., corresponding to effective depths occurring in the test slab. All beams were 10 ft long. The

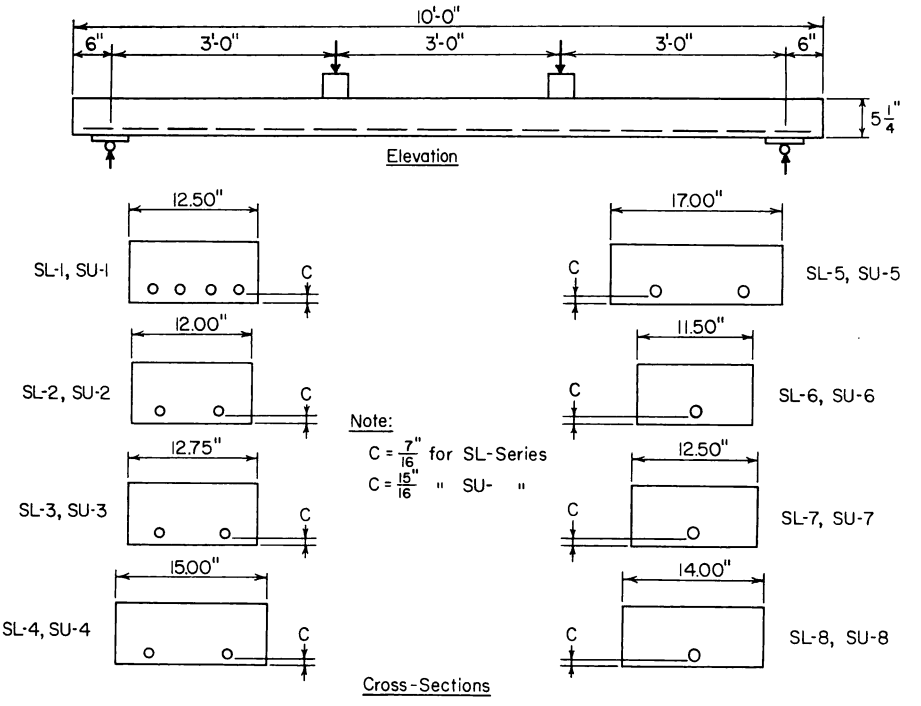

Fig. A1—Dimensions and reinforcement of strip beams

cross sections and elevation of these beams are shown in Fig. A1. The 16 strip beams reproduced the 16 different combinations of bar spacing and effective depth which occurred in the test slab.

The strip beams were simply supported with a 9-ft span between supports. Concentrated loads applied at the third points on the beams, as seen in Fig. A2, provided a constant moment region in the middle third of the test specimens.

Steel strains were recorded continuously during each test by SR-4 strain gages attached at the midpoint of one bar in each beam.

Materials and tests

The materials used in the fabrication of the strip beams were identical to those used in the test structure.

The concrete mix proportions were as shown in Table 2. The 28-day cylinder strength for each beam, f_c', is listed in Table A1.

Reinforcement consisted of #4 deformed bars from the same lot as the slab reinforcement; intermediate grade steel with a yield point of 44,500 psi.

Fabrication of strip beams — The beams were cast in plywood forms in groups of four, over a period of 19 days. Steel chairs tied to the formwork provided support for the reinforcement and maintained the proper cover.

The concrete was placed with the aid of an internal vibrator. The beams were covered by polyethylene plastic sheets which were removed after 3 days, at which time the forms were struck. Subsequently the specimens were stored at 70 F and 50 percent relative humidity. Two 6 x 12-in. cylinders were cast for each beam and cured alongside the beams.

TABLE A1—PROPERTIES AND TEST RESULTS OF STRIP BEAM SPECIMENS

Beam	d, in.	b, in.	f_c', psi	No. of bars	Bar spacing, in.	A_s, sq in.	p, percent	Computed design moment, M_D, in.-kips	Computed yield moment, M_y, in.-kips	Test ultimate moment, M_u, in.-kips	$\frac{M_{u\,(test)}}{M_{y\,(calc)}}$
SL-1	4.56	12.50	4160	4	3⅛	0.80	1.40	61.8	150.0	144.0	0.960
-2	4.56	12.00	4270	2	6	0.40	0.73	32.6	78.4	77.4	0.987
-3	4.56	12.75	2655	2	6⅜	0.40	0.69	32.7	79.0	79.4	1.005
-4	4.56	15.00	3640	2	7½	0.40	0.58	33.0	79.1	79.8	1.009
-5	4.56	17.00	3530	2	8½	0.40	0.52	33.2	79.5	83.5	1.050
-6	4.56	11.50	4125	1	11½	0.20	0.38	16.8	39.9	43.3	1.085
-7	4.56	12.50	3500	1	12½	0.20	0.35	16.8	40.1	44.0	1.097
-8	4.56	14.00	2580	1	14	0.20	0.31	16.9	40.0	44.8	1.120
SU-1	4.06	12.50	3385	4	3⅛	0.80	1.58	50.9	132.2	126.3	0.955
-2	4.06	12.00	4210	2	6	0.40	0.82	28.9	69.1	72.1	1.043
-3	4.06	12.75	2725	2	6⅜	0.40	0.77	29.0	69.3	71.1	1.026
-4	4.06	15.00	3720	2	7½	0.40	0.66	29.2	70.7	72.5	1.025
-5	4.06	17.00	3320	2	8½	0.40	0.58	29.4	71.0	74.2	1.045
-6	4.06	11.50	3870	1	11½	0.20	0.43	14.9	35.6	36.3	1.020
-7	4.06	12.50	2945	1	12½	0.20	0.39	14.9	35.2	38.5	1.094
-8	4.06	14.00	2775	1	14	0.20	0.35	15.0	35.6	38.0	1.067
										Average $M_{u\,(test)} / M_{y\,(calc)}$	1.037

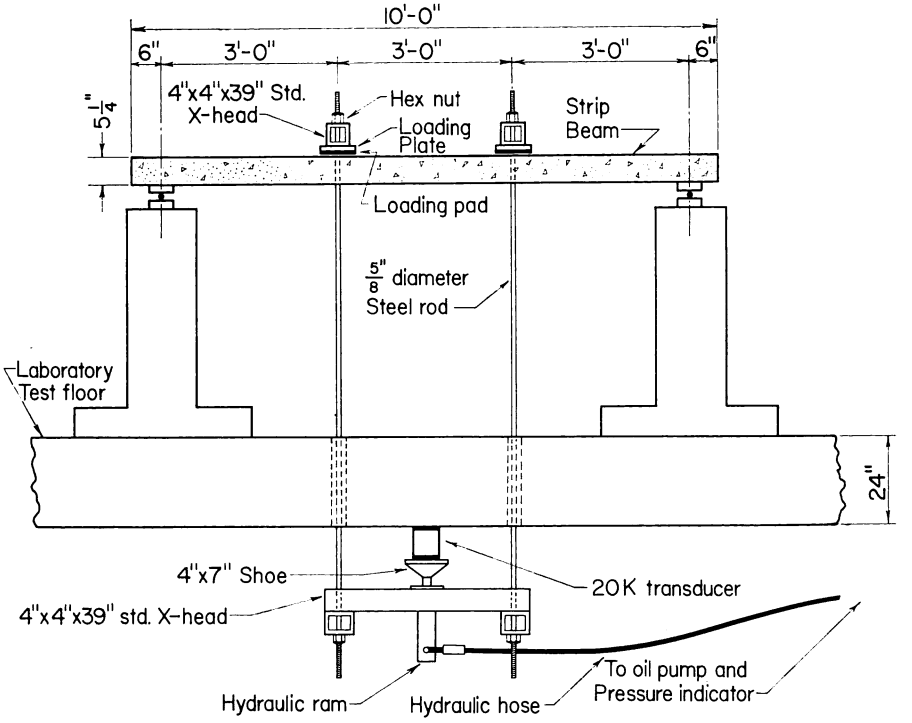

Fig. A2—Elevation of arrangement for strip beam test

Instrumentation — One SR-4 strain gage of 1 in. gage length was attached at the center of one reinforcing bar in each beam. These gages were mounted and waterproofed as described elsewhere.[2] The steel strain was recorded continuously on a strain recorder.

Loading arrangement — Two equal loads were applied at the third points of the span by a 20,000 lb capacity hydraulic ram acting through a system of cross-heads and pull-rods as seen in Fig. A2. The loads were monitored on an oil pump and pressure indicator unit, and were measured accurately by a load cell[2] positioned between the ram and the test floor. The test beams were supported on pedestals and rested on steel rollers placed between pairs of steel bearing plates.

Test procedure — All beams were tested at 28 days. They were loaded in three cycles by increasing the applied load in increments of ¼ total design load from zero to one design load and back to zero, zero to 1½ design loads and back to zero, and from zero to ultimate strength.

The working stress method of the 1956 ACI Building Code was applied to compute the design moments, using an allowable steel stress of 20,000 psi, an allowable concrete stress of 1350 psi and a modular ratio of 10. The computed design moment M_D, is given in Table A1 for each specimen.

Test results

Moment-strain curves were plotted for each beam from the experimental data. Idealized curves, characterizing the empirical curves, were then drawn so as to simplify the determination of bending moments.

A typical moment-strain curve is shown in Fig. A3. Since only live load

strains in the steel were measured during the tests, the curves were extrapolated to zero to include dead load moments and strains. This extrapolation was accomplished using the strains in the reinforcement due to the dead weight of the beams plus the loading equipment which were computed based on a transformed, uncracked section. The 28-day cylinder strength was used to compute $E_c = 1.8 \times 10^6$ psi $+ 460 f_c'$ for each beam. E_s was taken to be 30,000,000 psi.

The form of the moment-strain curves was found to be similar for all the strip beams. For any particular beam, the lower parts of the initial loading and reloading curves had approximately the same slopes up to the load at which flexural cracking first appeared. From this load to the highest previously applied load, the reloading curves had a steeper slope than during first loading. The upper parts of the three loading curves all tended to have the same slope.

The ultimate strength of all the beams was governed by yielding of the reinforcement. This type of flexural failure was expected, since the ratios of reinforcement in the beams were substantially lower than the balanced values for ultimate strength design.

Analysis of test results

The analysis of the strip beam test results involved producing idealized curves which approximate the empirical moment-strain diagrams. This was done so that the idealized curves could be used in an electronic computer program to convert slab reinforcement strain into moments per unit width when reducing the data obtained in the slab test.

As Westergaard-Slater[10] illustrated, the moment-strain diagrams consist of three parts: (1) that in which the concrete remains essentially uncracked; (2) that in which the concrete has cracked, but the stress in the steel remains below the yield point; and (3) that in which the steel stress is at or beyond the yield point. These first two parts approach straight lines which can be defined by the origin, the point at which flexural cracking of the concrete occurs, and the point at which the reinforcement yields. For strains greater than the yield strain of the steel, the bending moment in the beams is considered to remain constant and the moment-strain diagram becomes a horizontal line. The idealized curve for Beam SL-3 is shown in Fig. A3.

For the purpose of deriving the idealized moment-strain curve, the bending moment at flexural cracking was computed on the basis of a plain gross section and a modulus of rupture of 500 psi. The cracking moment, M_{cr} per unit width of the beams, is then

$$\frac{M_{cr}}{b} = \frac{f_r h^2}{6} = 2.30 \text{ in.-kips per in.} \quad \text{.....(A1)}$$

for $h = 5\frac{1}{4}$ in., the total depth of the strip beams.

The steel strain corresponding to initial tensile cracking in the concrete was estimated from the 16 experimental moment-strain diagrams and is designated ε_{cr}. An average value of 150 microin. per in. was utilized for all beams to facilitate the computer program. This figure should be somewhat less for the beams with smaller effective depth (i.e., SU beams), however, the error introduced is slight, particularly in the upper region of the curves. Thus the first point on the idealized curves is defined by M_{cr} and ε_{cr} and is identical for all beams if the ordinates are moments per unit width of the beams.

The coordinates of the second point on the idealized curve are the moment and strain at yield of the reinforcement. The moments at which yielding of the reinforcement first took place were predicted for each beam using Eq. (A1) in the Appendix of the 1956 ACI Building Code:

$$M_y = bd^2 f_c' q (1 - 0.59q) \quad \text{.....(A2)}$$

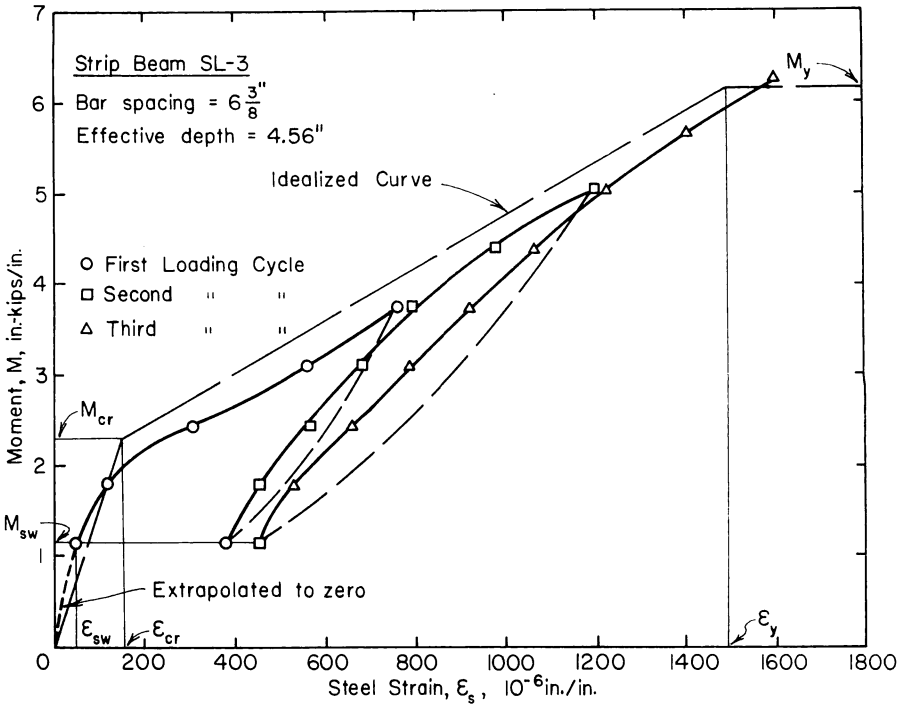

Fig. A3—Typical and idealized moment-strain curves for a strip beam

in which M_y is the ultimate resisting moment of the beams, $q = p\, f_y/f_c'$, $f_y = 44{,}500$ psi and $f_c' = 4715$ psi.* Table A1 lists the computed moments M_y, which are seen to be in close agreement with the measured ultimate moments.

The yield strain, ε_y, was obtained by dividing the yield strength of the steel (44,500 psi) by the modulus of elasticity which was taken as 30×10^6 psi. Thus, for all beams, ε_y is 1480 microin. per in.

Straight lines were drawn joining the origin, the point of flexural cracking and the yield point to form the idealized curves for first loading shown in Fig. A4 and A5. These idealized moment-strain diagrams approximate the empirical curves for first loading reasonably closely, as can be seen in Fig. A3.

For loading cycles other than the first, consideration must be given to the influence of residual strains remaining after earlier load cycles, and also to changes in shape of the idealized moment-strain diagram due to prior cracking.

The idealized moment-strain diagram for the second and all subsequent loading cycles will be of the form shown in Fig. A7. The diagram commences at a distance ε_r from the origin, where ε_r is the residual strain. ε_r was obtained in the tests by subtracting the initial zero load strain readings from the zero load strain readings for the test under consideration. Examination of the strip beam test data indicated that the first part of the reloading diagram could be represented as a straight line parallel to the first part of the initial loading diagram, and extending up to a mo-

*4715 psi is the 50-day compressive cylinder strength of the slab concrete.

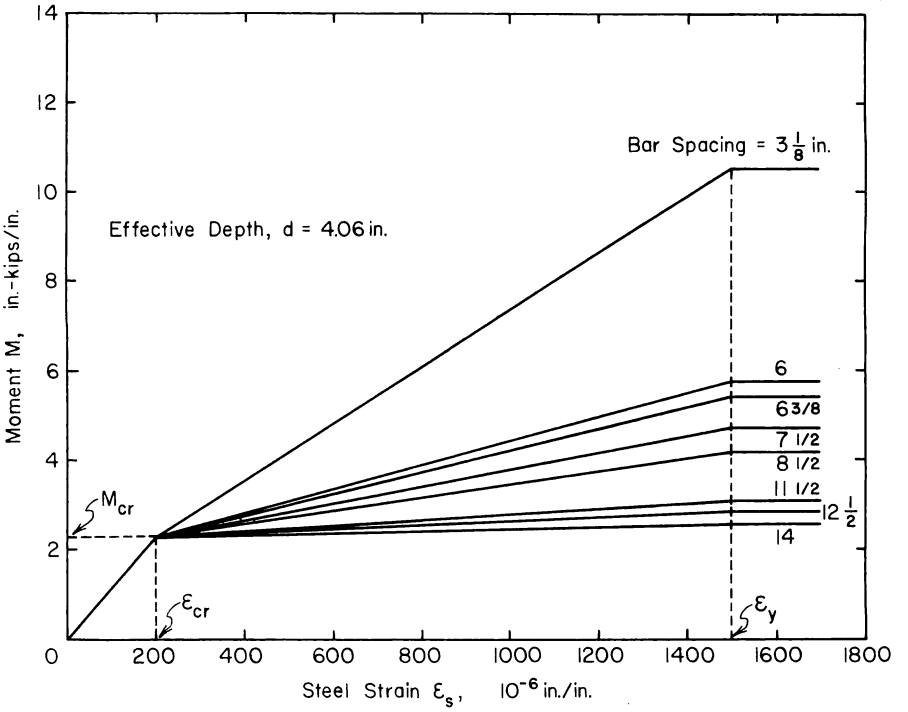

Fig. A4—Idealized moment-strain curves for strip beams with effective depth 4.06 in.

ment equal to the initial cracking moment. From this point onward, until the initial loading diagram was reached, the strain was found to increase approximately at the rate predicted by the straight line theory for reinforced concrete, assuming a cracked section and a modular ratio of 8.

The slope m_2 of the second part of the idealized moment-strain curve, for the second and all subsequent loading cycles, was therefore computed for unit width of beam, using

$$m_2 = \frac{M}{b\varepsilon_s} = \frac{A_s\, jdE_s}{b} \quad \text{(A3)}$$

This is simply an expression of the slope for the straight line cracked section theory using a modular ratio of 8. The slopes of the actual reloading curves on the third load cycle for the strip beams were measured and entered in Table A2 together with the computed slopes. It is seen that the measured slopes are always greater than the calculated slopes. Fig. A6 shows relationships between m_2 and bar spacing for the two effective depths.

Thus, with the additional consideration of residual strain and the effect of repeated loads on the flat plate test structure, the idealized moment-strain diagram is complete. This is shown in Fig. A7.

Application of idealized moment-strain diagram to interpretation of slab test strain data

The moment M, in Fig. A7 includes the moment due to the dead weight of the structure, in addition to the applied live load moments. Since the measured strains in the flat plate test structure were those due only to live loads, it was necessary to estimate the strains due to dead load before the idealized

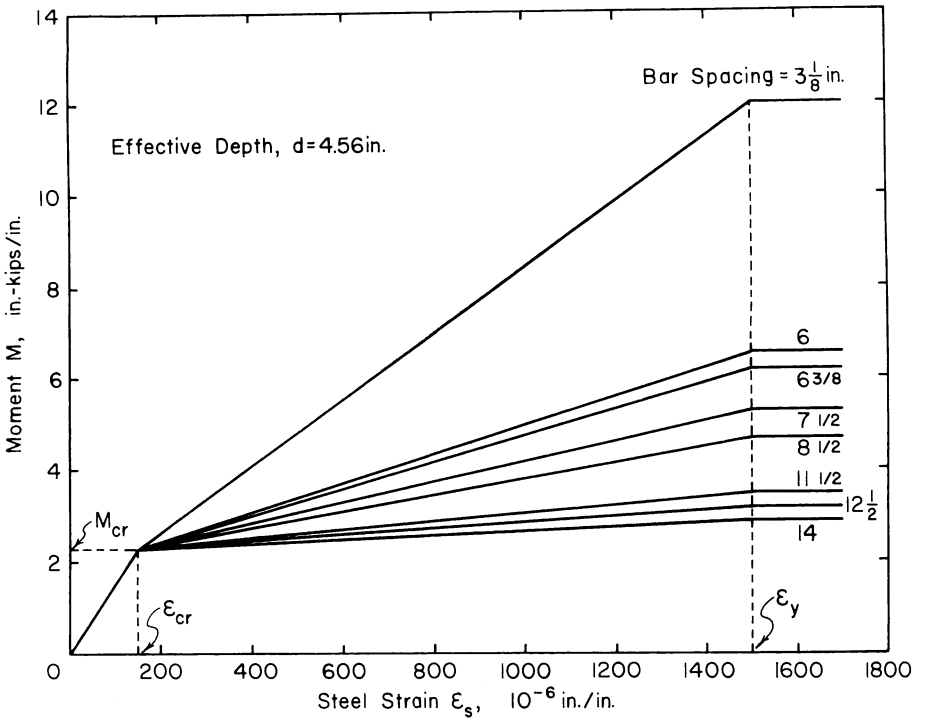

Fig. A5—Idealized moment-strain curves for strip beams with effective depth 4.56 in.

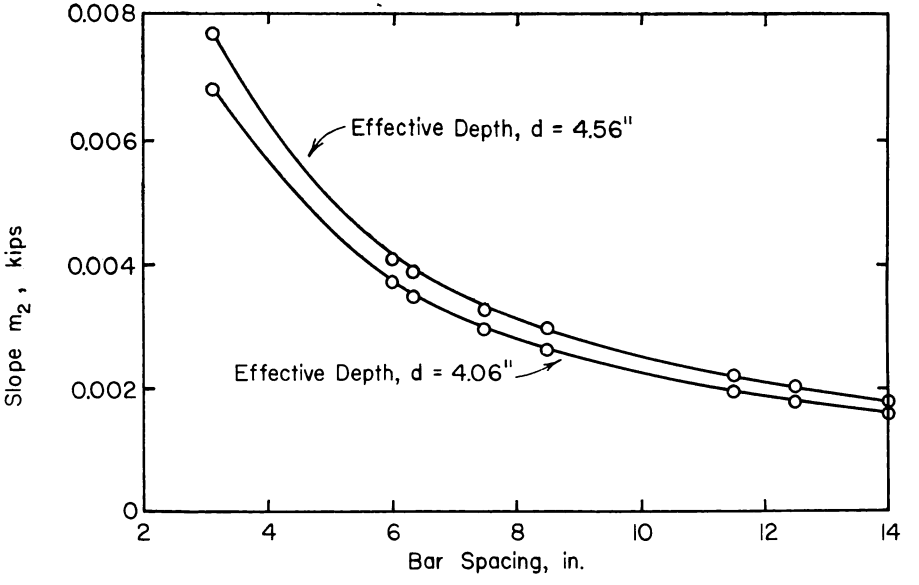

Fig. A6—Theoretical slope (m_2) of reloading curve versus bar spacing

TABLE A2—SLOPES OF MOMENT-STEEL STRAIN CURVES AFTER TENSION CRACKING HAS OCCURRED IN STRIP BEAMS

Beam No.	d, in.	Bar spacing in.	Computed slope of reloading curve, m_2, kips	Measured slope of reloading curve, kips
SL-1	4.56	3⅛	0.0077	0.0088
-2	4.56	6	0.0041	0.0059
-3	4.56	6¾	0.0039	0.0046
-4	4.56	7½	0.0033	0.0038
-5	4.56	8½	0.0030	0.0037
-6	4.56	11½	0.0022	0.0027
-7	4.56	12½	0.0020	0.0026
-8	4.56	14	0.0018	0.0022
SU-1	4.06	3⅛	0.0068	0.0079
-2	4.06	6	0.0037	0.0049
-3	4.06	6¾	0.0035	0.0038
-4	4.06	7½	0.0030	0.0037
-5	4.06	8½	0.0026	0.0043
-6	4.06	11½	0.0020	0.0027
-7	4.06	12½	0.0018	0.0024
-8	4.06	14	0.0016	0.0023

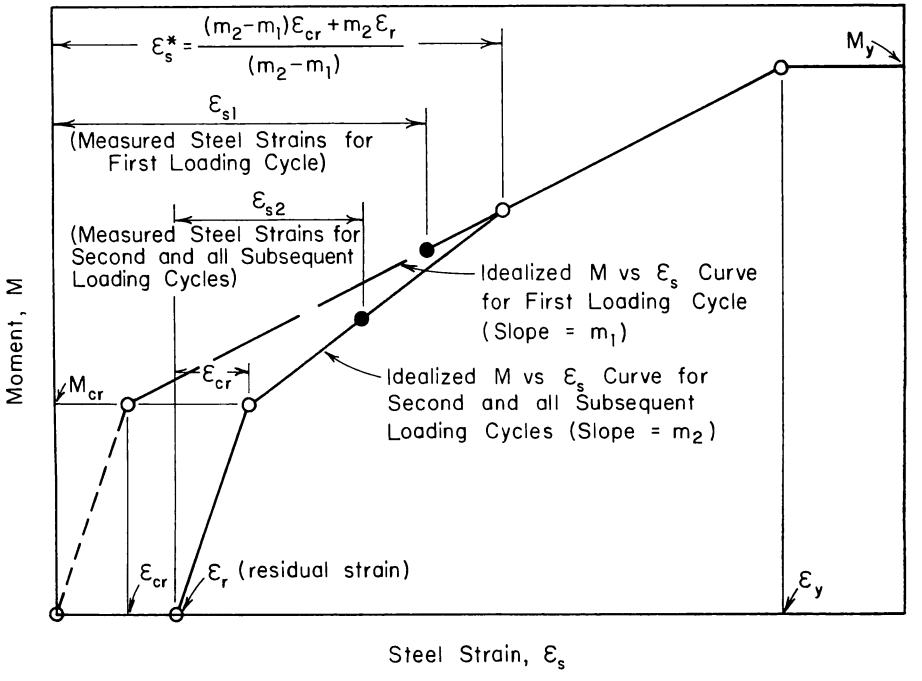

Fig. A7—Idealized moment-strain curves for strip beams subjected to repeated cycles of loading

moment-strain diagram could be utilized.

Load-strain curves were plotted using experimental data obtained from the strain gages in the slab. In these diagrams, the total load was plotted, and therefore the origin of these curves is actually at 73 lb per sq ft, the dead weight of the test structure. Since the lower part of these load-strain diagrams was essentially linear, it was possible to extrapolate to zero load, and the dead load strains were then obtained. These strains were averaged for each bar spacing, taking into consideration the location of the gage in the slab, and were added to the measured live load strains for the load stage under consideration. The load-strain diagrams were plotted from the data of Test 3 (see Table 3).

Bending moments in the test structure were obtained from the measured steel strains using a digital computer, programmed to interpret the strain data in terms of the appropriate idealized moment-strain relation. To facilitate the computer program, residual strains were neglected if the concrete was uncracked at the gage under consideration. This was done by inspection of the data. In this case the moments were calculated using the idealized relationship for initial loading. If the concrete was cracked, then the flexural moments were obtained using the idealized moment-strain relationship for the reloading condition.

The moment resulting from this computation is the total bending moment resisted by a strip of width equal to the bar spacing at the strain gage under consideration. Since nearly every second reinforcing bar was instrumented, the moment resisted by slab strips without a strain gage attached to the steel was taken to be equal to that of an adjacent instrumented strip of the same width.

NOTATION

A_s = area of tensile reinforcement
b = width of section
C_1 = constant
c = side width of a column in flexural computations
D_r = effective flexural rigidity of a plate per unit width
d = depth from compression face of beam or slab to centroid of tensile reinforcement
E = modulus of elasticity
E_c = modulus of elasticity of concrete
E_s = modulus of elasticity of steel
f_c = compressive unit stress in extreme fiber of concrete in flexure
f_c' = strength in compression of 6 x 12-in. cylinders
f_r = modulus of rupture of concrete
f_s = tensile stress in reinforcement
f_u = ultimate strength of steel
f_y = yield point of steel
h = total depth of slab
jd = distance between centroids of compression and tension
L = span length of a panel center-to-center of columns
M = applied bending moment
M_{cr} = bending moment at which flexural cracking takes place
M_D = computed design moment for strip beams
M_d = total ACI design moment for sections across entire structure
M_0 = numerical sum of assumed positive and average negative moments at the critical design sections of a flat slab panel
M_t = total measured moment acting on a section of slab extending across entire structure
M_u = measured ultimate bending moment
M_y = computed ultimate resisting moment
M_1 = total positive moment at midspan across full width of panel
M_2 = total negative moment on a column line and around the periphery of column capitals
m_1, m_2 = slopes defined by Fig. A7
n = ratio of modulus of elasticity of steel to that of concrete
p = ratio of area of steel to area of concrete, A_s/bd
q = intensity of distributed load, also reinforcing index, $p\, f_y/f_c'$

r = side width of column in shear computations
s = denotes scale of model
V = shear force
V_{flex} = ultimate shear force if flexural failure had occurred
V_u = ultimate shear force
v = shear stress
W = total dead and live load on panel
w = deflection of slab
ε_{cr} = steel strain at which flexural cracking takes place
ε_r = residual strain in concrete
ε_s = steel strain
ε_y = steel strain at yield
ϕ_v = V_u/V_{flex}

Received by the Institute Aug. 16, 1962. Title No. 60-55 is a part of copyrighted Journal of the American Concrete Institute, Proceedings V. 60, No. 9, Sept. 1963. Separate prints are available at $1.00 each, cash with order.

American Concrete Institute, P. O. Box 4754, Redford Station, Detroit 19, Mich.

Discussion of this paper should reach ACI headquarters in triplicate by Dec. 1, 1963, for publication in the Part 2, March 1964 JOURNAL.

Sinopsis — Résumés — Zusammenfassung

Ensayo en Laboratorio de una Estructura de Placa Plana de 45 pies Cuadrados

Se condujeron estudios coordinados, experimentales y analíticos, sobre sistemas de pisos de concreto reforzado en la Universidad de Illinois y en los laboratorios de la Asociación de Cemento Portland (PCA), con el propósito de proveer una base para métodos de diseño más racionales que aquellos shora en uso. Se espera que resulter sistemas de piso más económicos, de estos métodos mejorados de diseño. El programa experimentalen la Universidad de Illinois comprende el ensaye de modelos a un cuarto de escala de varios sistemas de pisos.

Para facilitar la interpretación de los ensayes con modelos a un cuarto de escala, se ensayó en los Laboratorios de la PCA una placa plana a escala tres-cuartos, midiendo en 45 pies cuadrados. Se compararó la distribución de momentos en la losa encontrados de los ensayes para cargas de servicio con valores de momentos en la losa obtenidos por los métodos usuales de diseño. También, el comportamiento observado a la rotura se comparó con valores para predecidos por la aplicación de las teorías de las lineas de fluencia y de la resistencia a cortante.

Essai au Laboratoire sur une Structure "Dalle de Plancher" Plate, 45 Pieds Carrés

On a fait des études experimentales analytiques coordonnées des planchers en béton armé à l'Université d'Illinois et au laboratoire de la PCA (Association de Ciment Portland), avec le but de fournir une base plus rationnelle des méthodes de calcul que celles en usage à présent. A la fin, on envisage que des systèmes de plancher plus économiques résulteront de ces méthodes de calcul ameliorées. Le programme experimentale à l'Université d'Illinois avait à faire avec un test sur des modèles de ¼-échelle de plusieurs planchers.

Pour faciliter l'interpretation des tests des modèles ¼-échelle, on a construit une structure plate à ¾-échelle mesurant 45 pieds carrés au laboratoire de la

PCA. La distribution de moments dans la dalle sous charge normale découverte dans les essais est comparée avec les valeurs de moment-dalle obtenues par les méthodes de calcul employées à présent. Aussi, le comportement observé à charge maximum est comparé avec les valeurs de charge ultime prédite par l'application de la théorie ligne de fluage et la théorie de résistance au cisaillement.

Modellversuch einer quadratischen Pilzdecke mit 45 Fuss Seitenlänge

Koordinierte experimentelle und analytische Untersuchungen von Stahlbetondeckensystemen wurden von der Universität von Illinois und der Portland Cement Association (PCA) in ihren Laboratorien durchgeführt, um Grundlagen für rationalere Berechnungsmethoden zu finden als sie gegenwärtig benutzt werden. Die Zielsetzung ist, durch diese verbesserten Entwurfsmethoden ökonomischere Deckensysteme zu erhalten. Das experimentelle Programm an der Universität von Illinois bestand aus Versuchen an Modellen verschiedener Deckensysteme in ein viertel der natürlichen Grösse.

Um die Auswertung der Versuche an den Modellen von ein viertel der natürlichen Grösse zu erleichtern, wurde von den PCA Laboratorien ein Pilzdeckenbau untersucht, der drei viertel der natürlichen Grösse war und 45 Fuss im Quadrat mass. Die Verteilung der Momente in der Platte, wie sie bei den Versuchen unter Nutzlast gefunden wurden, wird mit den Werten für Plattenmomente verglichen, die durch die gegenwärtigen Entwurfsmethoden erhalten wurden. Ausserdem wird das beobachtete Verhalten bei Bruch mit den Werten für die Bruchlast verglichen, die durch Anwendung der Bruchlinientheorie und einer Schubbruchtheorie berechnet wurden.